A STUDY OF CORROSION AND MECHANICAL CHARACTERISTICS OF QUENCHED AND SELF-TEMPERED (QST) OR TMT STEEL REINFORCING BARS USED IN CONCRETE STRUCTURES

A THESIS

submitted by

SOORAJ KUMAR A. O.

for the award of the degree

of

MASTER OF SCIENCE

BUILDING TECHNOLOGY AND CONSTRUCTION MANAGEMENT DIVISION

DEPARTMENT OF CIVIL ENGINEERING

INDIAN INSTITUTE OF TECHNOLOGY MADRAS, CHENNAI

JUNE 2017

The only thing we have to fear is fear itself.

Franklin D. Roosevelt

Dedicated to my late grandparents

THESIS CERTIFICATE

This is to certify that the thesis entitled "**A study of corrosion and mechanical characteristics of Quenched & Self-Tempered (QST) or TMT steel reinforcing bars used in concrete structures**" submitted by Sooraj Kumar A. O. to the Indian Institute of Technology Madras, for the award of the degree of Master of Science is a bonafide record of research work carried out by him under my supervision. The contents of this thesis, in full or in parts, have not been submitted or will not be submitted to any other Institute or University for the award of any degree or diploma.

Dr. Radhakrishna G. Pillai
Research Guide
Assistant Professor
Dept. of Civil Engineering
Indian Institute of Technology Madras
Chennai - 600036, India

Place: Chennai
Date: 2 June 2017

ACKNOWLEDGEMENTS

The research I took up would not have been successful without all the support and help gathered from my family, friends, colleagues and others. It has been my privilege to pursue this degree at IIT Madras, and I am grateful to all who were part of it.

I acknowledge the financial support from the Ministry of Human Resource Development (MHRD, India) and the Department of Science and Technology (DST, India) through IIT Madras.

I would like to thank my advisor, Dr. Radhakrishna G. Pillai for his immense support in and out of my research during the course of this degree. He had been such a great mentor in supervising the work and of immense support in times of need. I see his care and guidance as my privilege and am grateful to him for making me who I am today.

I am thankful to the staff and faculty from the Department of Civil Engineering for their complete support during the project duration. I thank Prof. Ravindra Gettu for his constant inputs and critical reviews at different stages of my research work. My sincere thanks to Prof. V. Gopalaratnam (University of Missouri, Columbia, USA) for his interest and efforts in guiding the project on fabricating an extensometer, and I am grateful for the opportunity given. I also thank Prof. Manu Santhanam and Prof. Ramamurthy for their comments and support in the timely completion of this work. A special mention to Prof. Koshy Varghese and Dr. Sivakumar Palaniappan for their help and support.

I thank Mrs. Malarrvizhi, Mr. Muthuswamy, Mr. Soundarapandian, Mr. Subramani, Mr. Krishnan and Mr. Gasper for their help in times of need. I am indebted to the staff of the Departmental Workshop - Mr. Murali, Mr. Prince, Mr. Balu, Mr. Nagarajan and Mr. Bala, for the amount of machining works for specimens and setups done over the course of this project. Thank you for your patience and perfection in the work delivered. Mr. Murali and Mrs. Malarvizhi had assisted a lot to get the extensometer work to fruition. Not to miss Mr. Shiva who was always there with the extensometer, taking the ownership on my behalf and looking after/improvising it. Mr. Prince and the supporting staff had done a good job in machining and fabricating, the mechanical and corrosion test specimens, TM-ring test setup, and bend test mandrel. Thank you all for your support.

A special mention to all those who helped me with the collection of steel samples from various countries. Thanks to Prof. Christoph Gehlen (*Technical University of Munich, Munich, Germany*), Prof. Frank Dehn (*Leipzig University, Leipzig, Germany*), Dr. Shashank Bishnoi (*Asst. Professor, IIT Delhi*), Nithin (*Ph.D student, IIT Madras*), Murshid (*Ph.D. student, NTU Singapore*), Tomo Ui (*Exchange student, Japan*), Mr. Sreekumar and Mr. Jayakrishnan (and Radhika) in this regard.

I thank Prof. Sampath, from the Department of Metallurgical and Materials Engineering, IIT Madras for permitting to use the lab facilities and assist in the microstructural and mechanical studies. Thank you Likin (*Ph.D. student, EED*), Mohan (*Ph. D. student, MME*), Anu (*M.S student., MME*) and Guhan (*Staff, Manufacturing Engineering Department*) for their support.

It was my privilege to mentor the interns during the summer and winter terms (2015-2016) and thanks to all for the support. It was Gokul, Sethu, Anupama and Sarvani who kickstarted the work out of Dr. Pillai's curiosity in TMT bars. Thanks to Vishruth and Susan for their super-enthusiasm in working with me. Thanks to Abhinav, Suhail, Anand, Mitra and Aiswarya for the support. It was a great experience to meet a few budding IIT Tirupati-ians including Sudhanshu, Leela, Aman, Chandru, and Tarani. I believe that you all had a great time with me and hope that the interactions were beneficial.

I thank my friends from the Department of Civil Engineering for their complete support and motivation throughout my research work. I thank all for their suggestions and laborious work support, especially when I stayed crippled towards the end of this project.

I would like to take a little (but significant) space to specifically thank everyone, who helped me at the crucial time of my project when I, unfortunately, got crippled. I thank Dr. Thirunarayanan (Ortho Specialist) who did the ankle-surgery and reviewed my condition in my recovery. I am thankful to Mr. Vijesh (Physiotherapist, IITM Hospital) for his patience and proper care in mobilizing my ankle. Thanks to Praveen for his brotherly care and consistent guidance (which I really needed at times of frustration) in documentation and completion of this work. His care and timely help in running around (literally) for me (and my parents) are unforgettable. Once again, thanks to Dr. Pillai for his sincere efforts in availing a temporary quarter on medical grounds and regular meetings to monitor the progress in my work. Special thanks to Dhanya Ma'am (Mrs. Pillai) also for all her care and well-wishes. Thank you Sanoop, for you lifted me (literally) when I fell and kept me moving during my recovery. Thanks to Sripriya and family (Karthik, Varun, and Uncle) for making a wonderful and friendly neighbourhood. Thank you, Nithya Nair, for helping me with the mobility accessories. Thanks to Rohit (cousin) and Shalu for your company and the good times we had. Thank you Saarthak for setting up a mini corrosion lab at home. Thanks to Deepak and Prabha for helping me out with the extensometer and tension tests and getting fruitful results. Thanks to Stefie for supporting me with the bend tests. Super-thanks to Yuvaraj and Aswathy for coordinating my work in and out of our department. Thanks to Sundar and Rameez for their timely help. Thanks to Ram, Shriram, Marimuthu, Santhosh, Aparna and Anand in keeping up my morale. Heartfelt thanks to Siva (Technician) again for helping me, despite his other works in MPCEM lab. Thanks to Anto (Project Staff) for his time and enthusiasm in my experiments, and meet the requirements. Thanks to Kanchana and Kavya for their help too. Special thanks to Achu for giving me company despite her hectic office work. Thank you Anzal, Vaisakh, Swathy and Abhi for the surprise visit. Thanks to Raveendran (Perappan), Saraswathiamma (Peramma), Rahul (cousin), Reshmi (cousin) and Rahul (brother-in-law), Latha (Chitta) and Nimmy (Chitta), Dr. Gafoor and family (Femi aunty, Chinnu, and Jilu), Prakashan Sir and Pushpa aunty, Vijayakumar uncle and Vidya aunty, for their concern and wishes.

For my friends (from BTCM division and other departments), big thanks for all the good moments we had. Thank you Ranjith, Madhumitha, Sai, Anna, Ranjitha, Shyam, Amrutha, Ganga, Tharun, Chackochan, Sonam, Varkey, Johan, Zaeem, Thangadurai, Vignesh, Sasidharan, Mani, Niveditha, Sindhu, Mathew, Manu, Sachin, Anil, Lijith, George, Khader, Anjitha, Rakishma, Akhila, Murugan, Nithya Banukumar, Priyadarshini, Manjari, Sujatha, Thirumalai, Pinky, Siva, Muthukumar, Ramaswamy, Mahesh, Swathy, Anusha, Dyana, Divya Rani, Sunitha, Cinderela, Nikhil, Sabari, Sooraj Shiby, Dibu, Hima, Arsha and Arathi. If I missed anyone, it was not intentional.

Most of all, my family who accompanied, supported and motivated me in that time of ill-health and frustration. Thanks to my Mom (Mrs. Sujatha Devi), Dad (Mr. Omanakuttan Nair) and my brother (Neeraj Kumar), for all the care throughout the last six months. This degree is your success too, and I have nothing but love to replace your time and energy invested in its completion.

A big thanks to all the haters too for bringing the bad experiences to me and making me stronger by overcoming them. I value that experience, and God bless you all.

ABSTRACT

Quenched and Self-Tempered steel reinforcing bars (rebars) consists of a hard peripheral 'tempered martensite' (TM) ring around a ductile 'ferrite-pearlite' (FP) core. These rebars are called by the name of Thermo-Mechanically Treated (TMT) steel rebars in the Indian market. The enhanced mechanical and corrosion properties of QST steel rebars over mild steel or cold-twist deformed (CTD) steel rebars is attributed to the composite behaviour of TM and FP. Despite the extensive research on QST steel rebars, there is a lack of consensus on the corrosion susceptibility of QST steel rebars. Also, it is difficult to have a full stress-strain curve of QST steel rebars without a costly extensometer. Hence, many engineering colleges are unable to procure these devices. To address these gaps, this study was executed in 3 stages viz. the evaluation of microstructural, corrosion and mechanical properties of QST steel rebars and the development of a low-cost extensometer.

Stage 1 involved macroetching of cross-sectional steel specimens collected from across different sources in India and other countries. QST steel rebars of 8, 12 and 16 mm diameters were etched using nital solution and the cross-sectional phase distribution (CSPD) was quantified. It was found that QST steel rebars with inadequate CSPD with discontinuous, eccentric, or non-uniform TM-phase exist in the market, owing to poor quenching and tempering processes. The presence and variation of non-uniform CSPD across different rebars are also found and reported. To address this quality control issue, a 'TM-ring test' procedure and setup was developed for site practice to produce repeatable and reproducible results, along with a 2 - level acceptance criterion.

Stage 2 studied the effect of the inadequate CSPD on the corrosion behaviour of QST steel rebars. The corrosion characteristics have been studied on isolated microstructural specimens (TM and FP separate) and a composite QST rebar (TM & FP combined). Linear Polarization Resistance (LPR) and Cyclic Potentiodynamic Polarization (CPP) tests, on TM and FP, extracted from a typical QST steel rebar showed a difference in the chloride threshold when immersed in simulated concrete pore solution. The chloride threshold for metastable and stable pitting of TM are 16 % and 11 %, respectively, higher than those of FP. Hence, FP could preferentially corrode over TM. However, immersion tests on composite QST steel rebars showed that pitting corrosion was more dependent on

surface defects than the microstructural difference. Also, the immersion test showed higher pitting propagation tendency of FP than TM.

In Stage 3, a low-cost clip-on extensometer (CoE) was designed and fabricated for the tension testing (as discussed in the next paragraph). Cylindrical specimens of TM and FP were extracted from a QST steel rebar and tension tests were conducted. The tensile test results showed that FP had a relatively ductile behaviour with low strength, whereas TM had a relatively brittle behaviour with high yield and ultimate strengths. Hence, QST steel rebars show a composite response. The rebars tested for cross-sectional studies in Stage 1 (and categorised into 'good' and 'poor' quality) were subjected to tension and bend tests, to correlate the effect of inadequate CSPD on the yield strength and elongation. There is a significant variation in the mechanical parameters exhibited by 'poor' quality steel rebar specimens with varying/inadequate CSPD. A few 'poor' quality steel rebars showed cracks under bending which could induce crevice corrosion.

The CoE (named as BTCoEM v1.0) is fabricated for a gauge length of 50 mm with a travel length of 15 mm (maximum 30% strain). The CoE design is based on a Wheatstone bridge circuit integrated with a fatigue-resistant aluminium body that translates the elongation in a test specimen into an equivalent output voltage. The device can record data with a resolution of 0.001 mm with an accuracy of ± 5%. The cost of the fabricated CoE is about one-tenth the market price of similar models and thus, acts as an economically-viable option for the low-tier institutions.

It is concluded that CSPD has a significant influence on the corrosion and mechanical properties of a QST steel rebar. The current BIS specifications for the manufacturing and quality check for QST steels needs to be stringent to tackle the issue. The study suggests the addition of 'TM-ring test' with the acceptance criteria as a compulsory quality control check at the end of a product line, or at the site. This can help to achieve a uniform and adequate CSPD, which is expected to give better corrosion resistance. Also, there is a need for upper limits (similar to Australian/British/Japanese standards) to draw a clear line of control on the yield strength. Hence, the adequate CSPD can indirectly help in achieving the desired yield strength also. Hence, the quality assurance of QST steel rebars in the microstructure level (regarding CSPD) will give an indirect control on the mechanical and corrosion performance. Better quality control will help in the better structural and corrosion performance of RC structures designed for earthquake

resistance and exposed to corrosive environment. This thesis will also help in creating an awareness among industry professionals on an existing lack of quality in QST steel rebars and the need for better quality control.

KEYWORDS: TMT, QST, steel, ferrite, pearlite, martensite, pitting, chloride threshold, cyclic potentiodynamic polarization, crevice corrosion, extensometer, Wheatstone bridge, tensile test, bend test

TABLE OF CONTENTS

LIST OF TABLES

LIST OF FIGURES

ABBREVIATIONS

ASM	American Society for Materials
ASTM	American Society for Testing Materials
AS/NZS	Australian/New-Zealand Standards
BIS	Bureau of Indian Standards
BS	British Standards
CE	Counter Electrode
CFPD	Circumferential Phase Distribution
CoE	Clip-on Extensometer
CPP	Cyclic Potentiodynamic Polarization
CPWD	Central Public Works Department
CRSI	Corrosion Resistant Steel Institute
CSPD	Cross-Sectional Phase Distribution
CTD	Cold-Twisted and Deformed
DA	Deflecting arm
DAQ	Data Acquisition
DIN	Deutsches Institut für Normung (German Institute for Standardization)
DP	Dual Phase
EDW	Electric Discharge Wire cutting
FP	Ferrite-Pearlite
FRP	Fibre Reinforced Plastic
GQ	Good Quality
HAZ	Heat Affected Zone
HYSD	High Yield Strength Deformed
IS	Indian Standards
JIS	Japanese International Standards
LCC	Life-cycle Cost
LPR	Linear Polarization Resistance
LVDT	Linear Variable Differential Transformer
MSP	Metastable Pitting
NIH	National Institute of Health
OCP	Open Circuit Potential
OES	Optical Emission Spectroscopy
OM	Optical Microscopy
PQ	Poor Quality
Q&ST	Quenching and Self-Tempering
QST	Quenched and Self-Tempered
RC	Reinforced Concrete
RE	Reference Electrode
Rebar	Reinforcement bar
SCE	Standard Calomel Electrode
SLP	Service Life Prediction
SP	Stable Pitting
SP’	Supporting Post
SPS	Simulated Pore Solution
STC	Self-Temperature Compensation

TM	Tempered Martensite
TMT	Thermo-Mechanically Treated
TRIP	Transformation Induced Plasticity
TS/YS	Tensile Strength to Yield Strength ratio
TZ	Transition Zone
UFG	Ultra Fine Grained
UTM	Universal Testing Machine
WE	Working Electrode
WFB	Wheatstone Full Bridge
YS	Yield Strength

NOTATIONS

A	Total cross sectional area of the steel reinforcement rebar
A_{FP}	Area constituted by FP core in a cross-section
A_{TM}	Area constituted by TM periphery in a cross-section
bwoc	By weight of cement
bwoC	By weight of concrete
Cl^-	Chloride
Cl_{th}	Chloride threshold
C_{TH}	Average chloride threshold
D	Designated diameter of the steel reinforcement bar
D_c	Diffusion coefficient
D_{FP}	Diameter of ferrite-pearlite core
D_{total}	Actual diameter of steel reinforcement bar
E	Young's modulus
E_{corr}	Corrosion potential
E_{OCP}	Open circuit potential
Fe_3C	Ferric carbide
I_{corr}	Corrosion current
L1	Level 1
L2	Level 2
ΔR	Change in resistance
t_{TM}	Thickness of tempered martensite ring
$t_{TM, max}$	Maximum expected thickness of tempered martensite
$t_{TM, min}$	Minimum expected thickness of tempered martensite
V_{input}	Input voltage
V_{output}	Output voltage

CHAPTER 1

INTRODUCTION

1.1 BACKGROUND

The reinforced concrete (RC) construction professionals resorted to Thermo-Mechanically Treated (TMT) steel rebars in the 1990s in India. Since then, TMT steel rebars are widely used in different grades and diameters across all scales of construction. The TMT steel rebars took over mild steel and Cold-Twist Deformed (CTD) steel, owing to it's enhanced mechanical and corrosion characteristics. However, the high demand for this wide usage has attracted a slight decline in the quality of these steel rebars manufactured in the local level supply. Although research has been done on the mechanical and corrosion properties of TMT steel rebars, studies point out the possible quality control issues which could potentially affect the quality of the subsequent applications. One such issue occurs in the quality control of cooling/quenching in the TMT steel manufacturing process. This could have an effect on the characteristic parameters specified (and unspecified) in the guidelines for quality control of steel rebars by the Bureau of Indian Standards (BIS). Since TMT is a market term coined while introducing these rebars in India, TMT steel will be termed by the scientifically correct term: 'QST' for Quenched & Self-Tempered steel, hereafter in this document.

QST steel rebars are expected to have an enhanced mechanical and corrosion performance. However, recent studies show that the corrosion propagation rates of QST steel rebars are similar to that of CTD steel rebars (Karuppanasamy and Pillai, 2016). Also, preliminary studies showed significant scatter in the mechanical parameters of QST steel rebars (Nair and Pillai, 2015). This unexpected behaviour in corrosion resistance and mechanical performance of QST steel rebars is focussed in this research. The thesis studies the microstructural phase distribution in QST steel rebars and co-relate the results to its corrosion and mechanical properties.

As a partial fulfilment towards the research objectives, this research also focusses on extensometers which are used to measure the complete stress-strain behaviour of materials. These devices are generally costlier and hence, difficult to procure for users in low-tier institutions. Thus, this research also looks at the possibility of fabricating a clip-on type extensometer which could be used in tension tests for steel rebars. The design details documented can substantially help the Indian community as well as other developing nations in producing indigenous devices.

1.2 PROBLEM STATEMENT

QST steel rebars are produced by rapid quenching technology to produce a composite microstructure in its cross-section. However, improper quenching produces a non-uniform and inadequate cross-sectional phase distribution (CSPD). The quality control in the Indian standard guidelines for identifying this problem is not adequate. The effects of this problem on the corrosion and mechanical characteristics of these steel rebars are unknown.

Also, the cost of extensometers used to record a complete stress-strain graph for materials like steel is a potential problem for the low-tier institutions in procuring such devices. As a partial fulfilment towards the main objectives, this issue was also identified as a potential problem in this research.

1.3 OBJECTIVES AND SCOPE OF STUDY

The objectives of this study are:

1. To assess the CSPD of QST steel rebars
2. To study the effect of CSPD on the corrosion resistance of QST steel rebars
3. To design and fabricate a low-cost clip-on extensometer for tension tests
4. To study the effect of CSPD on the mechanical performance of QST steel rebars

The scope is limited to 8,12 and 16 mm diameters from 14 different sources including construction sites and retail outlets across the world. The study also assesses the rebars from 11 different countries for comparison. The scope in corrosion studies is limited to pitting corrosion resistance. In mechanical studies, this work limits the scope to tensile parameters and bendability.

1.4 RESEARCH HYPOTHESIS

It is hypothesised that non-uniform and inadequate CSPD will result in early corrosion initiation owing to the difference in corrosion resistance of different steel microstructures present in a QST steel rebar. Also, the non-uniform CSPD could result in variability of tensile response (stress-strain behaviour) and could cause different failure mechanisms when compared to a typical good quality QST steel rebar.

1.5 RESEARCH METHODOLOGY

The research was executed in three stages as shown in Figure 1.1. Each stage corresponds to one of the objectives (from Section 1.3) in the framed research methodology.

1.6 THESIS ORGANIZATION

This thesis is organised into 9 chapters, adhering to the sequence of research methodology as follows:

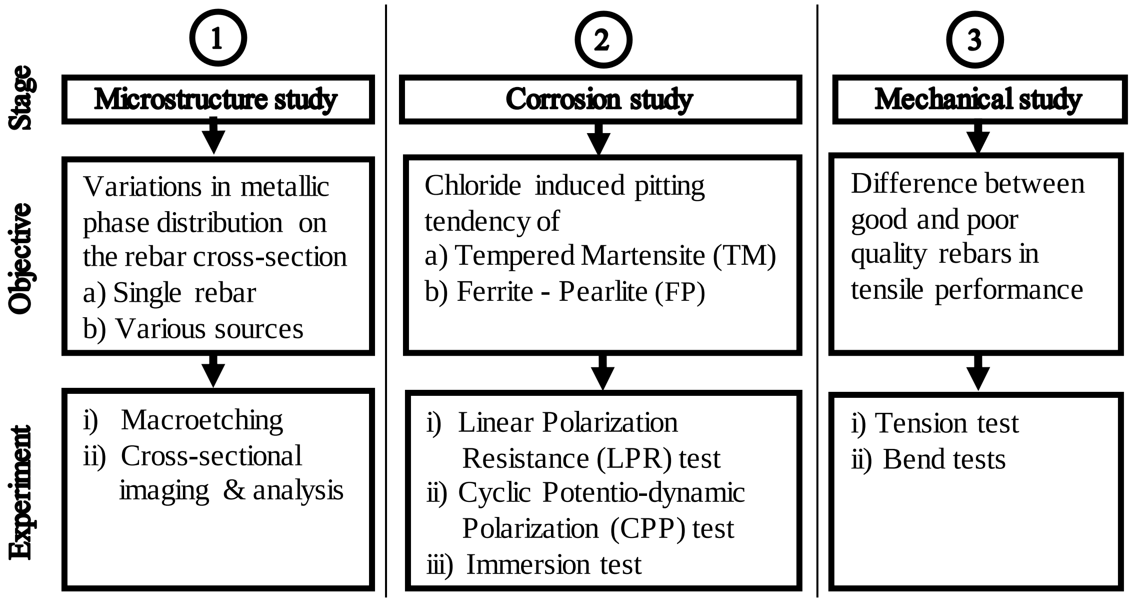

Figure 1.1: Research methodology

Chapter 1 gives an overall introduction on the research outline of this study including the definition of the problem statement.

Chapter 2 discusses the literature and available information on the current scope of this work. It also elaborated the need for current research based on the available information.

Chapter 3 briefly discusses the research significance of the overall work.

Chapter 4 is an overview of the materials and methods used in the scope of this study.

Chapter 5 discusses the microstructural study on the CSPD of QST steel rebars.

Chapter 6 looks at the corrosion characteristics of QST steel rebars based on the observations from Chapter 4 and correlates the effect of CSPD on the corrosion properties.

Chapter 7 studies the effect of the cross-sectional observations in Chapter 4 on the mechanical properties of QST steel rebars. The results of tensile and bend tests are correlated to the observations from Chapter 4.

Chapter 8 gives the design and fabrication of a clip-on extensometer (CoE) which was used for strain measurements in tension tests of steel rebars. This indigenously designed device was one-tenth the price of a commercially available extensometer and can be used for educational and research purpose.

Chapter 9 gives the summary, conclusions and scope for future studies for the overall work. The main observations on the effect of CSPD on the corrosion and mechanical characteristics within the scope of this study are reported. This chapter also enumerates the scope for future studies for individual sections of this study.

The following section gives the background information on QST steel rebars and previous research relevant to the current scope of the study.

CHAPTER 2

LITERATURE REVIEW

Iron and steel are widely employed in manufacturing appliances, tools, and infrastructure development. Steel is being used in developing roads, railways and buildings in the infrastructure sector for decades. The steels are used for reinforced concrete (RC) structures ranging from stadiums, bridges, and airports, to skyscrapers. Since concrete is weak in tension, it requires some help to take the tensile loads, which is provided by these steel reinforcement bars (rebars). Steel rebars have been used to cater the needs of RC construction industry for decades. The history of rebars in concrete started with mild steel reinforcement bars. The first usage of the steel rebars is dated back to the 1900s (CRSI 2001). Since its first use, the types of steel rebars in terms of physical and mechanical properties have changed to meet the requirements at different points in the history of RC construction industry.

2.1 REINFORCEMENT BARS USED IN CONCRETE STRUCTURES

There are different types of materials used as rebars in concrete in the RC buildings. These rebars have evolved in the history based on site-specific use and the need for better performance. Table 2-1 consolidates major types of rebars used in RC systems. These bars have been employed in existing RC constructions for site/region specific applications.

Steel rebars are used predominantly in the RC buildings because of its good mechanical properties at lower investment when compared to the other alternatives available. A variation of the steel rebars exists in the name of *epoxy coated rebars* where a coat of epoxy is provided over the steel surface by suitable methods. This is done (and marketed as) for enhanced corrosion resistance. There are *galvanized steel rebars* which are similar to epoxy coated rebars. The coating in these rebars is given using a galvanizing element (more anodic than steel) like zinc which protects the steel from corrosion. However, these coated bars cannot be bent without cracking.

There are studies on *bamboo reinforced concrete* (BRC), *fibre reinforced concrete* (FRC) and *textile reinforced concrete* (TRC) which are out of the scope of this study. The reinforcing elements like bamboo, fibres or textiles are advantageous in specific aspects like reducing overall weight, reducing the thickness, or crack resistance of the RC elements. This study focusses on QST steel rebars which emerged in India during the late 1990s.

Table 2-1: History of steel rebars in India

Reinforcing bar	Brief details
Mild steel (**MS**)[1]	Mild steel was the 1st type of steel rebar used as concrete reinforcement. These had strengths around 250 MPa and good ductility. This hot-rolled steel was predominantly ferrite-pearlitic in nature and is rarely/not used in current RC constructions across the world.
Cold-Twist deformed (**CTD**) steel[1]	This cold worked steel rebars were better in strength (400-500 MPa) than MS but brittle in nature. These were taken up in the market owing to the high strength when compared to MS bars. These rebars were also discontinued in most parts of the world.
Quenched and Self-Tempered (**QST**) steel[1]	QST steel rebars were better in many aspects where MS and CTD could not serve in RC systems. These rebars come in different diameters (6 – 36mm) and grades (415,500, and 550) in the Indian market. It has better strength along with good ductility and is expected to have better corrosion resistance than CTD or MS rebars.
Dual Phase (**DP**) steel[2]	DP steels are High Strength Low Alloyed (HSLA) rebars similar to QST steel rebars. These are ferritic-martensitic steel rebars with the difference in microstructural phase distribution. Unlike QST rebars with isolated areas of phases distributed in its cross-section, DP steels have a dispersed distribution in its cross-section.
Stainless steel (**SS**)[3]	These are relatively expensive. However, they are used in structures of high importance owing to the resistance to corrosion offered over the other variants of steel rebars. The earliest use of SS bars are dated back to 1940s in the Gulf of Mexico and were used in several sites in USA and UK ASTM A276 gives the variants of SS steel suitable for RC construction.
Fibre reinforced plastic (**FRP**)[4]	FRP rebars are lightweight and claim to have twice the tensile strengths of conventional steel rebars. These were used in bridge decks and docks in the USA where corrosion of steel rebars is a major concern. These are available in Glass (GFRP) and Carbon (CFRP) fibre variants. Although the initial cost is high, the life cycle cost (LCC) is economical.
Basalt[5]	An emerging type of rebar with comparable performance characteristics as of a steel rear. Major advantages include the absence of corrosion and lightweight nature. It is available in all diameters similar to QST steel rebars. These bars are claimed to have a similar coefficient of thermal expansion as concrete.

[1] Ambuja (2005); [2] Maffei et al. (2007); [3] Magee and Schnell (2002), Gedge (2003); [4] Malnati (2011), CIF (2003); [5] Smarter Building Systems LLC.

2.2 History of steel reinforcement bars in India

In India, ‘mild steel’ was used in the 1960s (Ambuja 2005) with a minimum yield strength of 250 MPa and good ductility. The ribbed version of mild steel also followed in the 1960s. Mild steel was succeeded by High Yield Strength Deformed (HYSD) steel rebars with better strengths of 400 to 500 MPa with adequate ductility. The HYSD steel bars had ribs on its surface to give a better mechanical bond performance. Cold working was employed in achieving high strength in the 1970s which brought Cold-Twist Deformed (CTD) steel rebars. CTD bars were also called TOR steel. However, CTD steel bars did not gain much acceptance in the market because of the reduction in ductility and corrosion resistance. This was because these rebars compromised on the ductility (which came down to approximately 12%) with an increase in the yield strength when compared to the expected ductility of 16% at that time. Also, CTD bars had residual stresses (as a result of cold-working) and surface cracks which led to poor corrosion resistance and durability in RC structures. Because of this, the developed countries banned CTD steel bars in few years. About a decade later, India also stopped the widespread usage of CTD steel bars.

The QST steel bars with sufficient strength and ductility succeeded CTD steel bars. The high costs in cold twisting and alloying with rare elements also helped in this transition. The modified manufacturing process (i.e., in the cooling stage to control the microstructure formation) of QST steel led to a better performance than its predecessors at reduced cost of production. Figure 2.1 shows the timeline and the evolution of steel rebars in India.

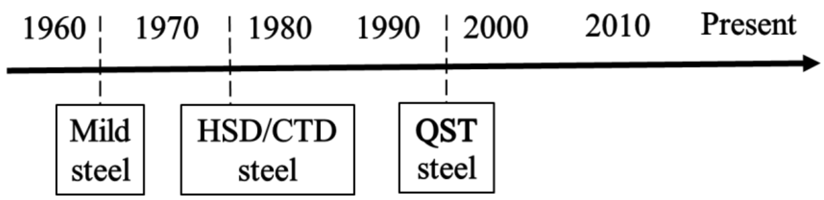

Figure 2.1: History of steel rebars in India

QST steel rebars are specially manufactured steel rebars with enhanced strength and ductility at the same time. Better mechanical performance at reduced production cost can be achieved through the special Q&ST heat treatment over cold-hardening or microalloying (Augusti 1995). This makes QST steel rebars being widely used in India today. The strength varies between 400 to 600 MPa with a minimum ductility of 20-24%. Guidelines have been written and established for the manufacture and quality check of steel rebars (including QST steel) by Bureau of Indian Standards (BIS).

QST steel is wrongly addressed in its name since any steel manufacture involves thermal and mechanical treatment processes. Thermo-mechanically treated steel could be any among QST steel, DP steel, Ultra Fine Grained (UFG) steel, and Transformation Induced Plasticity (TRIP) steel (Islam 2010). Although thermomechanical-treatment (involving a thermal and mechanical treatment) is common in the manufacturing of most steel types, the QST steel in India is industrially called as TMT steel - a market term.

2.3 MANUFACTURING AND QUENCHING TECHNOLOGIES FOR QST STEEL REBARS

The basic process of steel making is of two types: 1. Oxygen steelmaking and 2. Electric Steelmaking. The basic process in which iron is melted is different in these two techniques. In oxygen steel making, molten iron (with or without scrap steel) from the blast furnace is taken to a Basic Oxygen Furnace (BOF) to be blown with pure oxygen at speeds greater than the speed of sound. In an Electric Arc Furnace (EAF), the input materials (including scrap steel) are in solid state and electricity is used to melt the feedstock. This steel making process is followed by secondary steel making which includes processes to remove sulphur, remove unwanted gases and alloying to get the required composition. The molten steel is then cast and rolled to make products of required shape and sizes. The output of the casting stage is a billet, bloom or slab, depending on the shape and size of the product. A billet is rolled in the steel industry for the manufacture of steel rods. A brief flow of manufacturing process is shown in Figure 2.2.

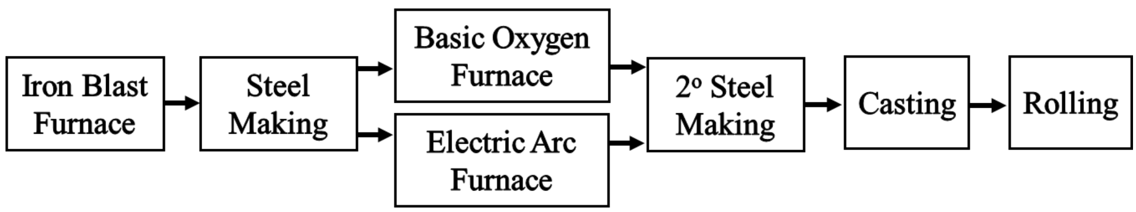

Figure 2.2: Brief flow of general steel manufacturing processes

The process that makes QST rebar special happens in the rolling stage. There is a specialized cooling process where the hot rolled product is rapidly cooled down (quenching) and then cooled in the air which results in surface tempering by the heat from the rebars own core (self-tempering). This cooling system has been patented and employed in different names with the same basic concept. Although there have been several references showing different points in history where the QST technology was introduced in the steel industry worldwide, the most common reference is to the mid-1980s. Different patented technologies for QST steel manufacture followed in the industry are given below and compiled in Table 2-2.

Table 2-2: Different quenching technologies

	Technology	Developers	Country	Year
1	Tempcore	CRM	Belgium	1960s
2	Thermex	HSE	Germany	1980s
3	Stelmor	Morgan Construction Company	USA	1960
4	Turboquench/ Thermoquench	Herbert Rothe Consulting Engineers	Germany	-
5	Evcon Turbo	Evo-Tech (India)	Germany	-

2.3.1 TEMPCORE ™

Tempore was developed by CRN Belgium in the 1960s and is believed to be one of the earliest patented technology established in the domain of cooling technology. The cooling pipe essentially has a tangential water flow. Unlike other technologies, it was noticed that Tempcore has a good background on steel research also and constantly try to improve their research and development (Rehm and Russwurm 1977, Simon et al. 1984). A notable document is Noville (2005) which discusses the effect of quenching parameters on the formation of CSPD.

2.3.2 THERMEX ™

This technology was developed by Franz Tamm (Managing Director HSM Germany) from HSM (Hennigsdorfer Stahl Engineering GmbH) Germany in the early 1980s. In India, the technology is delivered by H&K Rolling Mill Engineers (Mumbai) trademarked in the names of THERMEX, THERMEX QST and TMX. A few plants installed with Thermex systems are Mahalaxmi TMT (Wardha, Maharashtra; 4 strand Thermex Pipe Assembly), S.A.I.L. (Durgapur, West Bengal; First Thermex system in India in 1990) and Kamachi Steel plant (Chennai) (Refer H&K India website).

2.3.3 STELMOR ™

Developed by Morgan Construction Company in Worcester (Massachusetts) USA in the 1960s, it was acquired by Siemens in 2008. The Stelmor technology is a successful air patenting methods over the lead patenting methods for controlled cooling of steel rod (Campbell 1989). The competing technology is employed by JSW. There is a firm in the name of Stelmore Inc. from Canada which does not market the same technology. Stelmor is claimed to have a different cooling technique in products delivered as coils. For more details, refer Siemens VAI (2010).

2.3.4 TURBOQUENCH ™

A temperature controlled processing of wire rods and bar products provided by Herbert Rothe Consulting Engineers, the main difference told as the combination of laminar and turbulent flows within the nozzle, with an extremely high heat transfer coefficient (Reference: ThermoQuench website). 'Amravati' claims to be the authorized dealers of Turboquench technology in India. The technology is also called by the name of 'Thermoquench'.

2.3.5 EVCON TURBO ™

The system delivered by EVOTech Inc. was approved to be used in the manufacture of QST steel rebars by the CPWD Specifications (2009). However, not much details on the developer are available. The system was identified in few Indian steel manufacturers like SAIL and GBR metals.

The quenching and self-tempering processes are employed in the manufacturing line with the help of various cooling technologies. These patented technologies like Tempcore™, Thermex™, Thermoquench®, Evcon Turbo™ (Approved by CPWD specification 2009) or Stelmor™ essentially have a cooling system, which uses air, water or both at specified temperatures and flow rates. Noville (2015) discusses the effect of the quenching parameters (line speed, water temperature, and quenching time) on the microstructure and mechanical properties QST steel rebars using Tempcore™ technology, and Gamble (2003) discusses Thermex™ processed reinforcing steels. Other than these, scarce documentation on the differences in the quenching and self-tempering processes and outputs, across various quenching technologies could not be found by the authors.

The modification document for CPWD specifications (2008) allows the contractors in India to procure bars from marketing companies with BIS approved cooling technologies mentioned above. The sources of procurement have been categorised into primary and secondary sources, probably owing to the expectation in the quality of steel rebars employed in the structures.

2.4 MICROSTRUCTURAL FORMATION OF QST STEEL REBARS

QST is a special heat treatment done in the stage of rolling in the manufacture of QST steel rebars. The schematic of a QST process is given in Figure 2.3(a). The resultant cross section of a typical QST steel rebar is given in Figure 2.3(b). In the rolling stage, billets are heated and extruded, step-by-step to transform the shape and bring the cross section shape and size as desired. At the end of the rolling stage, the hot rolled product is cooled. In conventional rebars like mild steel, the hot rolled 'austenitic' rods are cooled in air slowly resulting in a ferrite-pearlite (FP; soft and ductile) phase formation at the microstructural level of the steel bar. In the case of QST steel rebars, the hot 'austenitic'material is rapidly cooled with the help of water at high pressure sprayed over the surface. The surface temperature of the rolled product drops from about 1000 to 200 ^{o}C (i.e., a reduction of about 800 ^{o}C) within about a second. This transforms the austenite to 'martensite' at the periphery and hot austenite at the core. The radiant outflow of heat from the austenite tempers the martensite to form 'tempered martensite' (TM; hard and brittle). The austenite slowly cools down in air to form an FP core. The combination of these two microstructures is the speciality of QST steel rebars. The hard TM gives high strength to the rebars and the soft FP gives enhanced ductility. A third transition layer between TM and FP also exists called 'bainite'. Bainite is again divided into two regions - the upper bainite and the lower bainite.

Figure 2.4 and Figure 2.5 shows the typical FP and TM phases (repectively) observed under the optical microscope in this study. The microstructure of TM has predominantly needle-shaped martensitic phase seen as dark in colour. These are not clearly distinct since the martensite had undergone softening due to tempering. FP is theoretically a lamellar structure of ferrite dispersed between pearlitic phase. The ferrite is seen as black/dark (carbide Fe_3C) and pearlite as white in colour. FP shows a plate-like structure with more grain boundaries when compared to the needle-shaped TM. These orientations are responsible for the strength and ductility of FP and TM. The amount of grain boundaries also indirectly shows the susceptibility to corrosion in these phases.

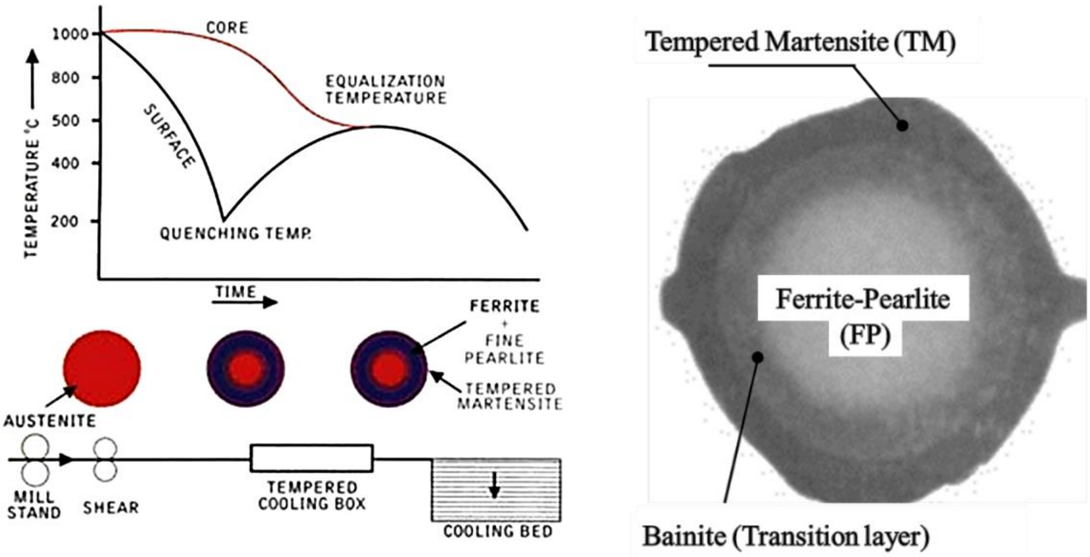

(a) (b)

Figure 2.3: (a) QST temperature profile with respect to time [TPSL (2015)] (b) QST rebar cross section with TM, FP, and TZ

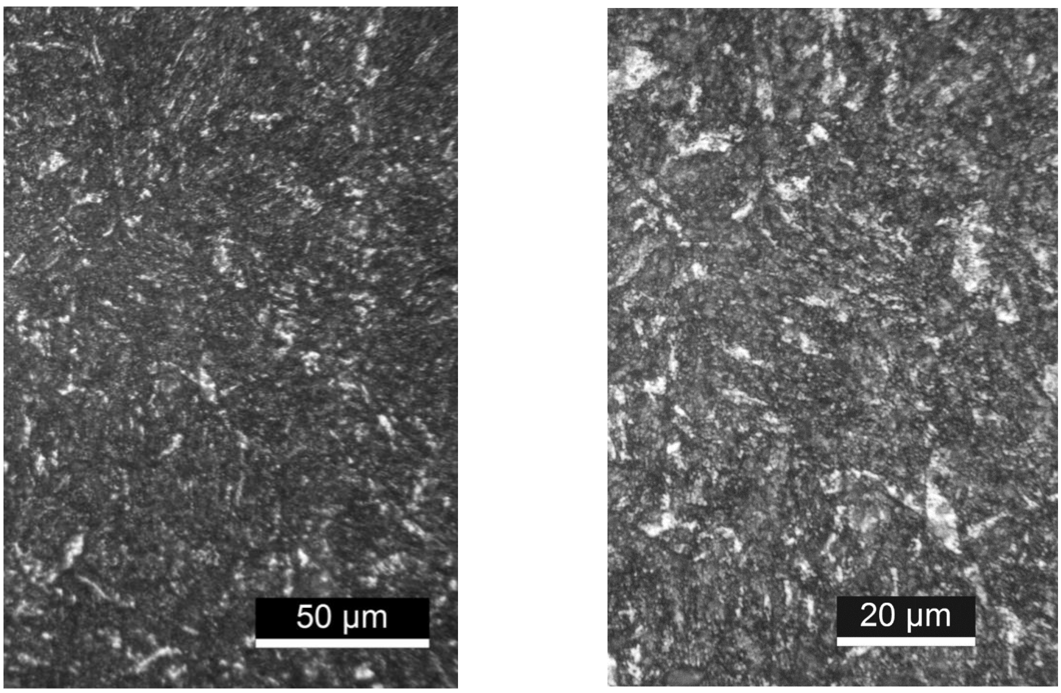

Figure 2.4: Micrograph of TM (On left: 500X; On right: 1000X)

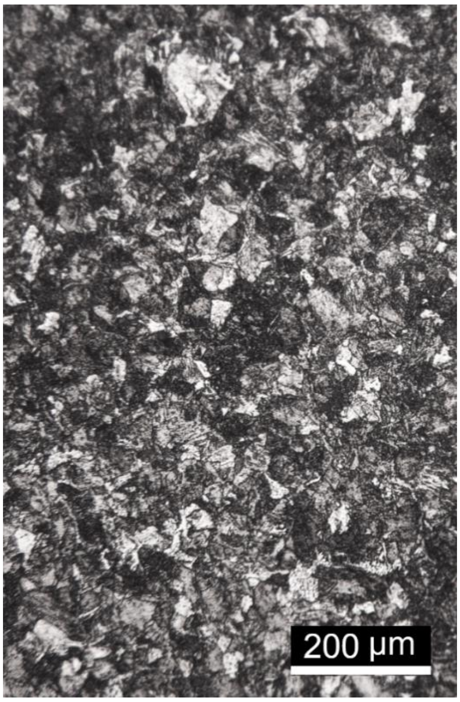

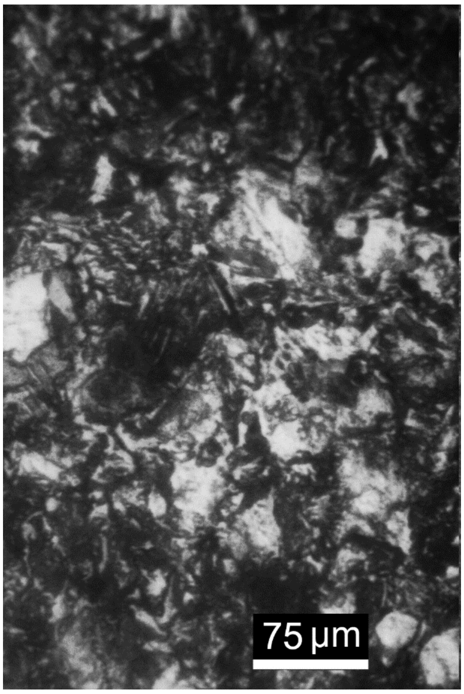

Figure 2.5: Micrograph of FP (On left: 200X; On right: 400X)

2.5 INDIAN STANDARDS FOR THE QUALITY CONTROL OF QST STEEL REBARS

2.5.1 General Guidelines

The guidelines in Indian Standards (IS) for the manufacturing of QST bars may not be sufficient enough to ensure quality in terms of the CSPD or corrosion resistance. The BIS specifications (similar to other international codes of practice) for the manufacturing or QST process is not available. IS 1786: 2008 (*High Strength Deformed Steel Bars and Wires for Concrete Reinforcement*) gives the end product requirements in terms of mechanical, physical and chemical properties. It does not incorporate any specific guidelines for the quenching and tempering process along the manufacturing line. In this code, there are no tolerance limits for the tensile parameters of QST bars. IS 1786:2008 specifies lower limits for parameters like yield strength, percentage elongation, and ultimate strength. Even though the code lays emphasis on the tensile characteristics, there are no references on the upper limit of yield strength for a bar of specific grade (except for 415S and 500S grades). Therefore, a bar with a measured yield strength greater than 500 MPa can be graded as both Fe415 and Fe500. This gives freedom for the industry to meet the minimum limit with very high tensile strengths for a particular grade. This lack of upper limit may lead to over-reinforced sections (instead of under-reinforced sections). This might be why the BS and JIS codes for reinforcing steel properties specify maximum yield strength as well for a single grade. ASTM A913/913M (*Standard Specification for High-Strength Low-Alloy Steel Shapes of Structural Quality, Produced by Quenching and Self-Tempering Process*) has given an upper limit for Grade 50 [315 N/mm^2] steel alone; although for structural steel shapes. The QST process has been briefed as a non-mandatory information in the same.

2.5.2 Annex A: Information on controlled cooling process

IS 1786:2008 *(High Strength Deformed Steel Bars and Wires for Concrete Reinforcement – Specifications)* provides guidance on the manufacturing and quality control of high strength steel bars for reinforced concrete. Irrespective of the method of manufacturing, the code is applicable for the quality control of QST steel rebars, primarily based on mechanical properties. However, it *does not mandate* the requirement of attaining the desired CSPD with TM-ring and FP-core, as shown in Figure 2.3. Moreover, Annex A of IS 1786:2008 is titled '*Information on controlled cooling process'* and provides minimal details for assessing the CSPD of QST steel rebars. A snapshot of Annex A is provided in Figure 2.6. Further, the last portion of Annex A states, "…*this test is not to be regarded as a criterion for rejection*…". However, it should be noted that Annex A in IS 1786 is intended to provide information on how to identify QST steel rebars and not to provide a standard method for the assessment of QST steel rebars based on microstructure. Also, the author has witnessed poor practices in the assessment of the microstructure of QST steel rebars at the manufacturing plants – mainly due to the lack of a standard procedure from Bureau of Indian Standards (BIS). Hence, there is a need for a standard and detailed method of assessment to obtain reproducible results/images (via etching and imaging).

The author could not find any specifications on the critical manufacturing parameters such as line speed, water temperature, and quenching time, for the heat treatment of rebars with different diameters. It should be noted that these parameters have a significant influence on the formation of appropriate CSPD and are dependent on the technology adopted in the manufacturing line such as Tempcore™ and Thermex™. and could not be generalized. Noville (2015) shows the change in CSPD with respect to the quenching parameters in a Tempcore™ cooling system. Further discussions on the control over these parameters are beyond the scope of this paper.

IS 1786 : 2008

ANNEX A

(*Foreword*)

INFORMATION ON CONTROLLED COOLING PROCESS

A-1 The processing of reinforcing steel is usually through one or combination of processes which may include hot rolling after microalloying, hot rolling followed by controlled cooling (TMT process) and hot rolling followed by cold work.

Heat treatment is a thermal process undergone by the steel in the solid state. The most common practice is finishing online heat treatment while rolling, commonly known as thermomechanical treatment (TMT) process. After leaving the last stand of the rolling mill, the bars are quenched (rapidly cooled) in water from a final rolling temperature of about 950°C. The quenching is partial, only until a surface layer has been transformed from austenite (a steel phase stable only at very high temperatures) to martensite (stable at temperatures below 350°C). This controlled quenching is achieved in one or more online water cooling devices through which the steel passes at a very high speed before reaching the cooling bed.

Because the quenching is only partial, a part of the original heat remains in the core of the steel and, on the cooling bed, this heat migrates towards the surface. This results in an automatic self-tempering process where the surface layer of martensite is tempered; this 'tempering temperature' (or equalization temperature) refers to the maximum temperature attained by the bar surface after quenching. Tempering enables a partial diffusion of carbon out of the extremely brittle but strong martensite, thus relieving the inherent stresses locked in during the sudden quenching of the red-hot steel in cold water. The resulting tempered-martensite shows improved deformability compared to the as-quenched martensite.

The core of the heat treated reinforcing bars/wires consist of ferrite and perlite – more ductile but less strong than the martensite. Computerized process control is used to dynamically adjust the many rapidly changing parameters depending on the chemical composition of the steel, the desired grade and size of the reinforcing bar/wire etc. For the larger diameters, small addition of microalloys is usual.

Sometimes it becomes necessary to determine if a particular reinforcing bar/wire, or lot, has undergone proper heat treatment or is only a mild steel deformed bar. Because the two cannot be distinguished visually, the following field test may be used for purposes of identification. A small piece (about 12 mm long) can be cut and the transverse face lightly ground flat on progressively finer emery papers up to '0' size. The sample can be macroetched with nital (5 percent nitric acid in alcohol) at ambient temperature for a few seconds which should then reveal a darker annular region corresponding to martensite/bainite microstructure and a lighter core region. However, this test is not to be regarded as a criterion for rejection. The material conforming to the requirements of this standard for chemical and physical properties shall be considered acceptable.

Figure 2.6: Snapshot of the reference from Annex A of IS 1786: 2008 specification

2.6 MICROSTRUCTURAL STUDIES ON QST STEEL REBARS

2.6.1 Microstructural properties of QST steel rebars

QST steel rebars have a ductile core and hard outer layer - the composite action gives sufficient ductility and yield strength. The pearlite core gives ductility to the bar and the martensite layer gives the tensile strength. It is believed that the corrosion resistance of QST steel bar is better than CTD bars, which is attributed to its tempered martensite periphery. Rebars of good quality constitute 25 to 35 percent (by the total cross-sectional area) of martensite (Ambuja 2005).

2.6.2 Defective CSPD in QST steel rebars

The basis of any Q&ST system is to drastically decrease the temperature of hot austenite to form martensite at the periphery. This is followed by slow air-cooling, allowing the heat from the core to radiate outward and temper the martensite. However, a standard cooling system is not followed and the control parameters in the employed cooling systems might vary across each other. Authors could not find guidelines on the Q&ST process, with a common scope on the process parameters across various technologies like Tempcore™ and Thermex™. The international guidelines for the quality control of QST steel rebars (IS 1786: 2008; ASTM A615/615M -16: 2006; AS NZS 4671: 2001; JIS G3112: 2004; DIN 488-1: 2009; BS 4449: 2005), are primarily based on the mechanical properties, with minor differences in the limits on the mechanical parameters. However, for a good QST steel rebar, mechanical and corrosion properties are equally important. Literature indicates that there is a possibility of improper TM-ring formation owing to poor 'quality control' in the manufacturing line of steel rebars (Noville 2015; Ambuja 2005; Markan 2005).

The defects in the peripheral TM-phase in a poor quality QST steel rebar can be broadly classified into discontinuities and eccentricities (Nair and Pillai 2017). In this context, a QST steel rebar with a uniform and continuous TM ring is considered as a good quality rebar with adequate CSPD. In contrast, a rebar with a defective TM-phase is considered as a poor quality rebar with an inadequate CSPD. However, the details on these defects (in TM-phase) and their implications on the strength and corrosion resistance of these rebars are not well-documented.

2.7 CORROSION STUDIES ON QST STEEL REBARS

The corrosion resistance of QST steel rebars is a debatable topic. There are researchers who report that the corrosion resistance of QST steel rebars is better than conventional rebars like CTD (Ray et al. 1997). However, Lunderberg (2002) reports that quenched and tempered bars always have a lower corrosion resistance than conventional rebars. Also, the corrosion resistance is said to increase when tempering temperature decreases (Say 600 ^{o}C for good corrosion resistance). But the type/mechanism of corrosion should also be specified while reporting corrosion rates or resistance to corrosion.

2.7.1 Pitting and crevice corrosions in QST steel rebars

Among the various types of corrosion in steel rebar, a good number of publications discusses pitting and crevice corrosions. Possible mechanisms and explanations for these phenomena are explained, for different types of steels and testing environments (Hoar 1937; Pistorius and Burstein 1992; Szklarska 2002; Strehblow 2002). However, the results are mostly probabilistic. Scientists could still not deterministically predict the corrosion initiation and propagation mechanisms (or rates) since the phenomena are dependent on multiple variables like chloride concentration, the surface condition of steel, the composition of steel, and anode to cathode ratio (Hoar 1937). However, there are 3 major mechanisms for pitting explained in literature (McCafferty 2010), and results are generally produced on a comparative basis, rather than on absolute terms. In most of the established mechanisms, it is generally agreed that a minimum chloride concentration [Chloride threshold (Cl_{th})] is required for the pit formation and propagation. Different steel microstructures form passive layers of different thickness. A passive layer formed over ferrite is comparatively unstable than martensite (Li and Luo 2007). Hence the Cl_{th} for two different phases in a composite steel rebar is theoretically expected to be different. Thus, in a poor quality QST steel rebar, the surface could form a passive layer of varying thickness at zones of TM and FP. This could result in earlier pitting when compared to a uniformly thick passive layer formed in a GQ - QST.

Crevice corrosion in chloride environments is a special case of pitting corrosion (Szklarska and Mankowski 1978; Postlethwaite 1983; Schafer et al. 1960). Crevice corrosion propagates through minor cracks in the steel rebars embedded in reinforced concrete. This could be an issue in the case of bent up bars, stirrups or hooks where steel rebars are bent approximately through 45^{o}, 135^{o} and 180^{o} (close bend), respectively. Although Ray et al. (1997) and, Rehm and Russwurm (1977) reports good bendability, for QST rebars, the effect of an inadequate CSPD on the bendability is not known. Unlike good quality QST steel rebars, it is hypothesised that the poor quality rebars will show cracks under bending, which would result in crevice corrosion.

2.7.2 Multiple chloride thresholds (Cl_{th}) for a composite microstructure

Cl_{th} for steel-cementitious systems is reported in numerous publications (Alonso et al. 2000; Angst et al. 2009; Poulsen and Sorensen 2012). The established Cl_{th} values are represented mostly as a concentration in pore solution, percent by weight of cement and percent by weight of concrete. These established threshold values are used in service life prediction (SLP) by engineers using diffusion models (Pillai and Annapareddy 2013) or software tools like Life 365™ (Life-365^{TM} 2014). However, these predictions depend on a single value of Cl_{th} of the embedded steel in the SLP calculations. But, there exist a possibility of multiple threshold values in steel rebars with composite microstructure. The possible reduction in estimated service life between the threshold levels may be impactful in such cases of QST steel rebars.

2.7.3 Higher activity of ferrite over martensite in DP steels

General corrosion rates and localized corrosion (crevice or pitting) effects depend on the microstructure of the steel. There are 3 major forms of microstructural phases present in a low carbon steel – namely ferrite, pearlite and martensite. Preferential pitting corrosion occurs on ferrite phase and is reported to have an activity in the order of 'ferrite > martensite > pearlite' (Lu et al. 2012). Based on potentiodynamic tests in DP steels, Bhagavathi et al. (2011) have shown that the number and frequency of pits observed on the surface of the steel specimen decreased, with an increase in the martensite volume fraction (12-28%). Hence FP phase is susceptible to preferential pitting over TM in a poor quality rebar with discontinuities. Although in DP steels, (Sarkar et al. 2005) finds that a martensite-ferrite morphology can act as a cathode-anode combination. In continuation of the work by (Bhagavathi et al. 2011), a 27-48% increase in the martensite, increased the cathode to anode ratio in DP steels and lead to higher corrosion rates (recorded using galvanostatic polarization) (Sarkar et al. 2005). This indicates a possibility of galvanic corrosion at an exposed TM-FP interface.

2.7.4 Higher corrosion rate for QST steel rebar with inadequate CSPD

Nandi et al. (2016) present a clear image of an inadequate CSPD used in the scope of a corrosion research. It was observed that the average corrosion rate is higher for this rebar when compared to the other specimens in the scope. Thus, the inadequate CSPD could possibly lead to unexpected results in corrosion resistance and compromises the expected quality in corrosion performance of QST steel rebars.

2.7.5 Mixed opinion on the susceptibility to corrosion between FP and TM

Research has shown that the corrosion rates of CTD rebars can be 8.4 to 52% higher than that for QST steel rebars (Ray et al. 1997). This is attributed to the heterogeneity in the microstructure of CTD rebars, due to the high carbon and manganese content. This results in increased pearlite volume fraction in FP, which increases the probability of electrochemical cell formation. A recent 2-year long study (Jayachandran and Pillai 2016) also reported relatively same general corrosion rates for QST and CTD steel rebars embedded in chloride contaminated mortar. Further, the corrosion studies on microstructural phases isolated from QST steel rebar have shown the possibility of preferentially localized corrosion of FP over TM (Nair et al. 2016). However, a few other studies conclude that TM phase at the surface is more susceptible to pitting corrosion than FP (Angst and Elsener 2016; Al-rubaiey et al. 2013; Jang et al. 1988). In general, the conclusions from various studies form a mixed opinion on the relative corrosion resistance of TM and FP.

2.8 MECHANICAL STUDIES ON QST STEEL REBARS

Tempered martensite steels have better tensile strength and hardness when compared to the conventional hot-rolled steel rebars. This is the result of a composite microstructure of FP and TM. TM has higher yield strength but brittle in nature, whereas FP is ductile in nature but has a relatively lower yield strength. These well-established steel rebars are proven to have better mechanical properties than its predecessors. However, studies have tried to compare the properties with other steels in terms of hardness and bendability. Few studies report about the composite action of different microstructures, variation in tensile parameters (Nair et al. 2015), and geometrical characterization (Rocha et al. 2016) of QST steel rebars.

2.8.1 Differential mechanical behaviour of TM and FP

Studies have checked the relative mechanical parameters, bendability, hardness and weldability of QST steel rebars. However, only a few have tried to address the mechanical performance as a composite behaviour of the microstructure. Cadoni et al. (2013) show the tensile stress-strain behaviour of TM and FP microstructures which adhere to the expected theoretical behaviour. The actual rebar was found to show an intermediate response.

However, the tests were done at high strain rates and might have to be checked for lower strain rates.

2.8.2 Composite mechanical behaviour of QST steel rebar

Since the tensile response is a composite behaviour, the failure pattern and fracture mechanics would also closely follow an intermediate behaviour. This is corroborated by Kabir and Islam (2014) by showing fracture patterns for as-received QST steel rebars against a milled QST steel rebar. The stress-strain behaviour is close in terms of yield strength for as-received and milled rebars. However, there is a marked difference in the elongation at failure and ultimate strength values. Cadoni et al. (2013) also show a superimposed stress-strain graph for FP, TM and an as-received rebar. The as-received rebars were closer towards FP's behaviour as observed in Kabir and Islam (2014) although the yield strength had a marked difference as reported in Cadoni et al. (2013).

However, the gauge length across which the strains have been calculated has not been mentioned. This is probably why the young's modulus (E) has also not been discussed in these documents. An approximate calculation from the graphs presented in Kabir and Islam (2014) shows 14 and 16 GPa for milled and as-received specimens, respectively, which is an underestimated value. In Cadoni et al. (2013), although the graphs almost coincide in the elastic region, an approximate E-value calculated is close to 200 GPa. Also, the as-received bar has a longer plateau near the ultimate strength when compared to the graph for which is not as expected. Rather, the combined TM-FP graph is expected to meet the ultimate strength at a much lesser elongation when compared to the case of FP.

2.8.3 Bendability and flexural stress concentrations in QST steel rebars

As mentioned in Section 2.7.1, Ray et al. (1997) and, Rehm and Russwurm (1977) reports good bendability in bend tests studied on QST steel rebars. The rebars are expected to be formable without any visible cracks. The scope of the rebars bent varies across these documents and included 8, 10, 12, 16 and 32. The position of specimens in bending (with transverse ribs or longitudinal ribs on the convex side of the bend) was not defined and the load-deflection behaviour has not been discussed. These might give a better understanding of the mechanism of bending and the possible crack formation at in-situ bending.

Research on the rib/surface profile and the stress concentration are discussed in Paul et al. (2014) and Rocha et al. 2016. Paul et al. (2014) report that in fatigue cycles, there occurs a plastic deformation localization at the transverse rib root which initiates a fatigue crack. Rocha et al. (2016) conclude that the surface imperfections from the manufacturing lines originate near the transversal and longitudinal ribs. Because these imperfections are zones of stress concentration, these are potential failure zones in the service life of QST steel rebars under flexure. These observations could apply to the response on bending the bars at the site, which could form localized stress locations and subsequent cracking.

2.8.4 Variation of hardness across the cross-sectional rebar diameter

Studies have tested QST rebars of various diameters for the variation in hardness across the diameter of a QST steel rebar (Rehm and Russwurm 1977; Nikolaou and Papadimitriou 2004; Cadoni et al. 2013, Rocha et al. 2016). It is known that FP is softer than TM and the hardness profile across a diameter will show higher values near the periphery and lower values at the core. The values observed in the studies above are given in Table 2-3 and the graphs are compiled in Appendix A: The hardness values seem to lie approximately in the same region.

Table 2-3: Hardness of TM and FP from literature

Year	Author (s)	Sample	Average Hardness		
			TM	TZ	FP
1977	Rehm & Russwurm	Heat 1	240	200	175
		Heat 2	250	200	165
2003	Gamble	Set 1	295	-	210
		Set 2	295	-	235
2004	Nikolaou	8 mm Tempcore B	310	-	225
		12 mm Tempcore C	300	-	200
2013	Cadoni et al.	32 mm	275	-	165
		40 mm	290	-	185
2016	Rocha et al.	16 mm	270	-	155
		26 mm	275	-	155
		34 mm	280	-	175
		Average	**280**	**200**	**186**
		Std. Deviation	21	0	28
		Coefficient of Variation	8	0	15

2.8.5 Comparison of international codes for tensile performance of steel rebars

The international codes for the quality control of steel rebars to be used in concrete does not mandate on the method of manufacturing. All the codes mandate on the requirement of minimum tensile parameters for the manufactured steel rebars which include yield strength YS), ultimate strength (TS), TS/YS ratio and % elongation. However, the availability of different grades of steel and the closeness in their properties may result in compromising the quality of steel rebars with the expected values. For example, an Fe 550D steel rebar could pass the specifications for an Fe 500D bar also. This is because the requirements are pointed out with minimum limits. However, a clear demarcation with maximum limits is not present in most of the international codes of practice. Figure 2.7 compares the YS from various international codes.

The international codes for Australia/New Zealand, Japan, Britain, and a few cases in BIS and ASTM codes does have specifications on the upper limits of yield strength. The YS is a crucial factor in the design of RC structures and needs to be controlled inside stipulated limits. An Fe 500D bar might not exactly have 500 MPa as the YS, nor 550 MPa. It could be any value above 500 MPa. Comparing this case with an Fe 500S bar which has an upper limit of 625 MPa, a design for an under-reinforced concrete element or a seismic prone building, could anticipate the maximum yield strength possible in-situ.

Most of the steel grades in the international codes for China, Hong Kong, India, Germany or USA mostly does not put upper limits on the YS. Irrespective of the technology by which a bar is manufactured, the mechanical parameters should be met as per these codal provisions. However, an additional advantage of providing upper limits on YS will be an indirect control over the quenching and optimized parameters to achieve a good quality QST steel rebar in its microstructural requirements. Unlike YS, this issue is not profound for other parameters like TS or % elongation, since higher values are better in these cases.

In Sections 2.8.2, 2.8.3 and 2.8.4, the effect of an inadequate CSPD is still not well-documented. Section 2.8.1 could help explain the tensile and flexural observations in rebars with inadequate CSPD. However, the hardness of rebars need not be checked in the case of inadequate CSPD, since the underlying fact that FP is softer than TM is applicable in both the cases of cross-sectional adequacy (adequate and inadequate CSPD).

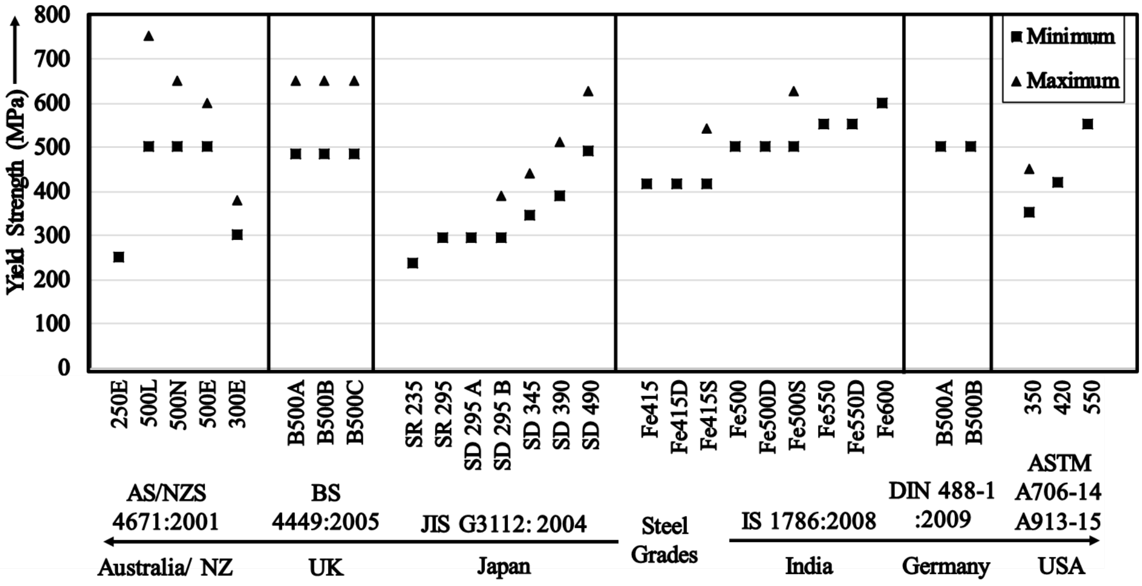

Figure 2.7: Yield Strength limits in different international standards

2.9 Effect of inadequate CSPD on the corrosion properties of QST steel rebars

A good quality QST steel rebar must have a continuous, concentric and uniform TM ring, as shown in Figure 2.8. However, many poor quality rebars (including QST) - in terms of geometry, rolling and mechanical properties - do exist in the Indian market (Viswanatha et al. 2004). Although some key industry personnel are aware of such issues, very few articles (Ambuja 2005; Nair et al. 2015) mention about the inadequate quenching and the resulting discontinuous, eccentric, and non-uniform TM-phase. In such poor quality rebars, the peripheral TM-phase is discontinuous with FP exposed at the rebar surface or circumference. Figure 2.9 shows three typical CSPDs of good quality (Case A) and poor quality (Cases B, C, and D) QST steel rebars obtained from the laboratory experiments in this study. Cases B, C, and D could result in preferential and localized corrosion (Nair et al. 2016). Also, based on electrochemical experiments conducted on coupon specimens extracted from representative QST steel rebar collected from the market, Nair et al. (2016) reported that FP could have lower chloride threshold than TM. Hence, QST steel rebars with discontinuous TM phase at the periphery could experience an earlier initiation of corrosion than a good quality rebar. Also, the discontinuities could affect the mechanical properties of the QST rebars (Mamun Al-Rashed and Shorowordi 2015).

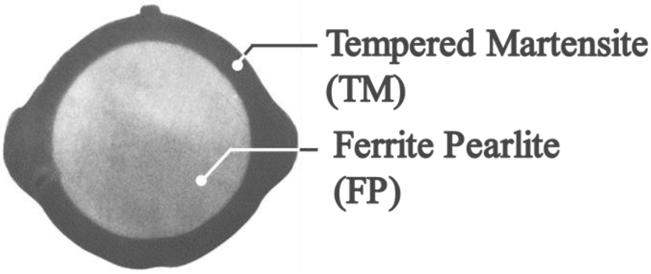

Figure 2.8: Typical QST rebar cross-section

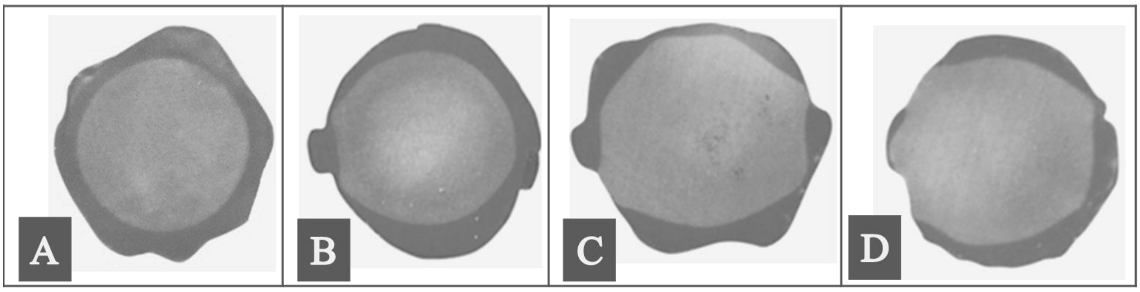

Figure 2.9: Cases of possible TM phase distribution in a QST steel rebar cross-section

2.10 Effect of inadequate CSPD on the mechanical properties of QST steel rebars

The strength and ductility of a QST bar are predominantly attributed to the quantity of TM and FP phases in the CSPD, respectively. The typical area constituted by FP in QST steel rebars is 65-75% (Markan 2005). However, the presence of discontinuities could lead to variation in the yield strengths from the specified strength-grade due to the higher area of FP. However, IS 13920 (1993): '*Ductile detailing of reinforced concrete structures subjected to seismic forces – code of practice*' and IS 1786:2008 do not specify any upper limits for yield and tensile strengths. This issue associated with the lack of upper limits on yield strength were raised by Rai et al. (2012). As a sign of improvement, the recent draft (CED 39 - 7941) for the amendment of IS 13920 (1993) recommends to incorporate upper limits in the yield strength for the rebars to be used in seismic applications. Also, the variations in CSPD along the length of a rebar can result in significant variability in the tensile properties along the length of the rebars. In addition, unsymmetrical cross-sections may result in the unsymmetrical flexural behaviour of rebars. In short, the variations in CSPDs can result in earlier and localized corrosion and variations in mechanical properties, which in turn can lead to unexpected structural behaviour of RC systems.

2.11 BACKGROUND ON EXTENSOMETERS

An extensometer is a general purpose device used to measure the extension (or elongation) of materials. Typically, these are used for obtaining stress-strain behaviour from laboratory tension tests (say, as per ASTM E8-16a) like steel, concrete, metals, acrylics, fibres, textiles, stones and soil. There are pre-defined types of extensometers based on the material tested and the technical specifications of the device. Presently, extensometers are available with different sets of the specification from various service providers in the market. Some manufacturers provide customized extensometers to meet specific client requirements. Clients value these devices for offering the advantage of measuring the complete stress-strain behaviour of materials and are widely used in research projects. Hence, these devices are of great demand on a single investment owing to its ease of application, repeatability, and reusability over a long duration. Because it is a single time investment, extensometers are relatively costlier than other strain measurement devices such as strain gauges and dial gauges. The extensometer designs for linear measurement applications can be categorized as discussed in Section 2.11.1.

2.11.1 Classification of extensometers

Extensometers could be broadly classified based on the method of measurement (Renganathan 2003) viz. direct and indirect comparison types. They could also be classified based on the type of contact with the specimen viz. contact and non-contact types. Table 2-4 gives the classification of a few extensometers into the categories above. Note that this work focuses on the clip-on type extensometers (CoEs) under the indirect and non-contact category.

Direct type extensometers measure the unknown displacement by comparing the displacement directly with a primary standard. An example is the conventional dial-gauge extensometer, which measures the length directly using a mechanical arrangement. The displacement is measured from the rotational movement of the dial gauge needle while the device is ‘in contact’ with the test specimen. In contrast, an indirect type extensometer measurement is compared with a secondary standard and correlated to the actual displacement. Typical displacement transducers work based on this principle of translating the physical input quantities into electrical output signal. These output signals are used to back-calculate the actual displacement (primary standard) based on a calibration chart.

Table 2-4: General classification of extensometers

Extensometer	Classification 1		Classification 2	
	Direct	Indirect	Contact	Non-contact
Dial gauge	✓		✓	
LVDT type		✓	✓	
Sensor arm		✓	✓	
Clip-on	✓	✓	✓	
Chain	✓	✓	✓	
Video		✓		✓
Laser		✓		✓

2.11.2 Transducers

Transducers convert the physical quantity to be measured into electrical signals. Transducers are classified based on the physical property employed, physical quantity converted, and the source of energy of their output (active or passive) (Renganathan 2003). The physical property employed includes the electrical resistance, inductance or capacitance to convert physical quantities like displacement, temperature, humidity, or pressure. An active transducer converts the input energy directly into an output signal. However, a passive transducer uses the input energy as a control signal to convert energy from a power supply into a proportional output. A displacement transducer is a subset of indirect extensometers and can be classified into electrical and optical types. The electrical type uses resistive, capacitive or inductive methods. Scientists have developed several displacement transducers based on different principles in the history of extensometry.

2.11.3 History on extensometry

Table 2-5 gives a non-exhaustive list of different types of extensometers developed. These devices are cited irrespective of the type of material tested and the technical specifications/limitations. As noticed in the literature, scientists had started around the mid-1950s developing extensometers for general-purpose and specific in-situ applications. These devices are used mainly to acquire a continuous correlation of load and displacements (or strains). The initial designs were predominantly based on direct visual measurements. Soon, the indirect extensometers working under the principles mentioned in Section 2.11.2 were invented. The mechanical/non-mechanical designs have improved over decades and the developing technology has led to advanced non-contact extensometers (visual viz. image or video) in the late 2000s. Also, there were extensometers which employed resistive circuits involving resistive bridge configurations to measure displacement. These studies are relevant in the current scope and are marked with superscripts (FB, MB, and HB) in the last column of Table 2-5.

Table 2-5: Review on various types of developed-extensometers

Reference	**Extensometer type**	**Principle**
Brace (1919)	Wire testing extensometer	Indirect visual
Samoilenko (1960)	Portable Extensometer at high Temp.	Direct visual
Sjostrom (1961)	An equiangular rosette type extensometer	**Resistance^{HB}** Inductance
Collins (1965)	RF cavity extensometer	Capacitance
Holister et al. (1966)	Moire extensometer	Indirect Visual
Zheingsheim & Pab (1969)	Inductive extensometer	Inductance
Chenchanna et al. (1970)	Resonance extensometer	Natural frequency
Johnstone & Elms (1972)	10" extensometer (low frequency strain)	**Resistance^{MB}**
Vekey (1974)	LVDT extensometer	LVDT/inductive
Smart et al. (1978)	Magnetic cantilever extensometer	Magnetism
Bennett (1980)	No-contact extensometer	Photodiode (Optical)
Lazarus (1980)	Torsional extensometer	Resistance
Seilig & Reinig (1983)	Vertical soil extensometer	Inductance
Alfimov et al. (1983)	Half-bridge electromechanical extensometer	**Resistance^{HB}**
Motoie et al. (1983)	LVDT extensometer (for high temperature)	LVDT/inductive
Bergqvist & Scherling (1987)	Resistive extensometer prototype	**Resistance^{FB}**
Bartlette & Saxena (1988)	Telemetric laser extensometer	Laser (Optical)
Barbieri & Corvi (1988)	An extensometer for fracture mechanics testing of thin composite laminates	**Resistance^{FB}**
Grediac et al. (1991)	Quadriaxial setup	**Resistance^{FB}**
Kenner et al. (1992)	Diametral extensometer	**Resistance^{FB}**
Blair et al. (1997)	A new reflective optical extensometer	Laser (Optical)
Tourlonias et al. (2005)	Contactless extensometer for textile surfaces	Photodiode (Optical)
Kobayashi and Yamaguchi (2008)	Non-contacting extensometer using digital speckle correlation	Laser speckle/digital image correlation
Note: Bridge configurations – HB: Half Bridge, FB: Full Bridge, MB: Modified Bridge		

In addition, there had been suggestions on the modification of designs and troubleshooting of design limitations by several authors for prevailing extensometers. These would help to make the devices compatible with the limited resources available (instrumentation) and improve the existing systems; For example, an attachment for measuring long distances (say 180 mm) in extensometers (Belyakov 1962), and epoxy points on specimens for the knife-edges to rest in contact type extensometers (Holm 1984). Also, it is stated that high strains result in non-linearity and the structural parameters need to be optimized for optimal linearity conditions (Zenxiang et al. 1997).

In summary, the existing literature help in assessing the pitfalls or drawbacks, and design user-friendly extensometers to meet the required specifications of the parameters that govern an extensometer design.

2.11.4 Parameters that govern an extensometer design

The governing parameters of an extensometer include travel length, accuracy, resolution and the number of cycles. These are briefly defined below.

(i) Travel length: Maximum deformation or elongation that the extensometer can safely measure with a tolerable error. (eg.: −5 mm to +15 mm)

(ii) Accuracy: Maximum error in the displacement measurements. (eg.: ± 0.005 mm)

(iii) Resolution: Least count of the displacement measurement. (eg.: 0.001 mm)

(iv) Number of cycles: The limiting number of test cycles after which there is a shift in the calibration of the extensometer due to fatigue. (eg.: 10^6 or 1 million cycles)

The range of motion, accuracy, sensitivity, repeatability of readings, readability, ease of mounting, size, and frequency response are other parameters considered while selecting a displacement transducer (Renganathan 2003, Lebow 1966). A few other characteristics like over-travel, concentricity, and hysteresis determines the reliability of the device (Norton 1989). Hence, there should be a better approach in sensing and addressing the sources of measurement errors in these transducers (Boyle 1992). These potential issues should also be considered in designing a reliable extensometer within its error limits.

The parameters discussed above are applicable in the case of strain gauges also. Strain gauges are widely used by the engineering community due to their ease of procurement, reliability, and user-friendliness in tensile strain measurements. However, they are good for a single use and have a limited strain measurement range.

Hence, the repeatability and maximum allowable strain (20 % or 20000 με) are limitations for a strain gauge attached permanently to a relatively flat surface on the test specimen.

2.11.5 Extensometer vs. strain gauge

Extensometers available in the market have gauge lengths (gauge lengths) ranging between 0.3 and 60 cm. The maximum strain measured is usually between 15 to 50 % of gauge length. Strain gauges are useful for relatively smaller gauge lengths (say less than 10 mm) which are difficult to measure by a general-purpose extensometer. Despite its one-time usability, strain gauges are relatively cheaper and take lesser space than the extensometers. However, an extensometer is advantageous over a strain gauge in the following cases:

1. It is reusable and could be employed in a large number of tests
2. It could be calibrated before each test (if needed)
3. It needs minimal specimen surface preparation for each test specimen
4. Complete stress-strain graph can be obtained (large deformation)

The calibration of an extensometer is usually done using the table-top calibrator shown in Figure 2.10.

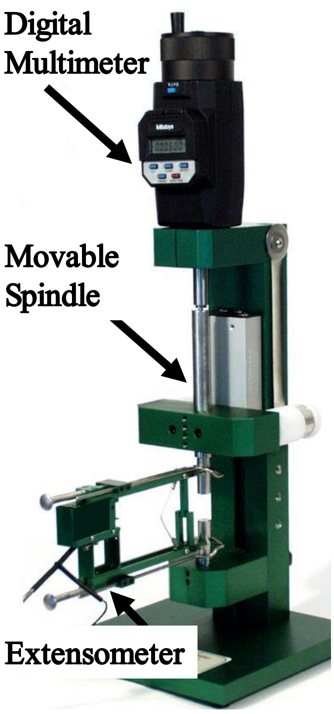

Figure 2.10: A commercially available calibrator for extensometer calibration

In the current scope, strain gauges are employed in a circuitry integrated with the mechanical body of the extensometer. This gives the advantage of reusing a strain gauge within its strain limits. Bannister and Whitehead (1991), and Sinclair (2000) briefs about mechanical sensors (specifically strain gauges) and the theory behind its use in displacement transducers.

2.12 SUMMARY AND RESEARCH NEEDS

2.12.1 Need for the development of a test method

TM-ring with uniform thickness and FP-core are necessary to ensure uniform mechanical properties and good corrosion resistance of QST steel rebars. Annex A of IS 1786:2008 briefly discusses a method to assess this, using etching techniques. Table 2-6 provides a summary of general guidelines available on specimen preparation and testing procedures (say, cutting, mounting, polishing, and etching) for metallographic studies. However, they do not provide specific protocols, which are required to properly execute the test in a manufacturing plant or construction site and obtain reproducible images/results. In particular, various steps in the cutting, polishing, and etching processes are intricate and need to be done with care to give reliable and reproducible results. Therefore, a standardized test method to assess the quality of CSPD is necessary.

Table 2-6: Summary of general guidelines available on specimen preparation and testing procedures for metallographic studies

Reference	Cutting	Mounting	Polishing	Etching
IS 7739 (Part I): 2003	✓	✓	✓	×
IS 7739 (Part V): 2003	×	×	×	✓
ASTM E3 (2011)	✓	✓	✓	×
ASTM E340 (2015)	×	×	×	✓
Vander Voort (1984)	✓	✓	✓	✓
Bramfitt and Benscotter (2002)	✓	✓	✓	✓
Geels et al. (2007)	✓	✓	✓	✓

2.12.2 Differential corrosion response of FP and TM – A summary

Based on Sections 2.7.4, 2.7.5 and 2.12.2, and the weightage over the literature that reports higher susceptibility of FP to corrosion, it is hypothesized that there exists a difference between the corrosion susceptibility of TM and FP microstructures. However, the preference of one microstructure to corrode over the other in chloride induced pitting in QST steel rebars is still not determinate. Hence, there is a need to evaluate the possible difference and quantify the relative difference, which could help in better estimates of corrosion initiation time in SLP.

2.12.3 Variation of mechanical properties in poor quality QST steel rebars

The difference in mechanical properties of TM and FP will have an implication on the tensile performance of a QST rebar with non-uniform and inadequate CSPD. An understanding on the scale of variability and the significance of the same in RC applications need attention. Hence there is a research gap as well as a need to see if improper quenching and the resultant inadequate CSPD seriously affect the expected mechanical performance of QST steel rebars.

2.12.4 Need for an economically viable extensometer

The technology involved in the extensometers are easily employable by students and researchers to develop indigenous devices. A good understanding of the working principle and careful fabrication can help to meet the need for an economical option for research/educational institutions which could not afford a commercial extensometer.

CHAPTER 3

RESEARCH SIGNIFICANCE

Based on the research needs given in Section 2.12, this chapter discusses the significance of each stage in this research. This research focuses on the quality control of QST steel rebars available in the Indian market. The work is expected to help and impact the manufacturers and end-users, in producing and using good quality steel rebars in RC applications.

Literature and preliminary tests on QST steel rebars from a few foreign countries have exhibited ideal CSPD with a peripheral TM-ring with uniform thickness and FP-core. However, many rebars collected from the Indian subcontinent did not exhibit such ideal CSPDs – thereby may exhibit inadequate corrosion resistance and high variability in the mechanical properties. At present, no standardized quality control tests are available to assess the CSPD of QST steel rebars - resulting in the production of poor quality rebars by many companies. A 'TM-ring test' can provide specific protocols to obtain reliable and reproducible results – facilitating the stakeholders to perform quality checks at both the steel plant and construction site. It is anticipated that the practice of this test can eventually enhance the quality of QST steel rebars in the Indian subcontinent.

Corrosion in steel is a major concern in SLP and life cycle cost (LCC) calculations in structural design. However, the quality control of QST steel rebars in the international codes is primarily based on tensile parameters. Although the corrosion resistance is expected to be reasonable in these bars, there are chances for early initiation of localized corrosion. This is because of the composite microstructure and hypothesized based on the differential response of TM and FP phases, in a corrosive environment. Understanding the difference in Cl_{th} of TM and FP can help to anticipate early and localized corrosion in QST steel rebar applications. Suitable factors could be employed by users in LCC and SLP of RC structures, for better estimates using the Cl_{th}. The results show that better quality control of the Q&ST process is required, especially in developing countries. This would help in extending the service life for structures of national importance over low-budget infrastructure projects.

Although QST has been used extensively across the globe for more than 3 decades, the presence of inadequate CSPD has been unnoticed and implications have not been reported. The presence of inadequate CSPD could result in the variation of mechanical properties for a single rebar. This could lead to the shift in design values of steel considered, say for under-reinforced design or strong column-weak beam design, and impact the RC design calculations. The results from this study could quantify an expected variation in yield strength to be accounted and suitably adjust the factor of safety in design. Also, poor quality QST steel rebar used in stirrups under mechanical bending could form cracks and attract crevice corrosion. The discussions in this scope are expected to build awareness on the need for good quality control and enhance quality in the manufacturing of QST steel rebars.

Generally, extensometers are procured from service providers in the market with high initial investments. These service providers supply extensometers compatible only for the test machines or data acquisition systems, manufactured by the same provider. There are others who specialize in manufacturing extensometers alone, and these devices would be compatible with any available test system. However, these customized extensometers are also relatively costly. This project on the design and fabrication of an extensometer could impact the low-tier educational institutions and research labs, to make indigenous devices at low cost. The prototype developed in this work has flexibility and space for improvisation, based on the user's test requirements.

The materials and methods used in the execution of each stage of this work are discussed in the following chapter.

CHAPTER 4

MATERIALS AND METHODS

4.1 Introduction

The study is broadly divided broadly into three stages as mentioned in Research methodology. Stage 1 constitutes the identification of the problem and, Stage 2 and 3 studies its potential effects at the application level. Stage 1 includes the microstructure study to check the cross-sectional phase distribution in a QST steel rebar. Stage 2 and 3 studies the effect of the observations on the corrosion and mechanical characteristics of the QST steel rebars. The overall flow of work is given in Figure 4.1.

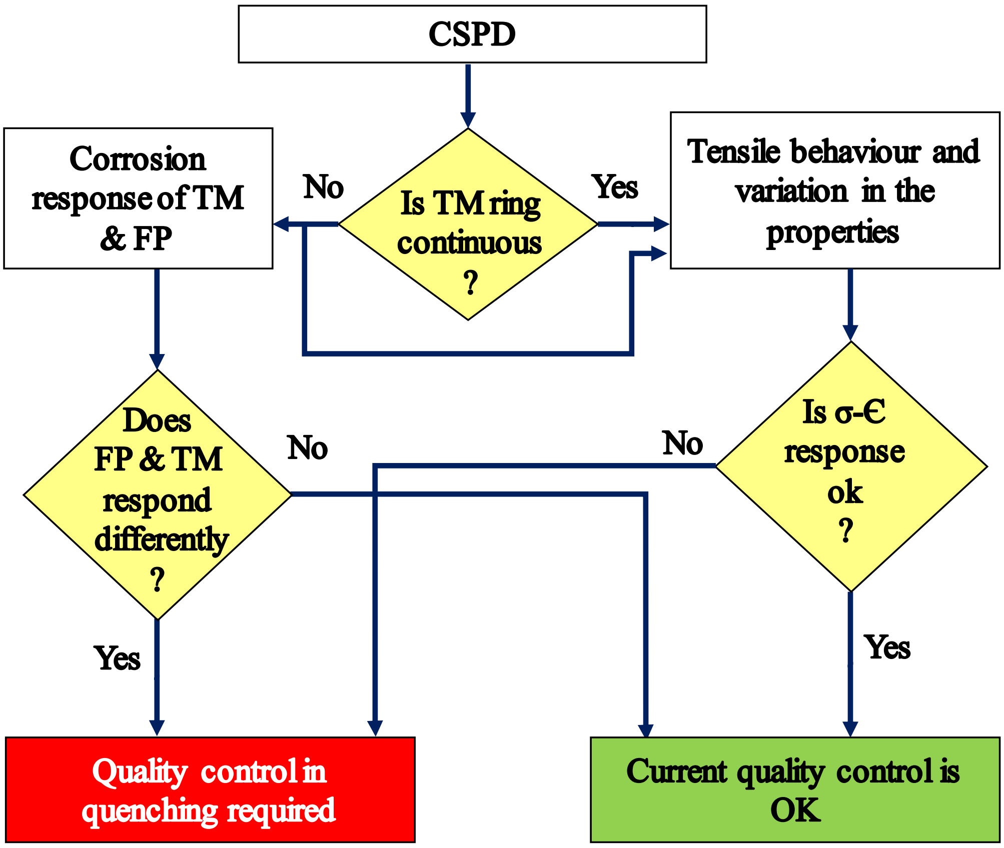

Figure 4.1: Overall workflow

As shown in Figure 4.1, problem identification stage is where the cross section is checked to confirm the quality of QST steel rebar in terms of the expected microstructural phase distribution. i.e. concentric and uniform TM ring over the FP core in a typical QST steel rebar as discussed earlier. This was followed by 2 paths based on the TM-ring continuity. The study revolves around the fact that defective TM rings exist. In that case, the corrosion resistance and tensile parameters of QST steel rebars are checked. If the TM-phase is continuous, it is assumed that corrosion resistance is not compromised, since the expected CSPD is obtained. However, the effect of thickness/area of TM ring on the variation in mechanical properties is assessed.

4.2 MATERIALS USED

The notable materials and specimen types used in the different stages are given below:

4.2.1 Steel bars

The steel material used throughout the study were QST rebars collected from various sites and retail outlets across India and other countries. The steel rebars tested was broadly categorized into 2 viz. Indian and Foreign.

The diameter is limited to 8, 12 and 16 mm of grade 500D as per IS 1786: 2008 specifications for Indian steel rebars. The expected chemical and physical properties as per IS 1786 (2008) are given in Table 4-1. The foreign rebar samples were of equivalent grades given in IS 1786: 2008 and not limited to 500D grade or diameter. The bars follow the national codal provisions of the region where it is manufactured and marketed.

Table 4-1: Properties of Grade 500D steel rebar as per IS 1786: 2008

<table>
<tr><th colspan="5">Chemical Composition (% maximum)</th></tr>
<tr><th>Carbon (C)</th><th>Sulphur (S)</th><th>Phosphorus (P)</th><th>S+P</th><th>Carbon Equivalent</th></tr>
<tr><td>0.25</td><td>0.040</td><td>0.040</td><td>0.075</td><td>0.53</td></tr>
<tr><th colspan="5">Allowed variations above the specified maximum</th></tr>
<tr><td>0.02</td><td>0.005</td><td>0.005</td><td>0.010</td><td>-</td></tr>
<tr><th colspan="5">Mechanical Properties (Minimum values)</th></tr>
<tr><th>Yield Strength YS</th><th colspan="2">Ultimate Strength TS</th><th>TS/YS</th><th>Elongation</th></tr>
<tr><td>500 MPa</td><td colspan="2">565 MPa</td><td>1.10</td><td>16%</td></tr>
</table>

A total of 14 Indian sources and 10 foreign sources were collected and tested in Stage 1. Typical QST steel specimens of 8, 12, and 16 mm diameter manufactured in Germany, Hungary, Italy and Russia (and collected from Germany), Australia, Bahrain, Singapore, Sri Lanka and Switzerland were included in the scope. The details on the sources and the designation of rebars from Indian and Foreign samples are given in Table

4-2. The diameter of rebars involved and the no. of specimens in the individual stages in the research methodology are given in Table 4-3.

Table 4-2: Sources, designations, and diameters of steel rebars tested

Indian

Source		1	2	3	4	5	6	7	8	9	10	11	12	13	14
Designation		T	J	K	S	I	SL	V	SD	TS	A	AG	GB	PC	SH
Main Scope	8	✓	✓	✓	✓	✓	✓	✓	✓	✓	✓	✓			
	12	✓	✓	✓	✓	✓	✓	✓					✓		
	16	✓	✓	✓	✓	✓	✓	✓		✓			✓	✓	✓
Addnl.		10													

Foreign

Source		Germany	Italy	Russia	Hungary	Switzer-land	Bahrain	Singapore	Sri Lanka	Australia
Designation		G	I	R	H	S	B	SG	SL	AS
Dia.	D1	8					8, 10		10	
	D2	12	12	12	14		12	12	12	
	D3	16	16		16	16	16, 18			16
	D4	18					22			

Table 4-3: Diameter and number of sources of rebars used in each stage

Stage	Test Procedure	Steel diameter (mm)	No. of sources: Indian	No. of sources: Foreign
1	Macroetching – various sources	8, 12, 16	14	11
	Macroetching – Single rebar length	12	2	-
	Macroetching - Longitudinal	8, 12	2	-
2	Linear Polarization resistance	36 (machined)	1	-
	Cyclic Potentiodynamic Polarization	36 (machined)	1	-
	Immersion test	12	2	-
3	Tension test – TM & FP isolation	40 (machined)	1	-
	Tension test – Single rebar length	12	2	-
	Bend test	8	10	2

The chemical composition of selected steels rebars was tested as mentioned in Section 4.7.2. The results are tabulated and given in Table 4-4.

4.2.2 Moulding epoxy

Several mounting resins were sampled/ used in the course of this work. There were 5 types of resins used in different stages. Brief details of these resin compounds are discussed in Table 4-5.

The Sikadur, CS1 and HS2 resins were majorly used for the primary specimens. A preliminary test showed unsuitability of other resins for the particular test type or test environment used. For more details on epoxies and selection criteria, see ASM Handbook 9 (2004) on metallurgy and microstructures.

Table 4-4: Chemical composition of steel rebars used in this study

Elemental Composition		Specimen Designation			
		German 12 mm	J 36 mm	K 8 mm	T 8 mm
Carbon	C	0.160	0.250	0.210	0.240
Silicon	Si	0.200	0.050	0.210	0.250
Manganese	Mn	0.885	1.232	0.735	0.826
Phosphorus	P	0.009	0.018	0.012	0.023
Sulphur	S	0.021	0.027	0.019	0.042
Chromium	Cr	< 0.001	< 0.001	0.305	0.224
Molybdenum	Mo	0.109	0.028	0.097	0.091
Nickel	Ni	0.126	0.015	0.398	0.359
Aluminium	Al	0.005	0.006	0.126	0.123
Cobalt	Co	< 0.010	< 0.010	< 0.010	< 0.010
Copper	Cu	0.165	< 0.010	0.208	0.145
Niobium	Nb	< 0.001	0.015	0.006	0.006
Titanium	T	0.001	0.002	0.004	0.005
Vanadium	V	< 0.001	0.056	0.020	0.023
Tungsten	W	< 0.010	< 0.010	0.054	0.035
Lead	Pb	< 0.002	< 0.002	< 0.002	< 0.002
Tin	Sn	0.008	< 0.010	0.048	0.027
Boron	B	0.000	0.000	0.001	0.002

Table 4-5: Epoxy specifications

Name	Resin Type	Colour	Components	Mix ratio or Specifications	Setting time	Edge retention	Alkaline reactivity
Sikadur	Epoxy	Straw Yellow	1 Resin 1 Hardener	2:1	24 hrs	Good	Nil
Cold Set 1 (CS1)	Acrylic	Pink	1 Powder 1 Liquid	2:1	15 min	Poor	Nil
Cold Set 2 (CS2)	Resin	Transparent	1 Resin 1 Hardener	2:1	24 hrs	Good	Nil
Hot Set 1 (HS1)	Phenolic	Black	1 Powder	180 ºC and 200 bar	30 min	Poor	Dissolves
Hot Set 2 (HS2)	Epoxy	Transparent	1 Powder	180 ºC and 200 bar	30 min	Good	Nil

The test methods/experiments done on specimens at various stages involves macroetching of steel rebars, general/pitting corrosion tests and mechanical tests (including tensile and bend tests). There are standard as well as modified testing methods used which are explained in the following sections.

4.3 STAGE 1 - MACROETCHING AND QUANTIFICATION OF CSPD

Stage 1 of this research is to check the cross-sectional phase distribution of QST steel rebars. The research begins with the observation of discontinuous rings of TM in QST steel rebars collected from the market in India. The study was then extended to identification of cross-sectional rings across several more rebars collected from various sources. The scope mainly includes 8, 12 and 16 mm diameter rebars. This section is executed in 2 stages:

1. Macroetching of steel rebars
2. Quantification of CSPD

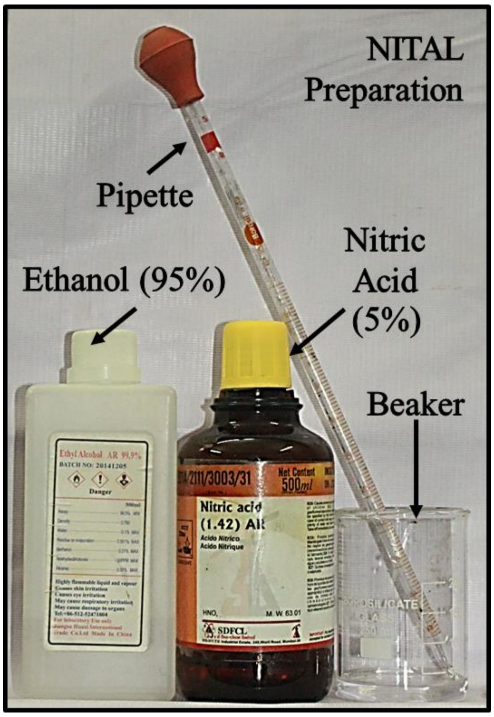

Figure 4.2: Nital preparation set

The CSPD cannot be seen by cutting the steel bar. The cross-section needs to be prepared and subjected to etching using standard etchants. The details of the solutions and procedure of etching is given in ASM Handbook 9 and IS 1786: 2008. Standard procedures suggest using a solution of 5% nitric acid in ethyl alcohol (ethanol by volume) for etching steel materials. This solution is also known by the name 'nital' and the components are shown in Figure 4.2 for making the solution. The detailed procedure for specimen preparation and etching is given as follows.

4.3.1 Specimen preparation

Any steel rebar specimen could be checked for the cross-sectional phase distribution by etching. The features could be analysed under a microscope or on a macroscopic scale. In this scope, we could identify and analyse the steel rebar cross sections on a macroscopic level (macroetching). This is proposed as a quality check test (non-mandatory) in IS 1786: 2008. The specimen should be prepared with care. The specimen should not be cut in a high-speed cutter/abrasive cutter which produce too much heat (temperature > 200 °C). Sufficient coolant should be provided while cutting to limit the temperature rise. If cut with a chop saw/high-speed cutter, sufficient length shall be cut off from the cut surface to remove the heat affected zone (HAZ). The length of HAZ could be taken as 3 times the diameter of the cut surface (Sommer 2005). Figure 4.3 gives the type of cutting facility preferred, and otherwise.

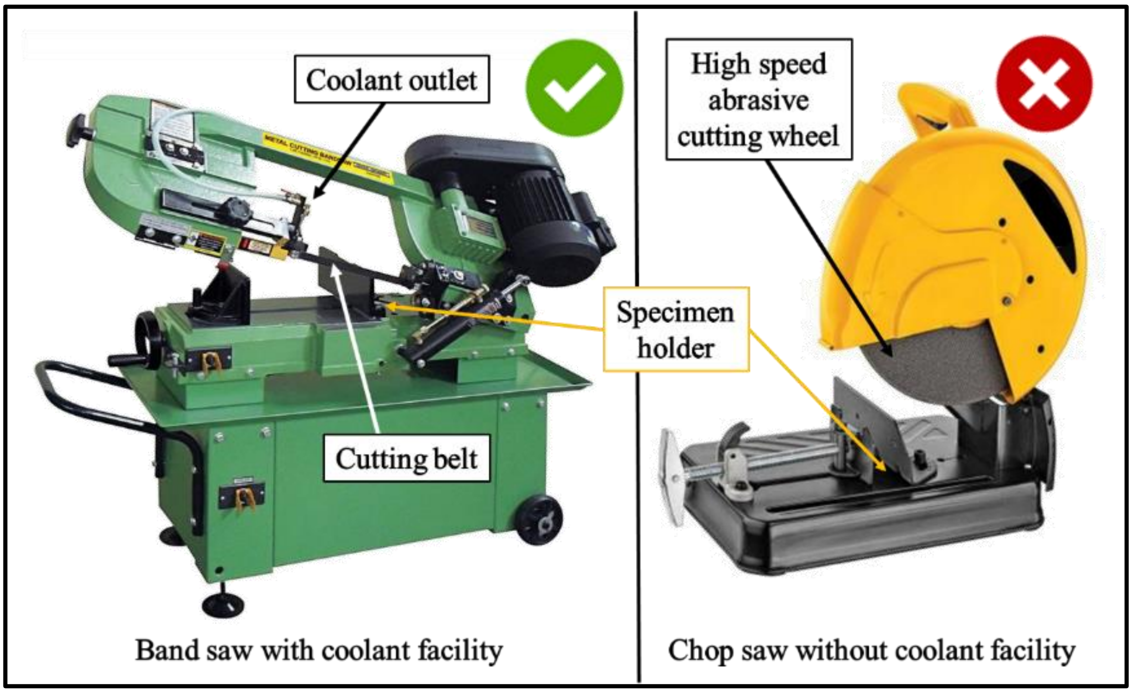

Figure 4.3: Steel specimen cutting machine with and without coolant

In the microstructure study, the HAZ is cut off under a band saw with coolant facility. The temperature is measured using an infrared thermostat and ensured to be within the tolerable limits. The heat signatures recorded or various processes with the study samples are shown in Figure 4.4. Figure 4.4 (1) shows the chop saw cut temperature which lies around 150 ^oC while cutting. However, band saw with oil as coolant shows a maximum temperature rise around 50 ^oC [shown in Figure 4.4 (2). Figure 4.4 (3) and Figure 4.4 (4)] are cases of epoxy embedment and milling (in lathe) processes, which will be discussed later. The temperatures are within the tolerable limits from the records.

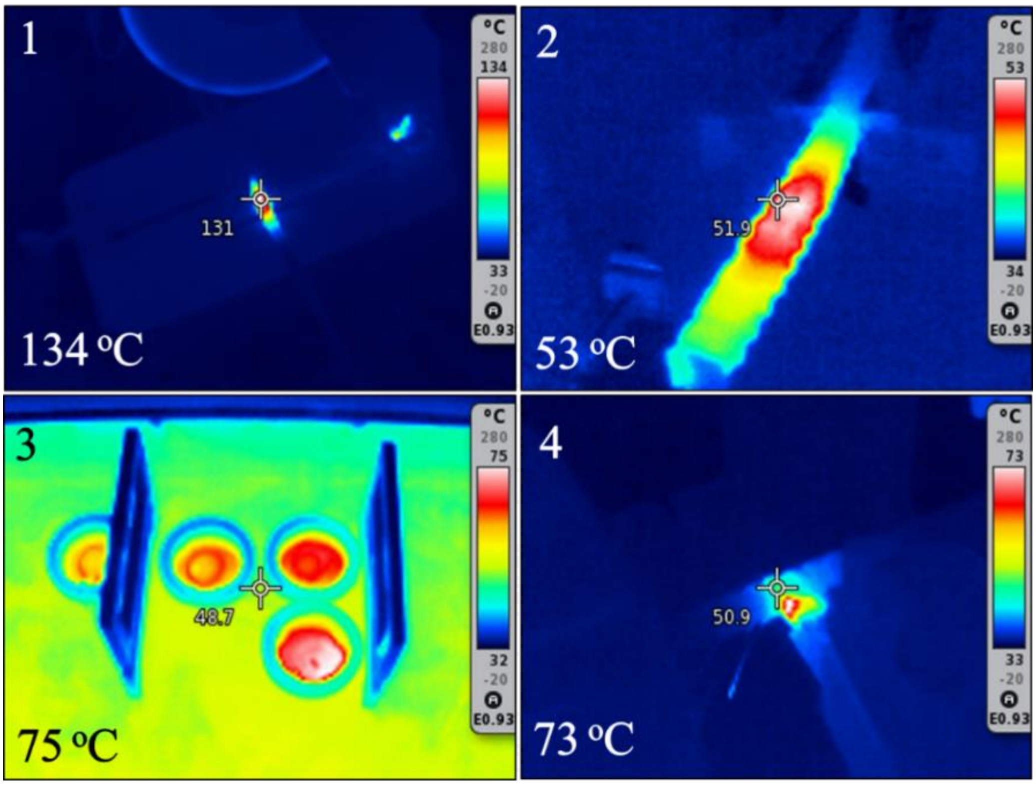

Figure 4.4: Heat signatures from different stages of specimen extraction

The step by step process of specimen preparation is given below:

1. Cut a steel rebar specimen of 1 to 2 cm length (Figure 4.5-1). The cutting shall be appropriately done under a coolant facility, or the HAZ should be removed as discussed earlier.
2. Mount the specimen (cold mount preferably) in an epoxy to isolate a single plain surface to etch and photograph.
3. The cold set compound used in this study is an epoxy based two-component compound (solid powder and liquid). The solid part to liquid part is taken in the ratio of 2:1 by weight The overall mixture is light pink in colour and the mixing reaction is exothermic.

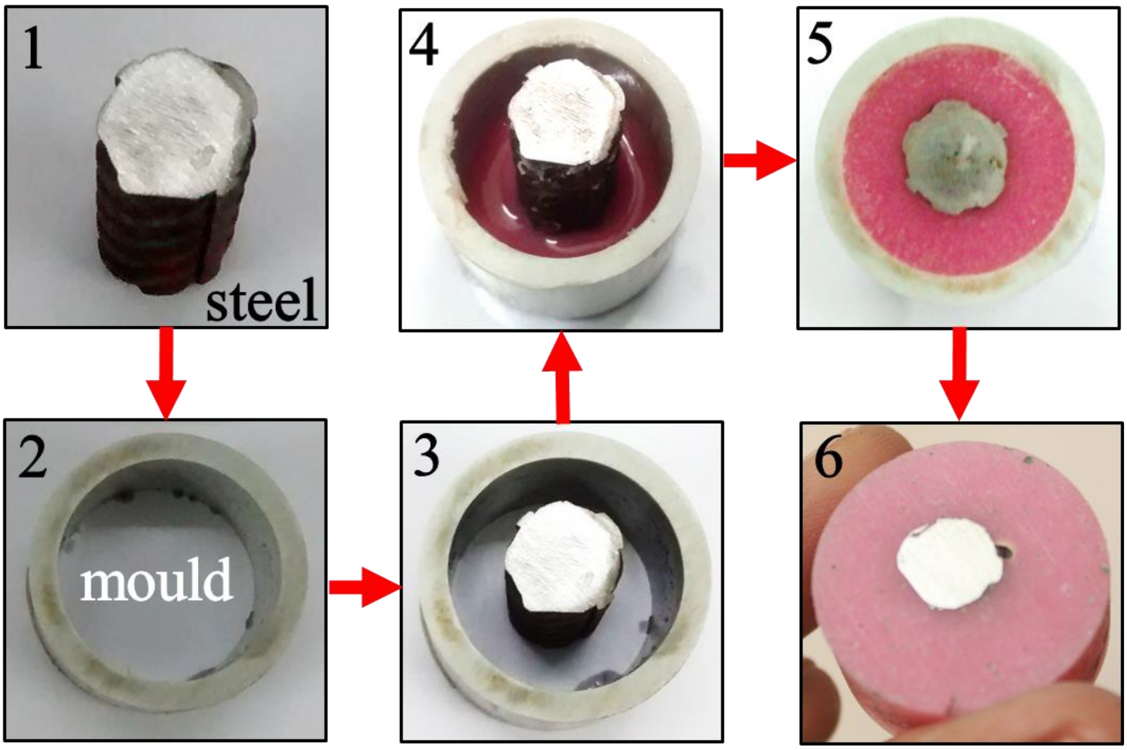

Figure 4.5: Specimen preparation stages in cold mounting

4. Plastic/rubber moulds (Figure 4.5-2) of 20 mm diameter were used. The sides of the mould should be lubricated by using oil/silica gel or easy demoulding of the specimen.
5. The specimen is placed inside the mould with the cross section under study at the base (Figure 4.5-3).
6. The mixing time is kept low (approximately 10-20 seconds) before pouring into the mould.
7. The setting time was around 15 minutes after the mould is filled (Figure 4.5-4) with the mixed epoxy. Figure 4.5-5 shows the set specimen before released from the mould.

The epoxy embedment is done for the following reasons:

1. While viewing the plan, transverse ribs in different planes disturb your 2D-image of the plane under study. Epoxy embedment helps to isolate and view only one plane at a time. Focusing on one plane is important if the image is taken for analysis.

2. While polishing the surface, the presence of mould is advantageous in getting a uniform polish. Higher the area to length o the specimen ratio, better the polish. In the case of small diameters, it helps to hold the specimen properly also.

   Note that hot mount shall be done, provided the temperature rise in the process does not distort the microstructure (temperatures less than 200 ^oC) under prolonged time intervals.
3. The specimen is polished in a belt grinder or a rotary polishing machine to smoothen the exposed surface under study by grinding or coarse polishing (Figure 4.5-6).

   Grinding is done with coarse emery sheets (grit size between 60 and 1200). This study had used coarse emery sheets of sizes 80, 120, 220, 320, 400, 600, 1000 and 1200 for grinding. Sufficient water as coolant should be provided to avoid temperature effects.
4. The specimen is finely polished (also called cloth polishing) in a rotary polishing machine with polishing cloths of different grades.

   The fine polishing is done using billiards cloth with 6μ diamond paste. This is followed by velvet cloth polishing using 1.5μ diamond paste. The fine polishing shall be done until a mirror finish is obtained. Fine polishing shall be done if the specimens are subjected to an optical microscope (OM) or scanning electron microscope (SEM) observations.
5. The polished specimens shall now ready to be subject to macroetching or microscopical studies.

4.3.2 Imaging setup

The prepared specimen for macroetching is placed under the imaging setup as given in Figure 4.6. A stereo microscope has been used in this setup with a limited 0.6X to 6X zoom. The details of the setup are given below:

1. An adjustable vertical head is used to contain and focus the etched surface for imaging.
2. A good resolution camera is mounted on the vertical head for imaging.
3. A light intensity of 350 - 450 lux is used to light the etched surface.
4. A connected data acquisition (DAQ) system (VMS^{TM} Image viewer or Tincam^{TM}) is used to record the images taken instantly.

5. Once the image is taken, threshold it at particular grey-scale so as to analyze the phase area distribution.

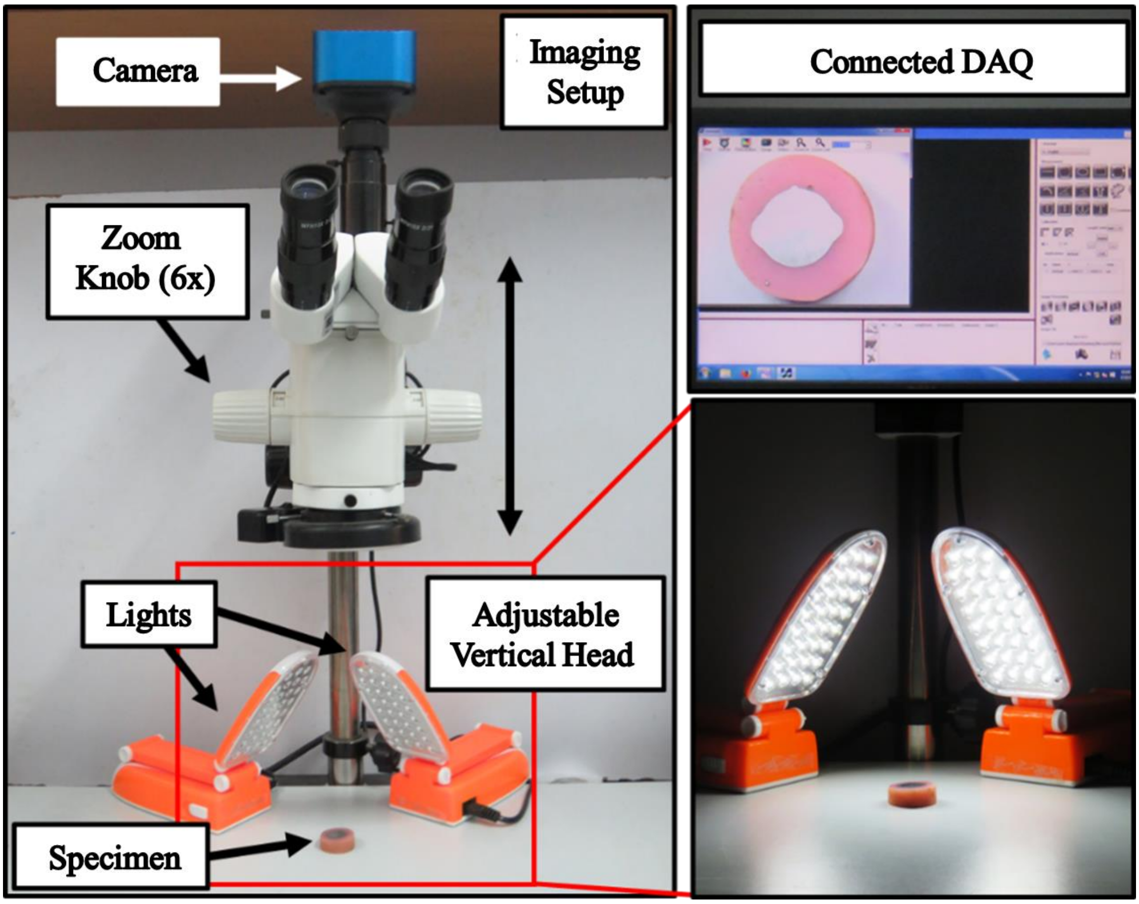

Figure 4.6: Imaging setup for nital test

4.3.3 Nital test

The prepared specimen from Section 4.1.1 is placed under the imaging setup. Etching (also called nital test in this context) is done using a standard etchant called nital as specified by IS 1786 (2008)/ASM Handbook 9. The steps given below shall be followed for the nital test:

1. The polished specimen mounted in epoxy is placed under the imaging setup.
2. The specimen is exposed to 2-3 mL of standard nital solution. Wait for 3-5 minutes.
3. The cross section will get etched and the TM and FP phases could be distinctly seen as shown in Figure 4.7.
4. The excess solution over the etched surface is absorbed using a tissue paper/cloth
5. The etched surface is photographed and subjected to further analysis

If used as a qualitative field test, visual analysis is enough and the user could skip the part of epoxy embedment in the specimen preparation as well as the imaging setup. All the cutting, polishing and testing requirements are still applicable. If the results need to be recorded for quantitative analysis, the moulding and imaging setups should also be included.

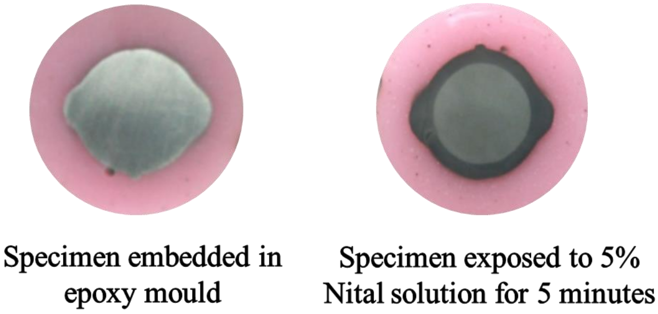

Figure 4.7: Polished specimen before and after nital test

4.3.4 Procedure for image analysis

The image taken after etching is analysed using a free software available called Image J® (Image Processing and Analysis in Java) developed by National Institute of Health (NIH), USA. The software interface is user-friendly to meet the analysis requirements in the scope of this study. Figure 4.8 gives the initial interface window of ImageJ.

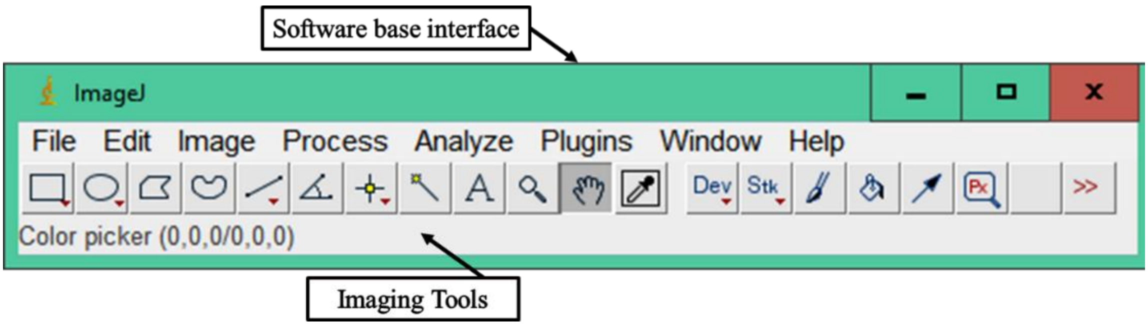

Figure 4.8: ImageJ software interface

A typical image taken after nital test (shown in Figure 4.9) is opened in Image J. The image has a scale placed on the side which is at the same level as the etched surface. This is to calibrate the scale in the image. This is an important step to be done at the beginning of analysis for all the images (the scale will be different across the images). The user marks a known distance on the scale or calibration. This distance is calibrated to the number of pixels per unit length by the software. Basic imaging operations shall now be executed to quantify the percentage area of TM and FP from the total cross-sectional area. For example, Figure 4.10 shows an image checked for the area of FP. The area of FP is marked along the boundaries using a polygon tool. The confined area is calculated using the calibration done for the image at the beginning.

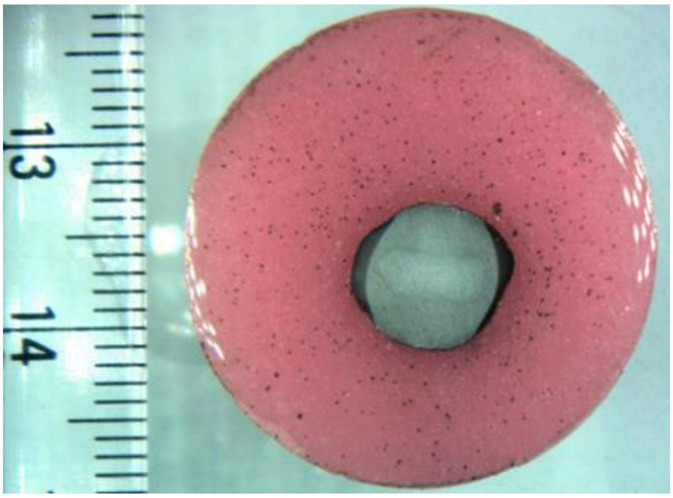

Figure 4.9: Image taken after nital test for analysis (with scale on the side)

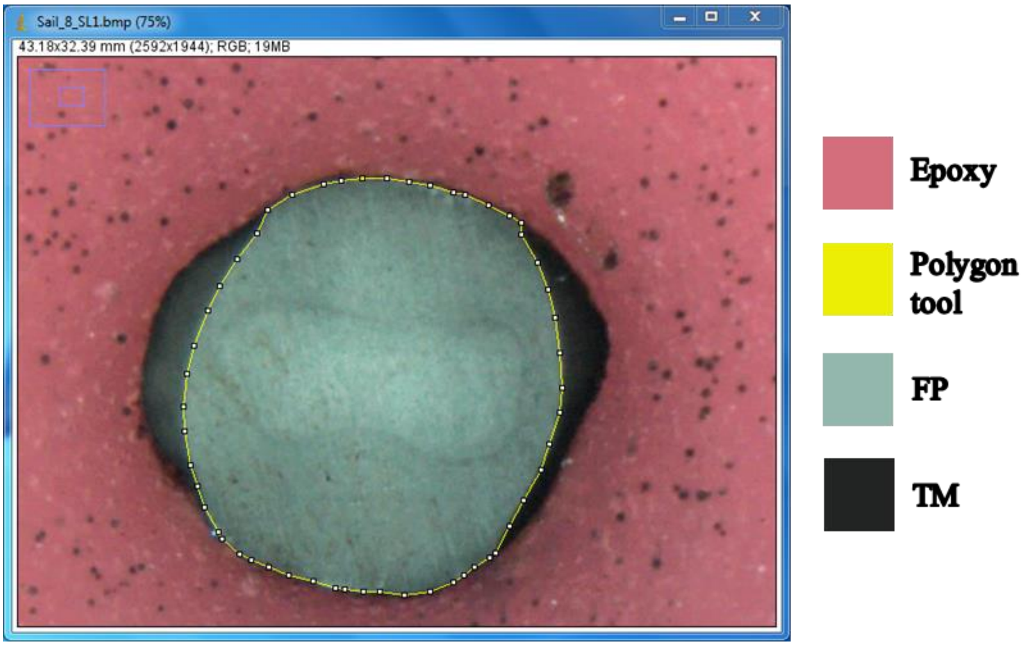

Figure 4.10: Area analysis by using polygon tool (area of FP marked in yellow border)

4.4 STAGE 2 – CORROSION TEST SPECIMENS AND PROCEDURES

This section is divided into three phases viz. LPR, CPP, and Immersion tests. Phase 1 tries to find out the Cl_{th} of TM and FP, by using LPR test method. Stage 2 with CPP tests identifies the difference between corrosion characteristics of FP and TM. Stage 3 tries to validate the result by exposure to chloride contaminated concrete pore solution (alkaline environment).

4.4.1 LPR test – Specimen preparation

TM and FP specimens were prepared by isolating the phases from a rebar of diameter 36 mm by EDW cutting machine. The chemical composition of the steel used is given in Table 4-4 under 'J 36 mm'. The cut directions and dimensions are given in Figure 4.11. The cutting was done under water at a temperature of 20 ^{o}C. This ensures that the phase is not disturbed by high temperatures. The area of each piece is approximately 225 mm^2.

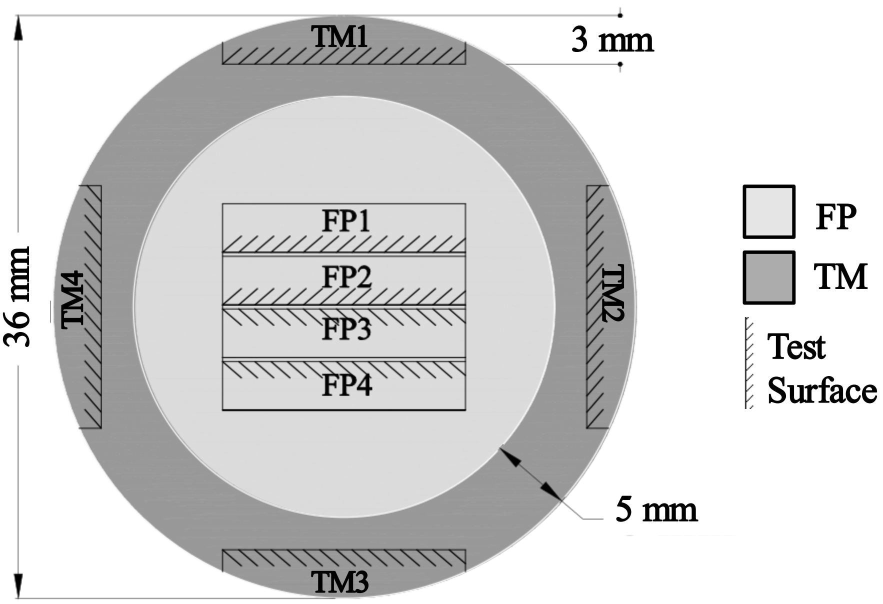

Figure 4.11: Schematic showing the locations of coupon specimens extracted

The steps of specimen preparation are shown in Figure 4.12. The specimens are polished or ground using a disc polisher shown in Figure 4.13(a). For each specimen, a wire is soldered onto one of the faces before mounting it in epoxy. These were cold mounted in moulds of 25 mm diameter, with the unsoldered side faced down. The cold mounting was done by vacuum impregnation using the setup shown in Figure 4.13(b). 30 bar pressure was maintained for 20 minutes to remove all the air bubbles near the specimen in the mould.

Grinding (coarse polishing) was done till 1000 μ grit size followed by cloth polishing (fine polishing) using 6-12 μ diamond particles. All rectangular specimens were ground at the corners to avoid preferential corrosion at the sharp edges. Three specimens each for TM and FP were prepared by this way. The typical test specimen is shown in Figure 4.14(a). The specimen placed in the test setup is shown in Figure 4.14(b).

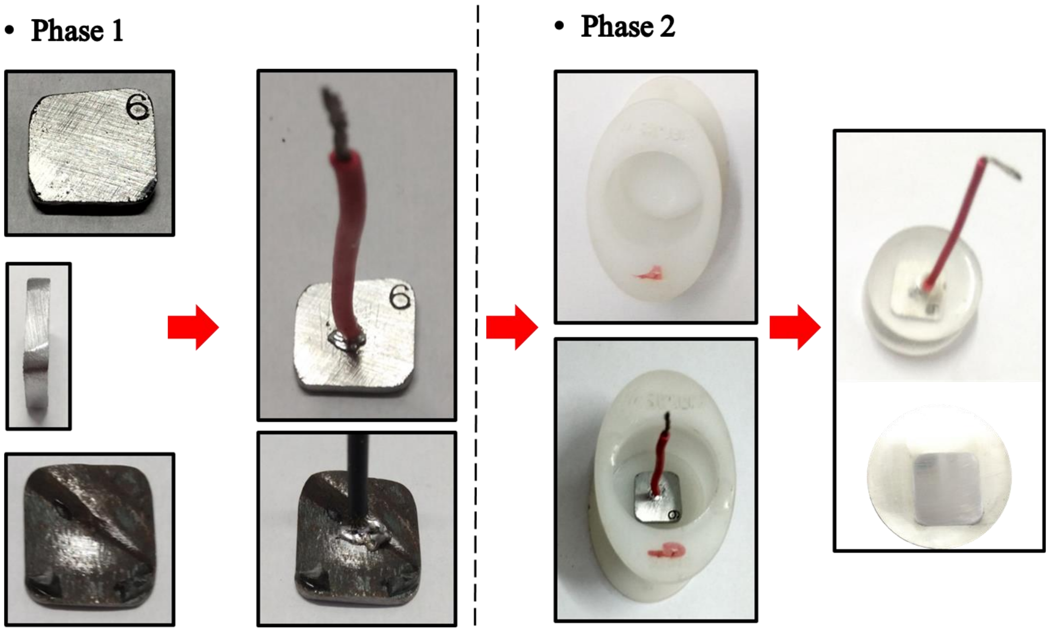

Figure 4.12: Specimen preparation of LPR test specimens

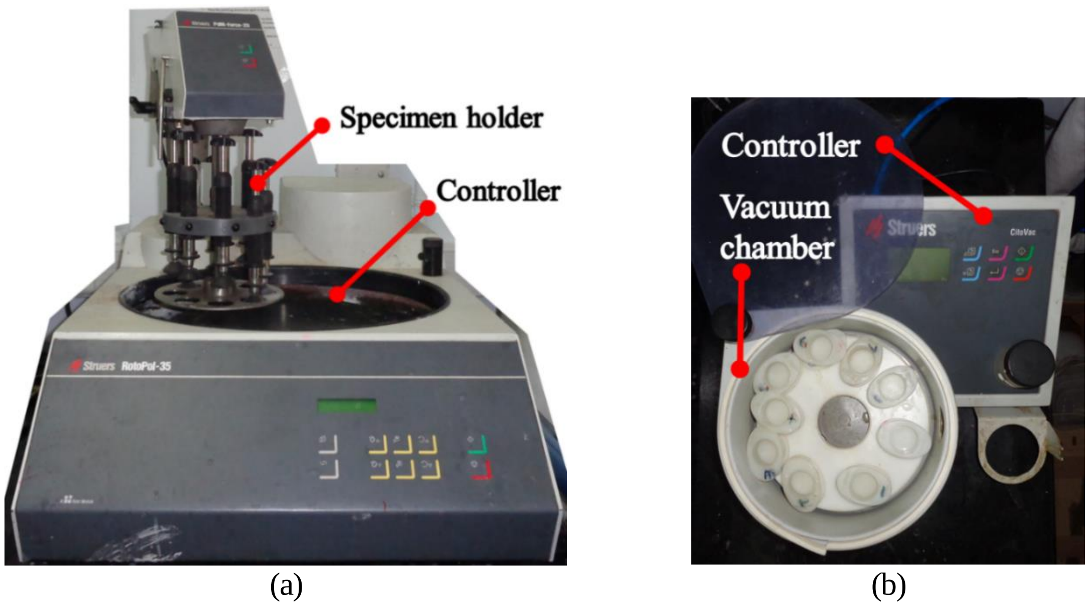

Figure 4.13: (a) Streurs Rotopol-35 disc polishing machine for specimen grinding/polishing (b) Streurs Citovac for vacuum cold setting

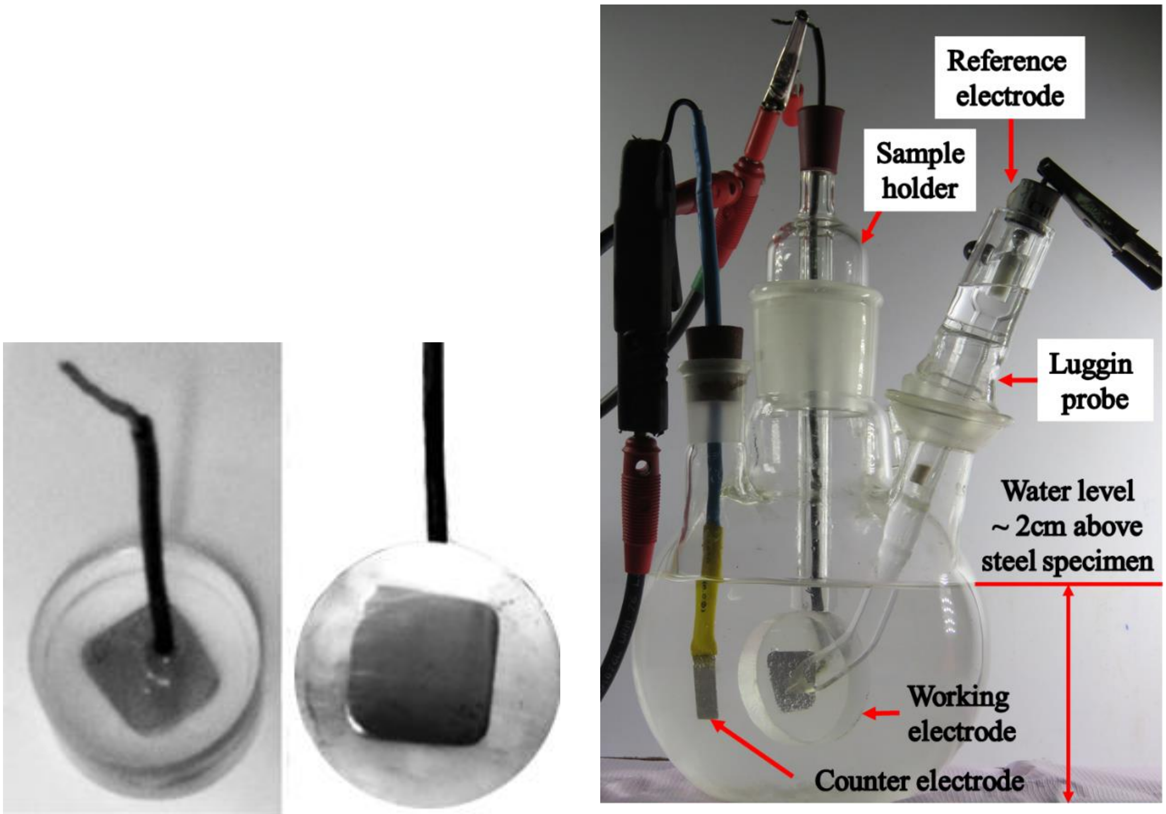

Figure 4.14: (a) Typical TM/FP specimen for LPR tests (b) Chloride induced corrosion test setup (ASTM G5)

4.4.2 LPR test – Test procedure

Figure 4.15 illustrates the LPR test procedure followed. The chloride induced corrosion test was done after immersion in SPS with the composition given in Table 4-6 for a duration of 3 days. All tests were done at a temperature range of 25-30 ^{0}C at a pH value greater than 13.5. Each specimen is immersed in a container with 20 mL SPS. The prepared specimen is placed in the standard corrosion cell with 400 mL of the same immersion solution. The corrosion cell setup ready for the test is shown in Figure 4.14(b). The cell consists of Standard Calomel Electrode (SCE) as the Reference Electrode (RE) and platinum as the Counter Electrode (CE). The immersion is continued till 3 days (Poursae 2007) for the formation of the passive film (hereafter termed initial immersion). A standard OCP and LPR test is conducted across the specimen as the Working Electrode (WE), to monitor the formation of the passive layer. At the end of 3 days, chloride ions are introduced into the containers. The concentration of solution started at 0.2% and increases at steps of 0.4 till 3% Cl- by weight of the solution (0.2, 0.6, 1.0, 1.4, 1.8, 2.2, 2.6 and 3.0%). R_P and E_{corr}

values are measured at 3 hours and 6 hours of immersion in the chloride-contaminated solution. R_P is used to calculate corrosion rate in terms of corrosion current (I_{corr}) using the Stern-Geary equation (Stern-Geary coefficient = 24).

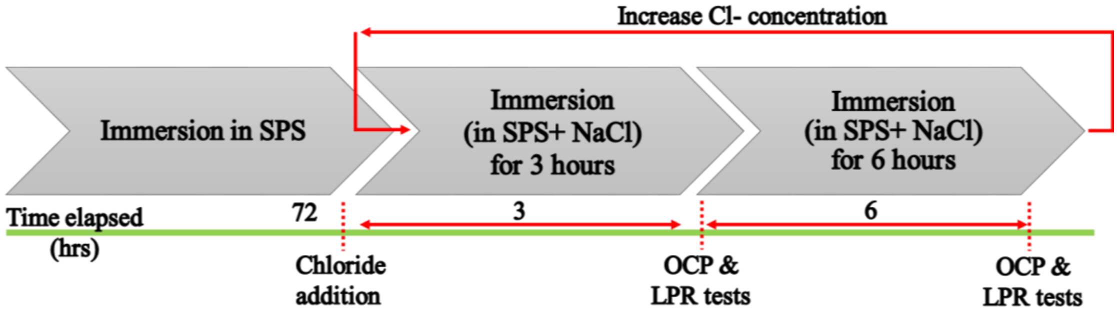

Figure 4.15: Schematic of the LPR test process

Table 4-6: Composition of Simulated Pore Solution (SPS)

Component	H_2O	$Ca(OH)_2$	NaOH	KOH
Quantity in grams (per kg of solution)	966.67	0.3	10.4	23.23

4.4.3 CPP test – Specimen preparation

Similar to the previous section, the specimens for evaluating pitting tendency were extracted from a good quality QST steel rebar (as defined in section 2.6.2) of 36 mm diameter and 15 mm length. The schematic of a ready-to-test specimen is shown in Figure 4.16, along with an isometric view of an actual specimen. EDW cutting machine was used to obtain coupon specimens of FP and TM regions. The cutting process under a water bath of 20 ^oC ensured a minimal heat affected zone (HAZ) in the specimens. The specimens were polished with coarse emery sheet to abrade approximately 0.2 mm depth, in which the HAZ was expected to fall.

The overall flow of specimen preparation is shown in Figure 4.17. The specimens were mounted on a hot mounting press using transparent epoxy (See Figure 4.18). A conducting wire spring was placed on the rear side of a specimen. A temperature and pressure of 180 ^oC and 200 bars, respectively, were applied. The spring got compressed and left an exposed point of wire at the rear side of the moulded specimen. At that point, an electrical wire (lead-wire) was soldered (See Figure 4.19) and the joint was epoxy coated to avoid current leaks. Two to three coats of a 2-component resin based epoxy were applied.

If a straight wire is soldered instead of the spring, the solder might detach or the wire might slant and fall inside the epoxy mould when the pressure is applied. This will fail to establish a proper lead wire connectivity.

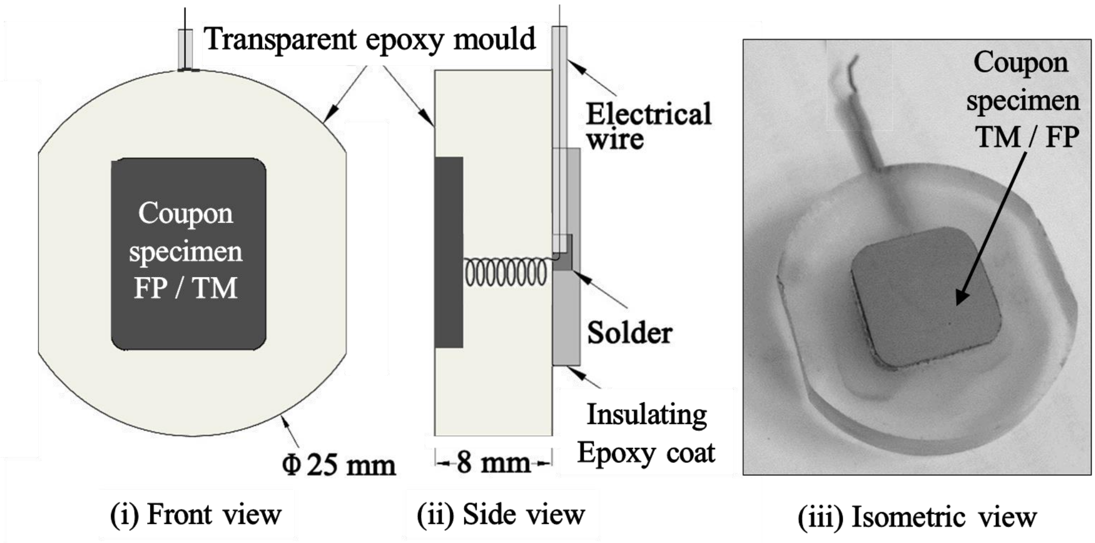

Figure 4.16: Schematic of a CPP test specimen

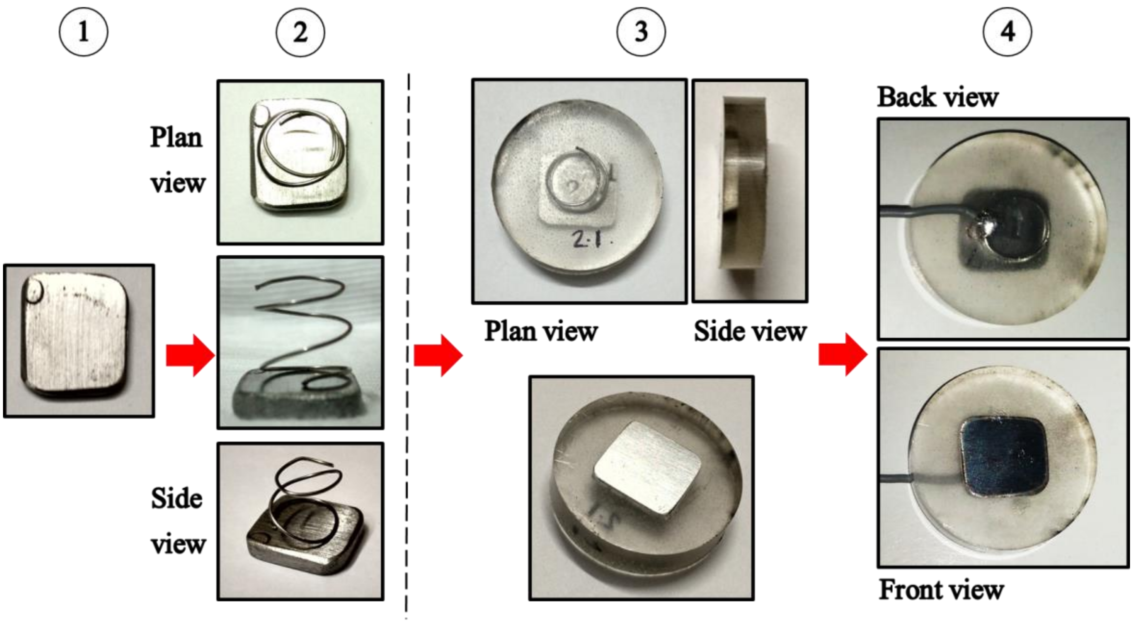

Figure 4.17: Overall Specimen preparation for CPP test

The moulded specimens were subjected to coarse polishing, (grit designations mentioned earlier) followed by fine polishing with diamond pastes of 6-12 μ (on billiards cloth) and 1-1.5 μ (on velvet cloth). A typical specimen is checked for connectivity between the test surface and the lead-wire end. The check for connectivity in the possible current leak is done between the lead-wire end and the epoxy coated surface. A set of 4 such specimens (from both TM and FP) were subjected to Cyclic Potentiodynamic Polarization (CPP) test to evaluate the pitting threshold in a chloride environment.

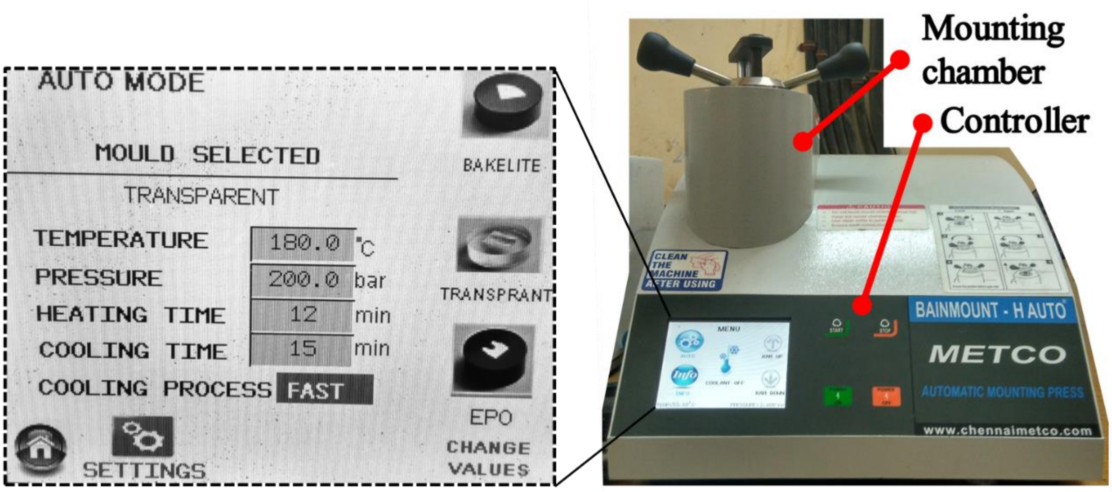

Figure 4.18: Bainmount-H hot mounting press used

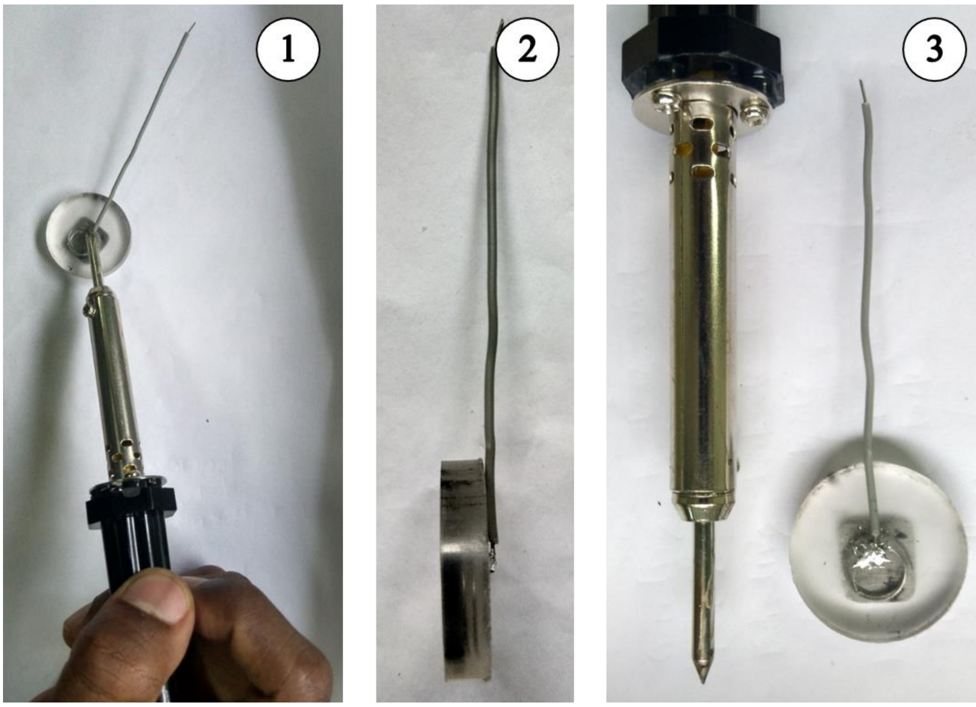

Figure 4.19: Establishing connections for the CPP test specimen after hot mounting

4.4.4 CPP test – Test procedure

The prepared test specimens in the previous section were immersed in a standard corrosion cell, filled with highly alkaline Simulated Pore Solution [SPS; 1000 g contains 966 g H_2O, 23.3 g KOH, 10.4 g NaOH, and 0.3 g $Ca(OH)_2$]. Figure 4.20(a) shows the standard corrosion cell setup used in this study. The overall CPP test setup is shown in Figure 4.20(b). The standard corrosion cell consists of the prepared specimen acting as the WE, an SCE as the RE) and nichrome as the CE. The RE is placed in a luggin probe filled with saturated potassium chloride (KCl). The luggin probe helps to position the RE between WE and CE, to measure the potential applied with respect to the RE. The chloride (Cl^-) concentration was varied between 0.2% to 2.2% by weight of the SPS and tested by CPP. 2.1% of Cl^- (by weight of solution) would simulate the seawater chloride level of 3.5% NaCl. The pH of the solution was monitored and maintained at values greater than 12.5. A 'Solartron' (model 1261) potentiostat was used for executing the corrosion tests. Data acquisition was done by using Scribner Associates' Corrware® software (Scribner Associates Inc.).

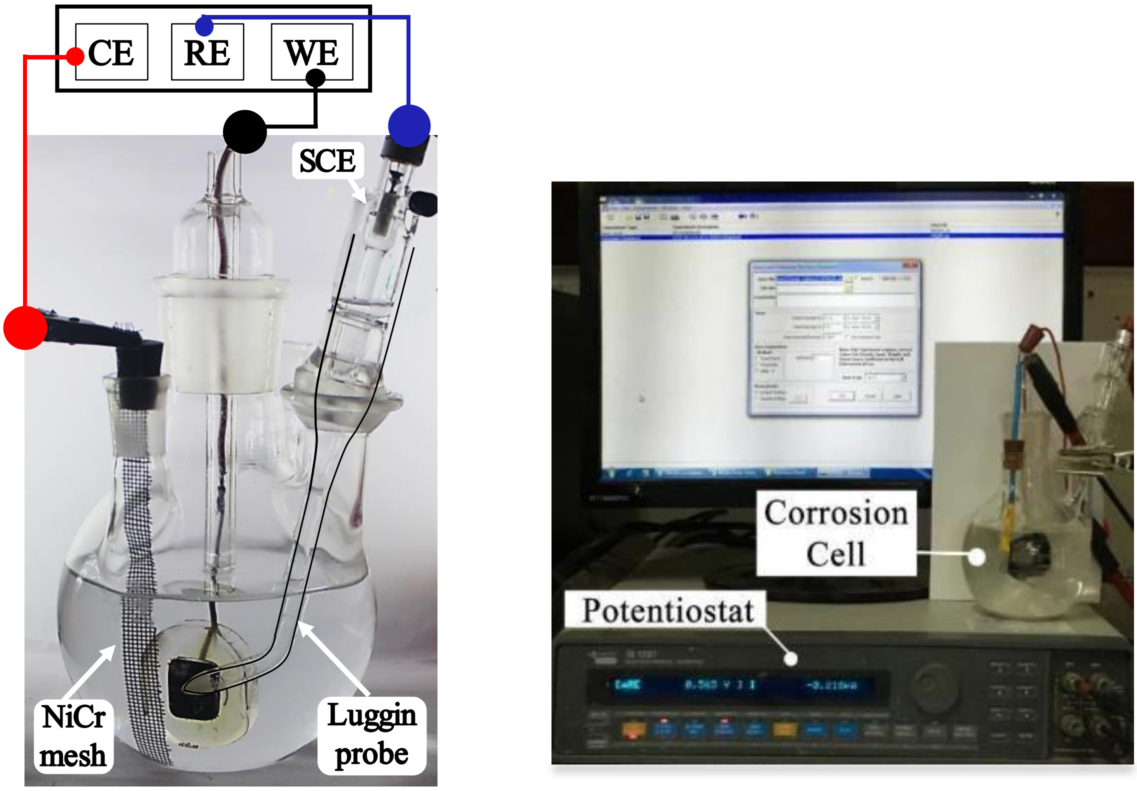

Figure 4.20: (a) Corrosion cell setup and (b) CPP test setup with Solartron-1261

CPP test was done on TM and FP specimens at an incremental concentration of Cl^- in SPS to find the chloride-induced pitting threshold. The specimen was first immersed in a known concentration of Cl^- in SPS solution. The concentration at which pitting was first observed is considered as the pitting threshold. The Open Circuit Potential (OCP) is measured first, followed by a potential sweep with respect to the measured OCP. The scan range of the test was -100 to +1500 mV with respect to OCP at a scan rate of 0.1667 mV/s. Apart from the voltage condition, a reversal condition when the current exceeds 1 mA/cm^2 (Princeton Application Note 4, Falleiros 1999) was also placed. This will avoid severe damage to the specimen under active corrosion. Each specimen was subjected to CPP test at increasing Cl^- concentration in steps of 0.1% Cl^- by weight of SPS solution.

All the specimens were used for repetitive tests at different Cl^- concentrations. The disturbed surface zone after a test completion was removed by polishing the exposed face. The measured current was calculated per unit area of the exposed face. The specimens were photographed and analysed in an image analysis software (ImageJ®) to find the area of the exposed face. The area of an exposed face lies between 1 cm^2 and 2.5 cm^2. The cathodic area was 2.5 to 6 times higher than anodic area, which is assumed to eliminate local effects.

4.4.5 Immersion test – Specimen preparation

For immersion tests, 100 mm long specimens of 12 mm diameter from good and poor quality QST steel rebars were extracted. Both the bars are turned on a lathe to remove the ribs and polished for a smooth surface finish. The schematic of test specimen preparation is given in Figure 4.21. Hence, the test specimens are divided into 2 types:

(i) Type 1: In the case of good quality rebar (Type 1), a depth of 1.5 mm is milled from the surface to expose a strip of FP as shown in Figure 4.21. Figure 4.22a shows a real-time specimen immersed in the solution. Figure 4.22b shows the milled plane with a strip of FP surrounded by TM. The CSPD is also given in the figure.

(ii) Type 2: For the poor quality bar (Type 2), there already exist an exposed FP area at the circumference at multiple points. The circumferential phase distribution (CFPD) is mapped by etching the circumferential area. Type 1 specimen is a simulated or artificially mimicked case of Type 2.

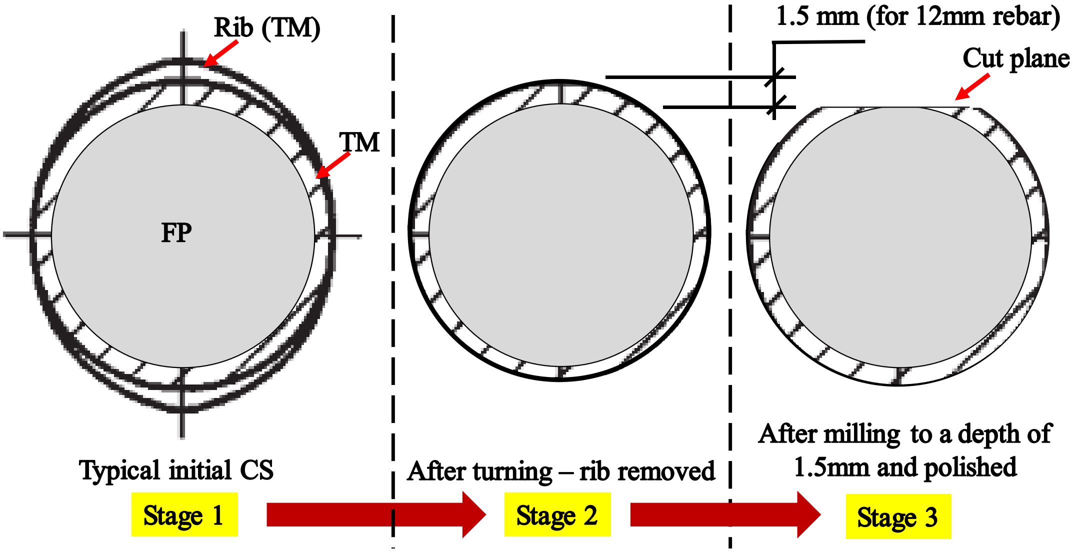

Figure 4.21: Immersion test specimen preparation

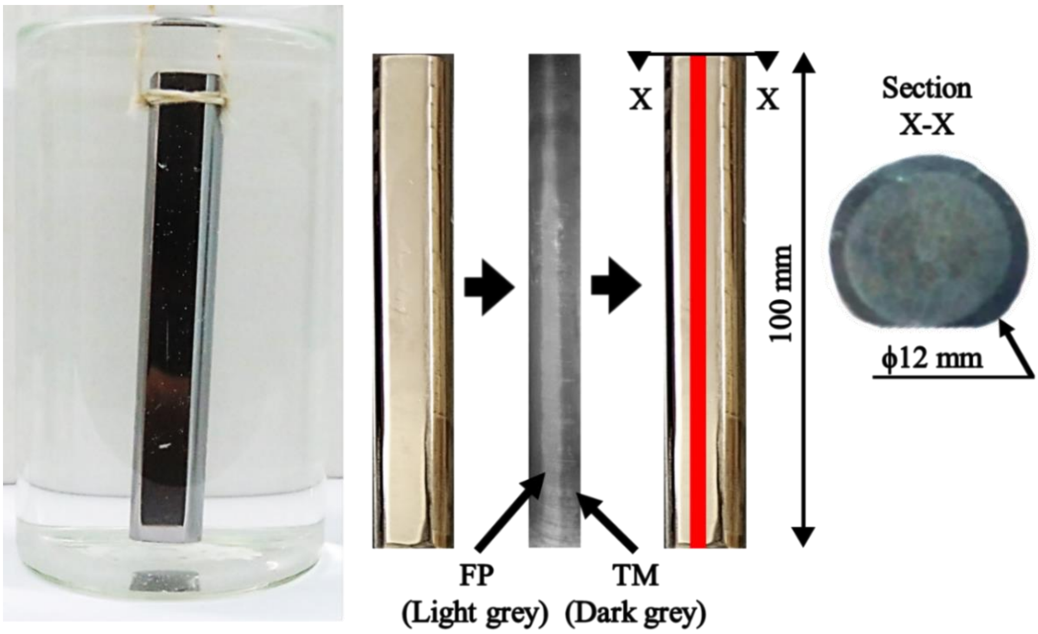

(a) Specimen immersed in solution (b) FP strip etched and mapped

Figure 4.22: Type 1 immersion test specimen

4.4.6 Immersion test – Test procedure

The immersion test is done to validate the observations from CPP. The test is expected to simulate the actual scenario where there is a simultaneous exposure of TM and FP areas on the surface of the steel rebar. The specimens were immersed for 3 days in simulated pore solution (composition given in Table 4-6) for passive layer formation (Poursaee and

Hansson 2007). Based on the CPP test results, 1.6% Cl^- (by weight of solution) is introduced, to observe natural corrosion initiation and propagation.

4.5 STAGE 3 – MECHANICAL TEST SPECIMENS AND PROCEDURES

Stage 3 focusses on the mechanical properties of TM, FP and QST steel rebars. The scope includes tensile and flexural properties evaluated by tension tests and bend tests, respectively.

4.5.1 Tension test

Tension tests were executed in for two different types of specimens.

(i) Type 1: TM and FP specimens were extracted from a 40 mm rebar as shown in Figure 4.23. The extracted cylindrical specimens were 7 mm in diameter and 200 mm long. These were milled down to 5 mm diameter for a gauge length of 25 mm at the centre (shown in Figure 4.24).

(ii) Type 2: As received specimens from GQ and PQ rebars were tested in this case. The specimens were prepared by milling the longitudinal ribs/seam alone to anticipate the breakage in the region. The length of milling depends on the diameter of the rebar and the corresponding gauge length

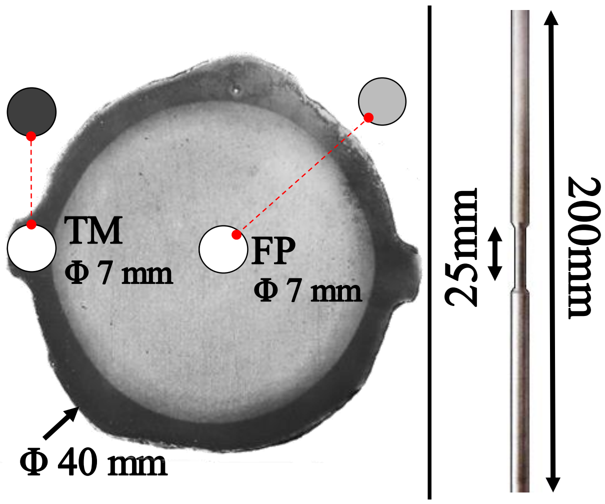

Figure 4.23: TM/FP specimen extracted for tensile test

Figure 4.24: Longitudinal rib milled as part of the tensile test specimen preparation

Tension tests were done on FP, TM and a QST bar specimens to compare the yield strength (YS), ultimate strength (TS), percent elongation, YS/TS, and modulus of elasticity (E). This was followed by as-received QST steel rebars with good and poor quality CSPDs subjected to tension test for comparing the tensile performance. The test results are given in Section 7.2. Additionally, the details of an indigenous extensometer, designed and fabricated for the use in these tension tests, are given in Section 4.6.

It is important to note that the tensile testing specimens are not turned on a lathe to reduce the cross-section as per the codal provisions. This is because the TM ring will be disturbed/removed from the picture giving an underestimated or wrong test result when compared to an as received bar. This is applicable only if the strain is measured for a specific gauge length where the is expect the specimen to fail. In industry, the technician puts marks (marker or dot punch) at equal intervals along the specimen length and test the specimen. The elongation percentage is calculated for the interval in which the specimen breaks. However, this is not the case in the current scenario. Hence, shows the way in which the specimens were prepared for the gauge length. The longitudinal rib/seam is milled or ground to make the effective area relatively lesser than the other areas.

Tension tests are done to find the mechanical parameters of materials under tension. The test parameters and dimension of specimens used varies and are decided based on the user's requirements and the standards of practice. Specimens in this study were tested in an MTS 311.12 Universal Testing Machine (UTM; Figure 4.25) with an HBM QuantumX MX 1310-B data acquisition system (DAQ; Figure 4.26) to record the strains measured by an extensometer.

4.5.2 Bend test

Bend tests were executed in rebars of 8 mm diameter as shown in Figure 4.27 to compare the bendability. The bend test was also divided into two cases.

(i) Case 1: A standard 135^{o} bend test as per IS 1599: 1985 was done in this case. The included angle will be 45^{o} at the end of the test. Visible cracks were checked.

(ii) Case 2: A modified bend test for a bend angle of 157.5^{o}. The included angle is 22.5^{o}. This case is intended to simulate excess bending.

The rebars were bent across a test span of 90 mm and a clear span of 40 mm. Rebars from 10 sources were tested which includes 2 sources with adequate CSPD and 8 sources with inadequate CSPD. IS 1599: 1985 specifies ‘3d’ as the mandrel diameter, where ‘d’ is the diameter of the rebar tested. However, the mandrel diameter used was 16 mm to mimic a site scenario of an 8 mm stirrup rebar, bent around a 16 mm primary rebar. The bars were checked for visible cracks for bend angles of 45^{o} and 22.5^{o}.

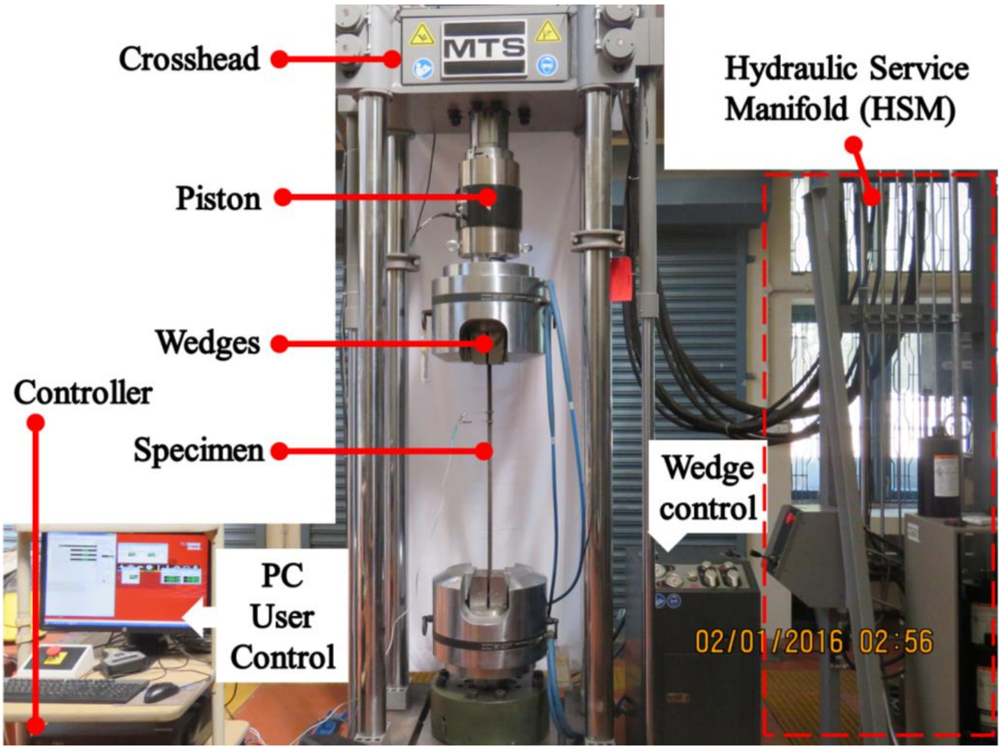

Figure 4.25: MTS 311.12 Universal Testing Machine (UTM)

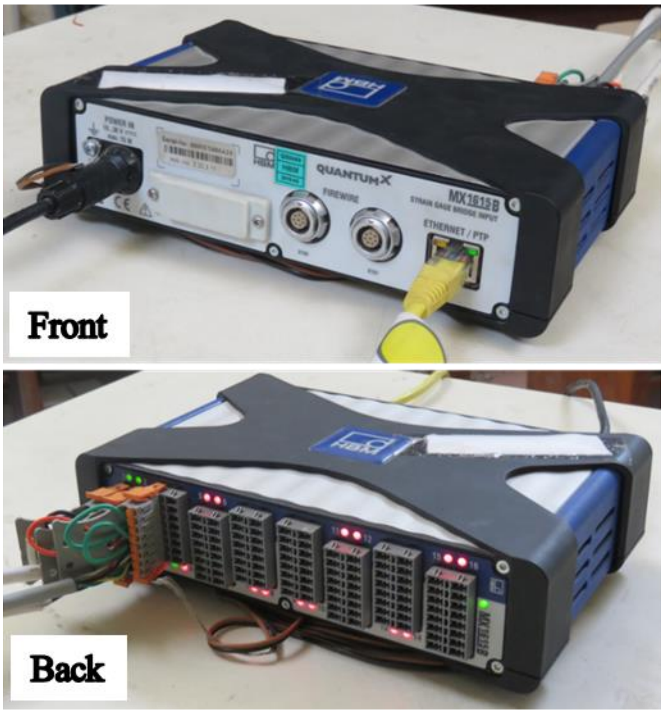

Figure 4.26: HBM Quantum X MX 1315B controller (DAQ unit)

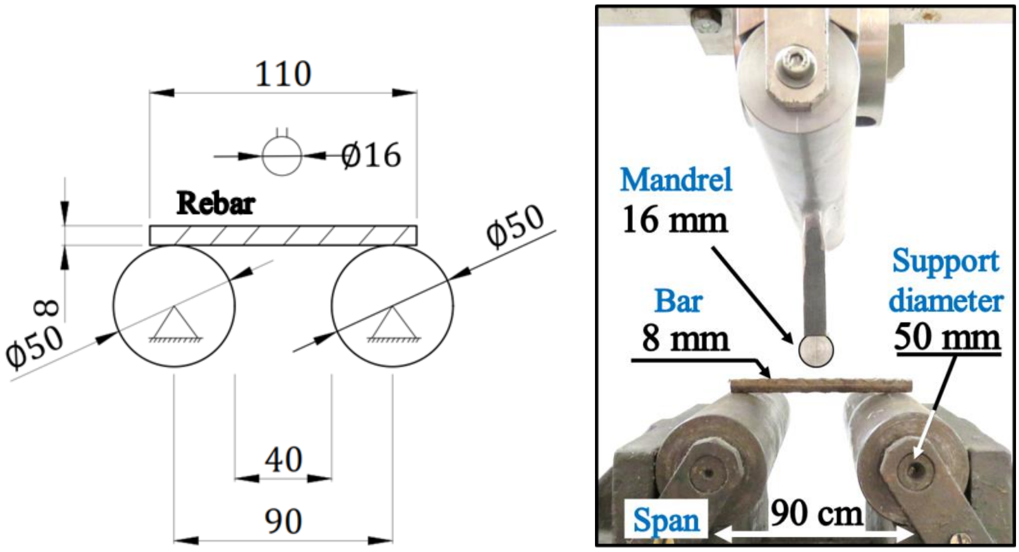

(a) (b)

Figure 4.27: Bend test setup (a) Schematic (b) Real-time test setup

4.6 EXTENSOMETER DESIGN AND FABRICATION

The design and fabrication of a clip-on type extensometer were done for measuring strain in the tension tests mentioned in Section 4.5.1. The design involves several mechanical and electrical components which are enumerated in Figure 4.28. The mechanical components are made of aluminium and stainless steel. Further details on the grade of materials, material selection, design, fabrication and testing are given as a stand-alone chapter (Chapter 8) for the ease of understanding.

4.7 OTHER EXPERIMENTS AND TEST METHODS

4.7.1 Optical Microscopy (OM)

An Optical Microscope (See Figure 4.29) is used to check the microstructural features in steel and concrete specimens. A wide range of magnifications is available, typically up to 1000X.

4.7.2 Optical Emission Spectroscopy (OES)

Optical Emission Spectroscopy was used to identify the chemical composition of steel rebars. There are two types of OES viz. Arc and Spark excitation **(**DeKalb 1966**).** The samples in the current study were subjected to spark excitation. The advantages of OES over EDX or XRD are the identification of period 2 elements (Carbon, Nitrogen etc.) and minimal specimen preparation. The limitation is the minimum size of the bars to be used for the test. Low diameter wires/bars of 10 mm and below, may not be accurately analyzed, unless the specimen is made flat.

4.7.3 Electron Discharge Wire (EDW) Cutting

These are precision cutting facilities used to extract specimens to the required shapes and sizes as per the drawings input to the facility. Computerized Numerical Control (CNC) was used in extracting the coupon specimens from a rebar, with minimal heat damage and time. The cutting is done under water at 20 ^{o}C leaving an HAZ of less than 0.25 mm.

4.7.4 Laser Cutting

Laser cutting is also a precision cutting tool used to cut materials into the desired shapes. The process is generally used in sheet metal research and was used to fabricate the knife edges from stainless steel, as per the design drawings.

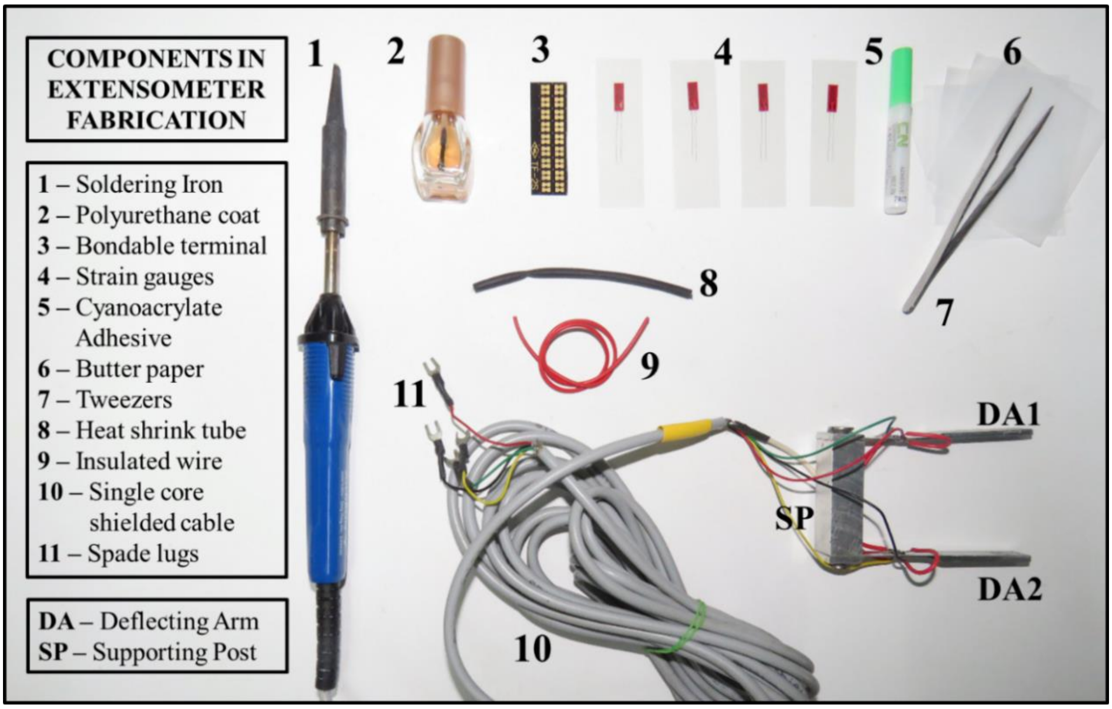

Figure 4.28: Material requirement for the extensometer fabrication

Figure 4.29: Olympus BX-41 Optical Microscope

The following chapters will discuss the work at each stage, namely the microstructural study, corrosion study and the mechanical study. The stand-alone Chapter 8 is a discussion on the design and fabrication of a low-cost clip-on extensometer.

CHAPTER 5

RESULTS: MICROSTRUCTURAL CHARACTERISTICS

5.1 INTRODUCTION

The scope of this section is limited to QST steel rebars of 8, 12 and 16 mm diameters. The specimen preparation and test methods are given in Section 4.3. The microstructure is evaluated in three cases:

(i) Case 1 checks the variation in CSPD of rebars collected from various sources. Test samples of 10 mm thickness are extracted from various rebars by using a band-saw with coolant.
(ii) Case 2 checks the variation in CSPD of a single rebar length of 1200 cm. Test samples of 10 mm length are extracted at every 70 cm approximately.
(iii) Case 3 checks the longitudinal variation of TM thickness along a 150 mm length. The test sample is prepared from a 150 mm length and 8 mm diameter rebar.

The specimens were moulded in a cold setting epoxy. These specimens were subjected to coarse polishing (grinding) using emery sheets of grit size 80, 120, 320, 600, 1000 and 1200 in the presence of coolant. The polished specimens were macroetched with 5% nital solution (5% nitric acid in ethanol) to reveal the CSPD. The exposed cross section with a dark grey region of TM and light grey region of FP were photographed. The epoxy moulding helps to isolate a single plane of cross-section (during etching) and avoids the disturbance created by the out-of-plane transverse ribs in the image recorded (for analysis). The details are explained in following sections.

5.2 EVALUATION OF CSPD: TEST CASES AND RESULTS

5.2.1 Variation across different sources of rebar

A total of around 100 specimens were subjected to macroetching. A good number of rebars in the microstructural study showed defective CSPD. However, only a few cases from the results of 'TM-ring test' are given in Figure 5.1. Each row corresponds to 8, 12 and 16 mm diameters of rebars tested. Column 1 shows rebars with an adequate TM ring. Column 2 through 5 shows the cases of discontinuous TM rings in all three diameters. It is observed that 8 mm rebars exhibit higher chances for having a defective CSPD when compared to 12 and 16 mm rebars. However, few 12 and 16 mm rebars also showed defective CSPDs. This suggests that improper quenching could occur irrespective of the diameter of the rebar manufactured.

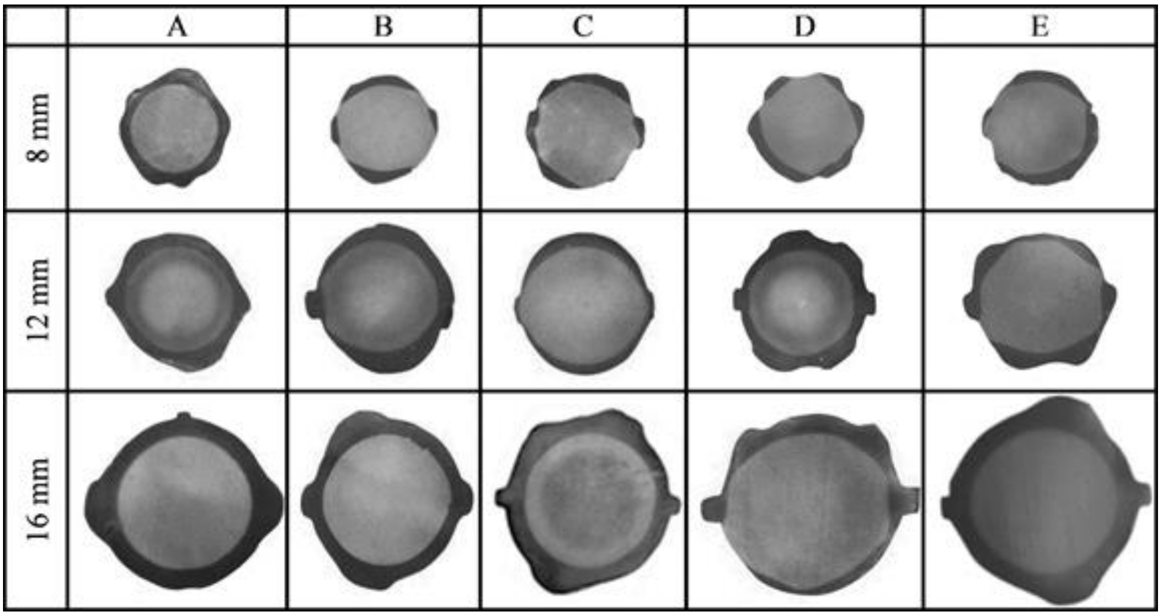

Figure 5.1: Nital Test results

Based on this, a good quality QST steel rebar is defined as a rebar with a uniform and complete TM ring (adequate CSPD). A poor quality QST steel rebar shows two peculiar cases of CSPD shown in Figure 5.2. There could be a case of discontinuous and non-uniform distribution of TM on the periphery as shown in Figure 5.2(a). However, there could be a case of continuous, yet non-uniformly distributed (or eccentric) TM phase as shown in Figure 5.2(b). The former case is observed in B8, C8, D8, E8, E12 and D16 from Figure 5.1, whereas the latter in B12 and C12. Further images are given in Appendix B and Appendix C.

The results imaged were analyzed to find the area of TM and FP constituting the total cross-sectional area (including ribs). Since the scope is limited to the area of TM and FP, AR_{FP} (equals 100 - AR_{TM}) will include the area of bainite (if present) as well. Figure 5.3 gives the range and variation of the observed AR_{TM} across different rebars. The average AR_{TM} was observed between 34-37%, with a negligible difference across the diameters. However, the majority of the observed areas were found to be (relatively) higher than the reported range of 25-35% (Ambuja 2005; Markan 2005) in literature. It is not clear whether the values reported in the literature are for a nominal area or the actual cross-sectional area, which could be a reason for this relative shift in data. The red marker denotes defective CSPD and black markers denote uniform CSPD. Then, it is clear from Figure 5.3 that the number of red markers decreases as the diameter increases i.e. the probability of finding an inadequate CSPD/defective TM-phase is higher, in lower diameters.

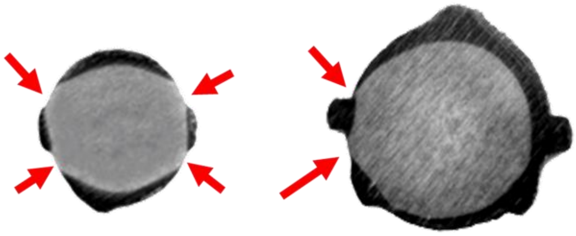

Figure 5.2: Poor quality rebars exhibiting (a) discontinuous and (b) eccentric CSPD

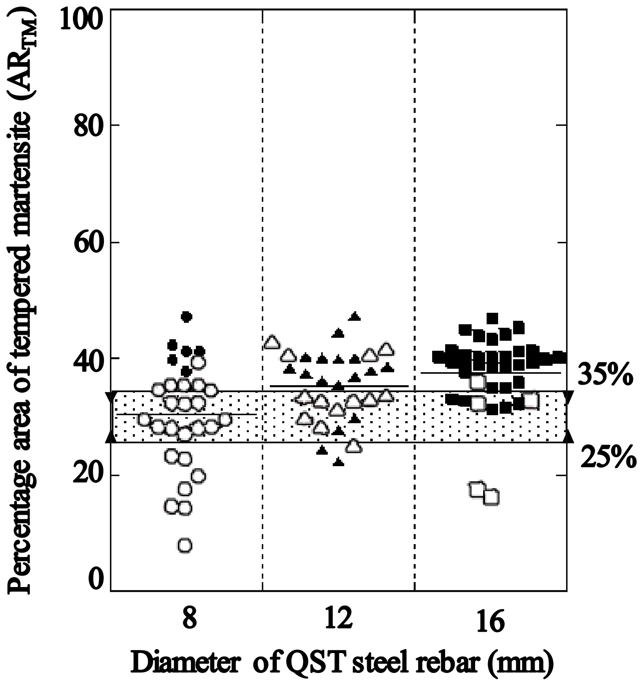

Figure 5.3: Dot plot showing AR_{TM} for good and poor quality QST steel rebars

5.2.2 Variation along a single rebar length of 1200 cm

From the results in the earlier section, the scope was narrowed to the variation in CSPD along the length of a single bar, one each from good and poor quality rebars. The results of the variation along the longitudinal length are shown in Figure 5.4. A good quality QST steel rebar showed a complete and uniform peripheral TM ring consistently across its length as shown in the 4 images (to the left) in Figure 5.4. However, the majority of the CSPDs tested showed defective TM in the case of poor quality rebars. A few relevant cases in the tested specimens along the length are given in Figure 5.4 (to the right). From Figure 5.4, cross-section at 9m (section 9-9) in poor quality rebar has a discontinuity (shown with an arrow). All other cross sections (3-3, 6-6 and 12-12) shown for poor quality rebar has a non-uniform thickness of TM ring with arrows pointing at locations of least visible TM-ring thickness. It is concluded that a poor quality steel may not necessarily have the same cross-section consistently throughout its length. An inadequate CSPD/defective TM-phase tends to vary across the length.

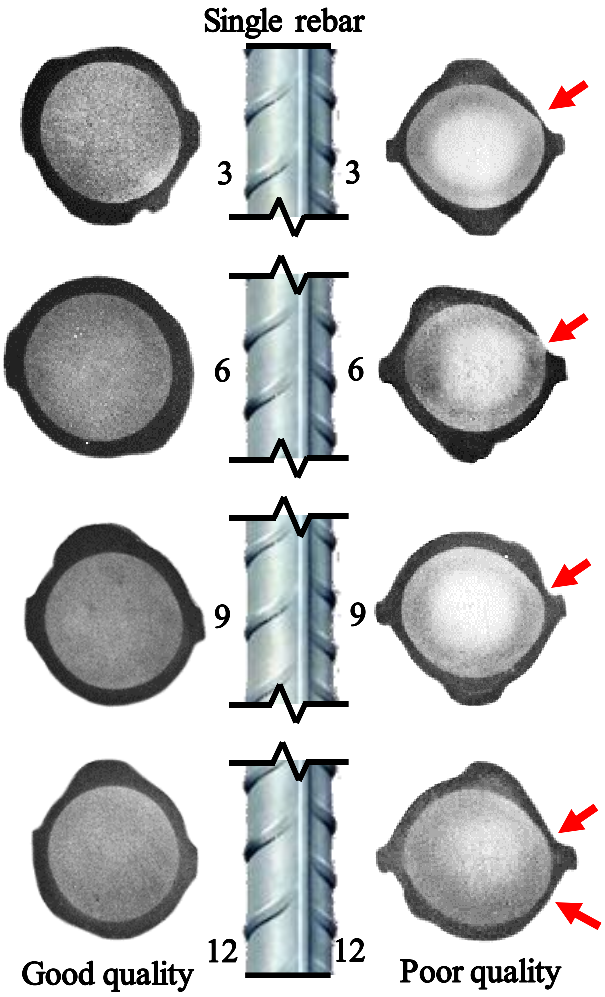

Figure 5.4: Variation of phase distribution along a single rebar of length 1200 cm

5.2.3 Variation of the TM thickness along a longitudinal section

A poor quality rebar specimen of 8 mm diameter was cut into a 15 cm long piece and milled in the longitudinal direction (See Figure 5.5). The cross-section at ‘0 cm’ of the milled piece is also shown. The depth of milling is such that the cross-sectional discontinuity lies within the milled plane. The cross-section of the cut piece was etched to find the variation in TM thickness. TM thickness is zero at discrete regions in the bottom edge, marked by the adjacent double-headed dashed lines. Also, the TM phase thickness in the bottom edge is found to vary along the length. The top edge in the figure seems to have a uniform thickness along the full length. The good quality 12 mm rebars showed consistent thickness across its length. In the poor quality 12 mm rebar, the portions where TM thickness varies are marked by white dashed lines. The cut plane did not coincide with any discontinuous TM portions. Appendix D shows the profile of a 12 mm rebar. There are no clear discontinuities visible. However, there is a change in thickness of TM which are marked by dotted lines and zoomed in for visibility.

In general, defects in QST steel rebars could be present in any diameter on poor quality control. These could be discontinuities or eccentricities as a result of the improper or uneven Q&ST process. These defects might not be present consistently across the length of a single rebar.

5.3 CLASSIFICATION OF CSPD

Figure 2.9 shows four typical images of CSPDs of QST steel rebars. A good quality QST steel rebar should exhibit continuous, concentric and uniform TM phase and a core with FP phase (as shown in Figure 2.9 A). On the other hand, a poor quality rebar could exhibit either of the three defects (i.e., discontinuous, eccentric or non-uniform) or a combination of these as shown in Figure 2.9. These defects could form due to improper quenching in the In-line QST treatments. This study proposes to classify these defects as follows:

(a) Eccentric and non-uniform TM-phase: Cases where the TM-phase at the periphery is continuous but eccentric; and have a non-uniform thickness.

(b) Discontinuous and non-uniform TM-phase: Cases where the TM-phase at the periphery does not form a complete ring and is discontinuous at one or more locations (i.e., both FP and TM phases are exposed at the surface); and have a non-uniform thickness.

Based on the observations, Section 5.3.1 discusses the possible outcomes of the 'TM-ring test' and their evaluation details.

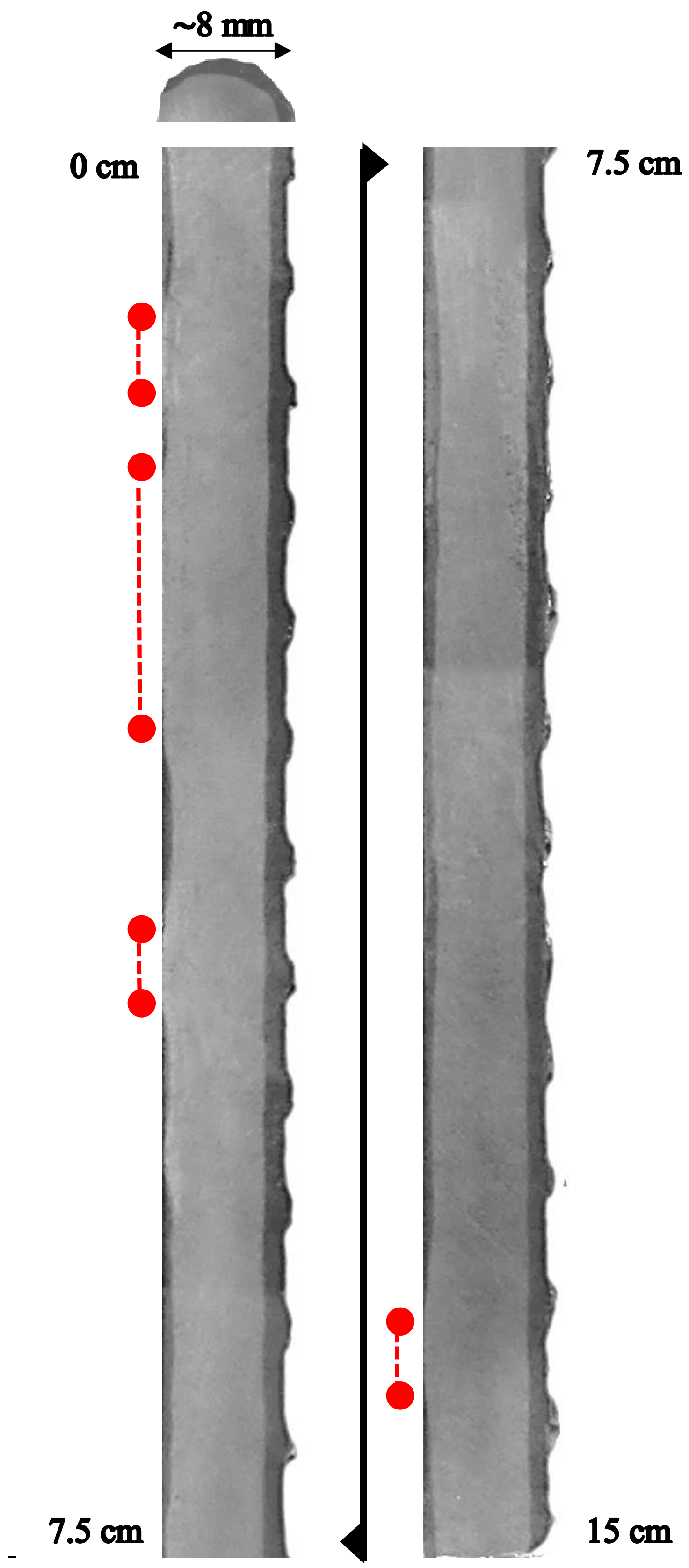

Figure 5.5: Longitudinal variation of TM phase in an 8 mm poor quality rebar

5.3.1 General classification of results of nital test

The Reference Cases A, B, C, and D in Figure 2.9 indicate four possible outcomes from the 'TM-ring test'. Case A indicate good quality, whereas Cases B, C, and D indicate poor quality.

Case A in Figure 2.9 indicates an ideal rebar showing a continuous, concentric and uniformly thick TM-ring. Through the laboratory tests on various steel rebars collected from the market, it was found that this kind of perfect TM-rings are mostly seen in large diameter rebars and lacking in rebars with less than 16 mm diameter. Moreover, such small diameter rebars are used as stirrups with smaller cover depth than that of primary reinforcement with a larger diameter. This hints that better quality control is required for such smaller diameter rebars.

Case B in Figure 2.9 is a case of continuous, eccentric and non-uniform TM phase. The ring thickness is very small at two regions on the left side in the image. This could probably occur if the coolant temperature or pressure is not uniform along the circumference. As a result, a differential temperature gradient occurs forming TM-ring with non-uniform and inadequate thickness at some regions. These types of defects were mostly found in 12 and 16 mm diameters. On the contrary, over-quenching at specific points can form TM-ring with non-uniform and more than the adequate thickness at some regions.

Case C in Figure 2.9 shows a non-uniform TM-phase with scattered discontinuities. This cannot be defined as a case of concentricity. This could occur when the quenching hardware fails (e.g., clogged nozzle) to work at some locations over the surface of the rolled rebar in the cooling stage. Theoretically, when the minimum thickness of the ring in Case B becomes zero, it forms a discontinuity.

Case D in Figure 2.9 shows a discontinuous and non-uniform TM region - with a relatively longer discontinuity (seen to the left side) when compared to Case C. The quenching and self-tempering of rebars require better quality control to avoid this.

Discontinuous TM-phases (Cases C and D) were mostly observed in 8 and 12 mm diameter rebars. However, note that such defective bars could also exist in 16+ mm diameter rebars. It is generally observed that the relative thickness of TM-ring increases with an increase in diameter of the rebar, reducing the chances for defects in TM-ring. Note that this increase in TM-phase will, in turn, result in a reduction in the FP-phase. The impact of this on the tensile strength and ductility needs to be studied. It is recommended that the CSPD must be assessed for at least one specimen from each rebar lot. Therefore, a feasible and easily employable acceptance criteria for QST rebars is necessary as part of the 'TM-ring test'.

5.4 ACCEPTANCE CRITERIA FOR QST STEEL REBARS SUBJECTED TO NITAL TEST

Figure 5.6 shows the proposed 2-Level acceptance criteria: (i) Level 1: Visual Analysis and (ii) Level 2: Thickness analysis. Level 2 assessment is to be done if the rebar is 'accepted' in Level 1.

5.4.1 Level 1 Acceptance Criteria: Visual analysis

Level 1 (L1) acceptance criterion is based on a qualitative visual analysis of the images obtained from Section 4.3.3. The L1 criteria will help categorize the image into one of the cases given in Figure 5.6. The user is instructed to check the formation of a ring and core on etching and evaluate the continuity, uniformity and eccentricity of the TM-phases formed. If the answer for all the four questions in the first table in Figure 27 is 'Yes', then the rebar lot can be 'accepted' for use. If any one or more answers are 'No', then the rebar lot must be 'rejected' for use. It is also recommended to polish adequately and repeat the 'TM-Ring test' on the same specimen surface – to confirm the visual observations.

5.4.2 Level 2 Acceptance Criteria: Thickness analysis

The Level 2 acceptance criteria shall be used only for the rebars 'accepted' in the Level 1. In Level 2, the thickness of TM phase (darker region) in the image of the etched surface is measured/analyzed. Any suitable instrument (e.g., Vernier Caliper or Crack Gauge) or an image analysis software could be used for this purpose. This study used ImageJ®, which is a free software developed by National Institute of Health (NIH), USA. As per Markan (2005) and Ambuja (2005), the recommended area of "TM- ring" is 25-53% of the rebar cross-sectional area. The corresponding minimum and maximum thicknesses of the TM-ring for 25% and 35% area of TM, respectively, are calculated as follows.

Minimum expected thickness of TM $t_{TM,min}$ =

$$\frac{D-D_{FP}}{2}=\sqrt{\frac{A}{\pi}}-\sqrt{\frac{A_{FP}}{\pi}}=\sqrt{\frac{A}{\pi}}-\sqrt{\frac{0.75A}{\pi}}$$

$$=0.134\sqrt{\frac{A}{\pi}}=0.134\sqrt{\frac{\left(\frac{\pi D^2}{4}\right)}{\pi}}=0.07D$$

where, D = Nominal diameter of rebar, and D_{FP} = Diameter of FP core area.

Similarly, the maximum expected thickness of TM, $t_{TM,max}$ = 0.1 D.

Therefore, for all the rebar sizes, the measured thickness of TM (t_{TM}) is recommended to be between 0.07D and 0.1D. In short, a rebar can be 'accepted' if the t_{TM} is between 0.07D and 0.1D, where D is the designated or nominal diameter of the rebar. This checks if a rebar with continuous TM-ring has been quenched properly to be acceptable. These acceptance limits on the thickness of TM phase have been established based on the expected cross-sectional area of TM and FP phases [Markan (2005) and Ambuja (2005)]. However, the evaluation of thickness is comparatively easier than cross-sectional area; hence, this research suggests an equivalent acceptance criteria based on the minimum and a maximum thickness of TM phase. These details have been included with illustration as a data sheet in Figure 5.6.

The datasheet could be used by an engineer at steel plant or construction site to check the quality of QST steel rebars. L1 criteria are recommended for quality-control engineers at construction sites. L1 followed by L2 criteria is recommended for steel rebar manufacturing plants, which could help them to determine the right quenching parameters to get the desired quality. The test setup for 'TM-ring test' is given in Figure 5.7. Note that the lighting provisions are not shown in the real-time setup.

Datasheet for ‘TM-Ring’ test

<table>
<tr><th colspan="17">REFERENCE CASES</th></tr>
<tr><td></td><td colspan="4">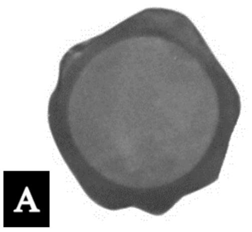</td><td colspan="4">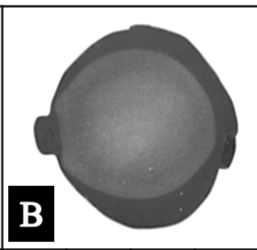</td><td colspan="4">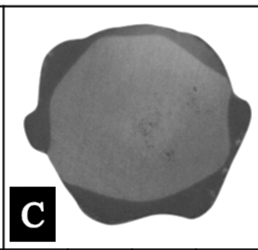</td><td colspan="4">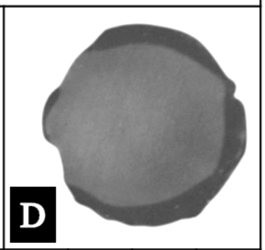</td></tr>
<tr><td>L1</td><td>Y</td><td>Y</td><td>Y</td><td>Y</td><td>Y</td><td>Y</td><td>N</td><td>N</td><td>Y</td><td>N</td><td>N</td><td>N</td><td>Y</td><td>N</td><td>N</td><td>N</td></tr>
<tr><td>L2</td><td colspan="2">Y</td><td colspan="2">Y</td><td colspan="4">-</td><td colspan="4">-</td><td colspan="4">-</td></tr>
<tr><td></td><td colspan="4">Accepted</td><td colspan="4">Rejected</td><td colspan="4">Rejected</td><td colspan="4">Rejected</td></tr>
</table>

LEVEL 1 (L1) ACCEPTANCE CRITERIA		
No.	Question	Answer (circle one)
1	Is a dark grey peripheral region and light grey core seen?	Yes / No
2	Does the dark grey peripheral region form a continuous outer ring?	Yes / No
3	Are the dark grey peripheral region and light grey core concentric?	Yes / No
4	Is the thickness of the dark grey peripheral region uniform?	Yes / No
Decision		
If all the answers are **‘Yes’**, then accept the rebar lot		
If any one or more answers are **‘No’**, then reject the rebar lot		

LEVEL 2 (L2) ACCEPTANCE CRITERIA		
No.	Observations	in mm
1	Diameter of rebar, D	
2	Measured thickness of TM, t_{TM}	
No.	Question	Answer (circle one)
1	Is $t_{TM} \geq 0.07$ D ?	Yes / No
2	Is $t_{TM} \leq 0.10$ D ?	Yes / No
Decision		
If all the answers are **‘Yes’**, then accept the rebar lot		
If any one or more answers are **‘No’**, then reject the rebar lot		

Figure 5.6: Datasheet for ‘TM-ring test’

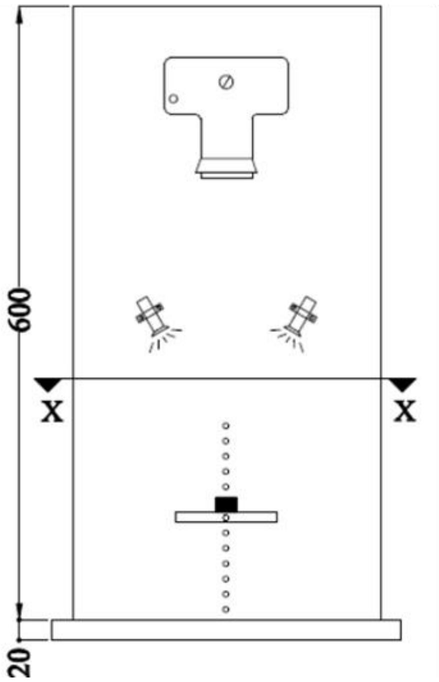

(i) Front view

(ii) Fabricated test setup

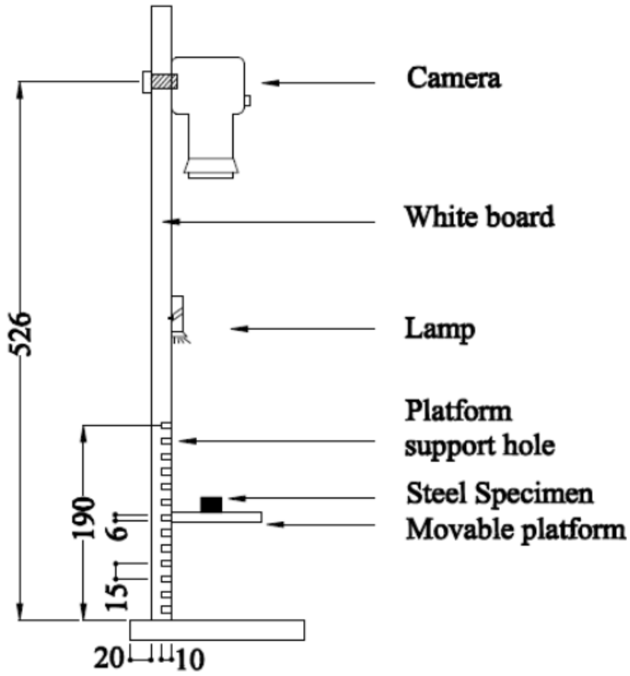

(ii) Side view

Figure 5.7: Imaging setup

5.5 CHALLENGES FACED

There were several issues faced in the course of the microstructure study. These should be kept in mind and addressed accordingly while specimen preparation and test procedure.

5.5.1 Specimen preparation

1. The formation of air bubbles while cold mounting is a primary issue in specimen preparation. The epoxy mix was too viscous to compact by tapping. The moulds could be subjected to ultrasonication at a mild temperature (Say 30 ^{o}C) to allow the trapped air inside to escape.
2. If plastic moulds are used, it will be difficult to demould as a result of the exothermic reaction, unless properly oiled. The user could prefer using silicone-rubber moulds for ease.

5.5.2 TM-ring test

1. Partial etching due to a slight incline in the etched specimen surface should be avoided. This could be done by polishing the surface so as to get a flat face or polishing the base so that the testing face becomes horizontal. In the case of this issue, a part of the surface will show clear rings whereas the other part will not. Figure 5.8 shows a typical case of partial etching.

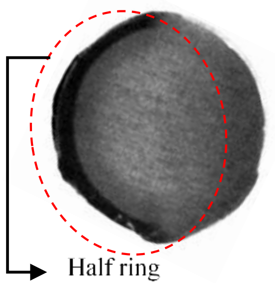

Figure 5.8: TM phase visible as a half ring

2. The scale should be kept in the same plane as the testing plane. Although the error associated could be negligible, it is better to be consistent with the practice of calibration the scale in the same plane as the testing surface. This could be done by maintaining the length of the moulded specimen or by having a platform with adjustable heights for the scale to be placed.

3. If no rings are observed, the specimen shall be polished again by removing a significant thickness of the specimen and redoing the test.

Figure 5.9 gives possible errors that a user could face in the 'TM-ring test' method. These are mentioned beforehand for the user to understand the errors and avoid them during the TM-ring tests. There are three results given in Figure 5.9 and discussed below.

a) Wiping the etch stain b) Poor polishing c) Heat damage when cut without coolant

Figure 5.9: Erroneous observations due to inappropriate/inadequate etching procedures

1. Result I shows the stains (which formed the dark ring) being removed while wiping the excess solution (by hand). In such cases, the user is advised to immediately wipe/clean the surface with a wet and soft cloth, polish the surface again, and repeat the 'TM-Ring test'.
2. Result II occurs under inadequate and inappropriate polishing. Partial or most of the surface area may remain dark. At the same time, some portion gets etched and shows the colour difference. It is instructed to polish the specimen again and repeat the testing.
3. Result III can occur when the test specimen is cut (from a rebar piece) without using any coolant and the cross-section gets damaged. It is instructed to procure a new specimen and continue the test. The user shall also extract a new test specimen from a distance of 3 times the diameter from the cut end (or heat affected zone) of the rebar. Also, ensure that a coolant is used for all the cutting procedures.

5.5.3 Photographing and image analysis

1. Dirt and dust trapped in the bubble holes and crevices near the specimen disturb the image analysis near the TM periphery.
2. Generally, the bainite ring is seen as a third phase in the cross-section. In some cases, the bainite ring could be distinguished only by increasing the contrast. The current scope of study focusses on TM and FP.
3. The images of the same format (lighting conditions) could not be recorded always. While comparing the images, the user may find different greyscales which are unique to that sample. The user could report the results within error limits while comparing general results.

The following suggestions may also be incorporated in the current scope to have a better experience in the overall testing procedure.

1. Use an alternate contrasting colour for the epoxy used to embed the specimen, if possible. However, transparent epoxy might not serve the purpose.
2. The photos shall be taken under the same lighting conditions to identify the transition ring.

The following chapter will focus on the corrosion aspects of QST rebars in the presence of inadequate CSPD.

CHAPTER 6

RESULTS: CORROSION CHARACTERISTICS

6.1 DETERMINATION OF CHLORIDE THRESHOLD USING LPR TEST

6.1.1 LPR test results for determining chloride threshold

Based on the literature, specimens were exposed to SPS solution for 3 days to allow passive film formation. E_{corr} and I_{corr} values were monitored at 3-hour intervals during this period. It is observed that there is no characteristic OCP value for TM and FP during the immersion period (without chloride contamination). The OCP value ranges between –180 mV and –350 mV. Figure 6.1(a) and Figure 6.2(a) gives E_{corr} and I_{corr} values after 3-hour immersion in the chloride-contaminated solution. Similarly, Figure 6.1(b) and Figure 6.2(b) gives E_{corr} and I_{corr} values for 6-hour immersion (subsequent to the 3-hour immersion). Note that the legend remains common for all the graphs.

Figure 6.1 gives the E_{corr} recordings for 3 hours and 6-hour exposures, respectively. In general, TM shows more negative E_{corr} values when compared to FP. This confirms that the metastable TM is more active than FP. As a result, in the case of inadequate CSPD, there is a possibility of galvanic corrosion. The results on FP1 is not used for comparison as the epoxy cracked across the face during the course of testing. As a result, FP1 lie out of the general response of the other specimens in Figure 6.1.

Figure 6.2 gives I_{corr} for 3 hour and 6-hour exposures, respectively. There is no specific threshold chloride concentration beyond which the I_{corr} increase drastically. For 3 and 6-hour readings, I_{corr} values decrease as chloride concentration increase, till 1% Cl-addition. This probably shows that the concentration is not high enough to induce corrosion and that the passive layer is getting stronger till 1%. However, at 1%, I_{corr} for all TM specimens increased in the case of 3-hour readings as given in Figure 6.1. Active corrosion for TM is expected to have started between 0.6 to 1.4% of Cl^- concentration in this case. For 6 hour readings, I_{corr} tends to increase for all specimens which could not be explained. Active corrosion was visible on the face of TM1 and thus shows a significant increase in the I_{corr} values compared to other specimens from Figure 6.1(b) and Figure 6.2(b). FP specimens started to show visible interfacial corrosion at the sides towards 1.8% Cl^-

contamination. This interfacial corrosion could be a reason for not capturing a similar range as in the case of TM.

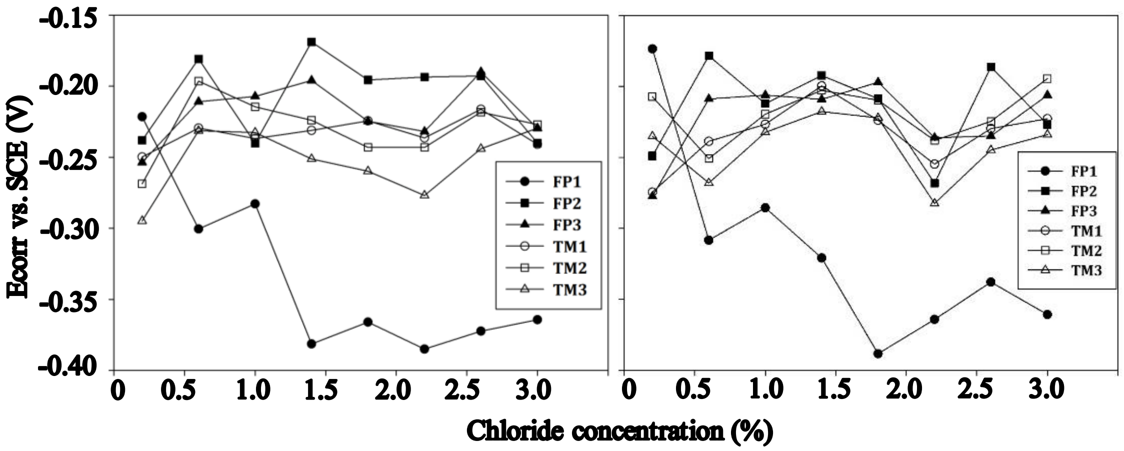

(a) (b)

Figure 6.1: E_{corr} vs. Cl^- % for (a) 3-hour immersion (b) 6-hour immersion

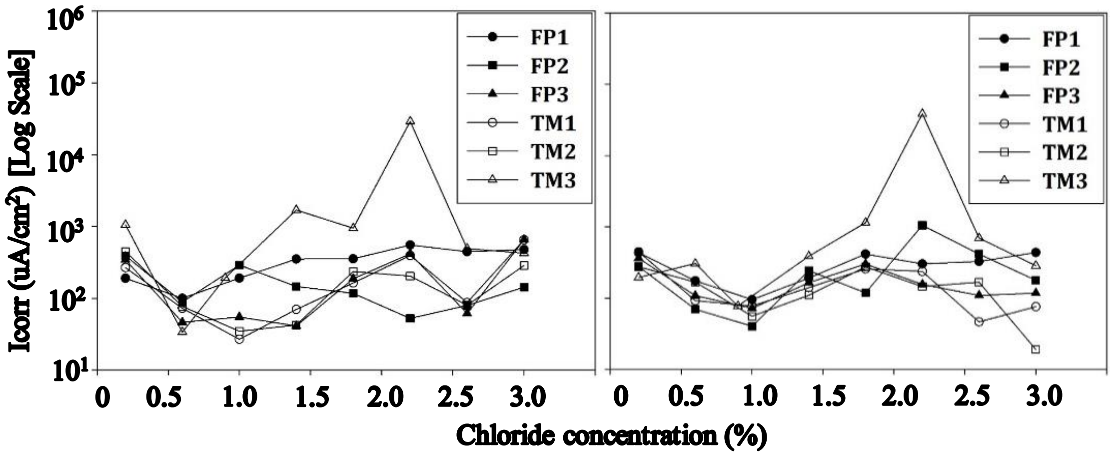

(a) (b)

Figure 6.2: I_{corr} vs. Cl^- % for (a) 3-hour immersion (b) 6-hour immersion

6.1.2 Challenges faced in LPR test method for Cl_{th} estimation

Several challenges faced during the course of corrosion response tests includes interfacial corrosion in FP specimens, instantaneous rise or dip in the records (for both TM and FP) and time-dependent response in corrosion. Micro level interfacial gaps induce localized corrosion. This affects the I_{corr} calculation with a highly underestimated value as we use the area of exposed face. In reality, the same rate should be calculated for a lesser area (the localized corrosion area) which could raise the Icorr readings. Variation in the testing environment may be the reason for the isolated rise and dips in Figure 6.1 and Figure 6.2.The specimens do not exhibit much difference between 3 and 6 hour exposure times in different chloride conditions. Thus, the 3-hour and 6-hour exposure times do not seem to have an effect on the susceptibility to corrosion for TM and FP. However, a standard exposure time is not established from the results obtained in this study. Considering these challenges, further set of studies are being done to trace the actual corrosion behaviour of TM and FP phases in a chloride environment.

The visible interfacial corrosion in FP specimens could give underestimated corrosion rates. Further detailed investigation considering the challenges faced in assessing the effect of discontinuous TM rings on the corrosion behaviour of QST steels was needed.

6.2 DETERMINATION OF CHLORIDE THRESHOLD USING CPP TEST

6.2.1 Pitting responses in CPP test results

Figure 6.3 shows the typical responses in a CPP test observed in the current scope. The test response in Figure 6.3(a) shows a ‘no pitting’ condition at a particular chloride concentration. As the concentration increase, cases of pitting as in Figure 6.3(b) are observed. The CPP test response moves from ‘a’ through ‘f’ (or f ’) and reverses at ‘d’.

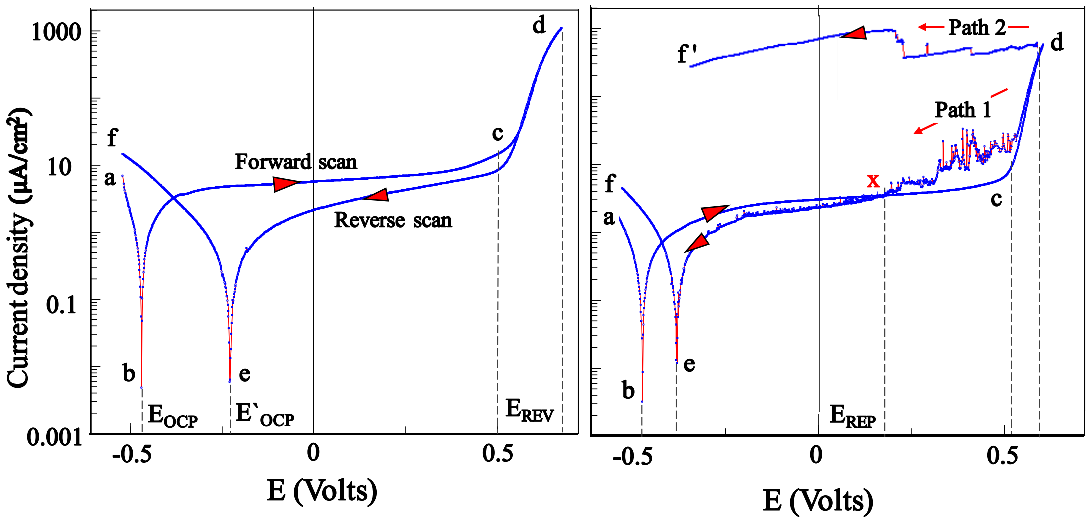

(a) Without pitting **(b) With pitting**

Figure 6.3: Typical Cyclic Potentiodynamic Polarization (CPP) curves

From the observed CPP test results, there are two possible responses for a TM/FP test specimen. Typical test responses as shown in Figure 6.3. Figure 6.3(a) is a non-pitting case where the scan starts at 'a' (E_{OCP} – 100 mV) and sweeps in the positive potential direction. This forward scan approaches the system's OCP at point 'b' where the current is negligible. Region a-b denotes the cathodic response of the specimen. Region b-d denotes the anodic polarization where the response current increases with increasing anodic voltage. The specimen remains passivated till point 'c' after which the current drastically increases. The region c-d is called the transpassive region. At a current of 1 mA/cm^2 given by point 'd', the scan reverses and follows a positive hysteresis curve through 'e' and completes at 'f'. In this case, there is no pitting visible.

In the case of pitting, a sudden current rise and a negative hysteresis loop are observed as shown in Figure 6.3(b). There are two cases of pitting shown by Path 1 and Path 2. In Path 1, the reverse scan crosses the forward path at the repassivation potential E_{REP}. The local current hikes observed near the reversal potential corresponds to a metastable (single or multiple) pit nucleation [Pistorius and Burstein 1992, Isaacs 1989]. Such pits formed does not propagate in an uncontrolled manner on the reverse scan. These could be observed on the surface after the test as shown in Figure 6.6(a) corresponding to 'metastable pitting'. In contrast, the reversal Path 2 does not cross the forward path on pit nucleation. This is defined as a stable pit since the response current increases or remains same (around 1 mA/cm^2) on decreasing the applied potential. A specimen which underwent stable pitting is shown in Figure 6.6(a) corresponding to 'stable pitting'. The stable pit seems to have originated from an edge as an edge effect. But the nucleation points were usually within the test face away from the edges. In both the cases, pitting occurs with the pit being metastable (repassivates in Path 1) or stable in Path 2. The classification and criterion for pit formation and growth, respectively, have been made by Pistorius and Burstein (1992) into metastable and stable pits.

6.2.2 Chloride thresholds of FP and TM phases from CPP test results

CPP test at varying chloride concentrations is to determine the Cl_{th} for TM and FP phases in metastable and stable pitting. Szklarska (2002) discusses different models of pit nucleation in literature and propose a mechanism by electrical breakdown of the passive film. Preliminary sample set had been subjected to CPP tests starting with a chloride concentration of 0.2% (by weight of SPS), and increments of 0.4% till 2.0 %. This is to narrow down the range of pitting threshold for the tested system. FP and TM pitted at 1.8% and 2.0%, respectively (in this case) which narrowed down the minimum testing Cl^- concentration to 1.5%. Hence further tests were done starting from 1.5, till 2.5% or stable pitting concentration, whichever occurred first. The incremental step was fixed at 0.1 % Cl.

Figure 6.4 and Figure 6.5 gives the CPP test results for selected chloride concentrations for FP and TM. Each plot consists of 3 graphs, one each before metastable pitting (MSP), at MSP, and at stable pitting (SP) chloride concentrations. The markers indicate the starting point of the forward curve with a circle, triangle, and square corresponding to each concentration mentioned earlier in its order. TM4 did not show unstable pitting and was not reusable at 2% since the specimen was worn off (upon polishing) with very limited thickness and exposed lead wire at the testing face. So the SP was considered as 2%, even though the graph does not show an unstable current hike.

From Figure 6.4 and Figure 6.5, the OCP for FP and TM specimens lie within 100 mV. There is no specific range of OCP values distinguishable for TM and FP. Hence, the possibility for galvanic corrosion is not supported by the CPP test results. However, Figure 6.6 gives the Cl_{th} for 4 sets of TM and FP specimens. The thresholds are shown for first/ MSP, and SP. The average threshold for TM is 16% and 11% greater than FP in initial and unstable pitting thresholds, respectively. This corroborates the observation in literature that ferrite is susceptible to pitting than martensite or pearlite. This is attributed to the higher activity for ferrite bands in FP phase over TM (Lu et al. 2012). Hence, at a TM-FP interface at the surface, it is expected that localized corrosion at an early stage would occur in QST steel rebars with discontinuities. To understand the effect of this difference in an actual structure, Life 365^{TM} was used for service life prediction using the Cl_{th} values obtained for a typical case.

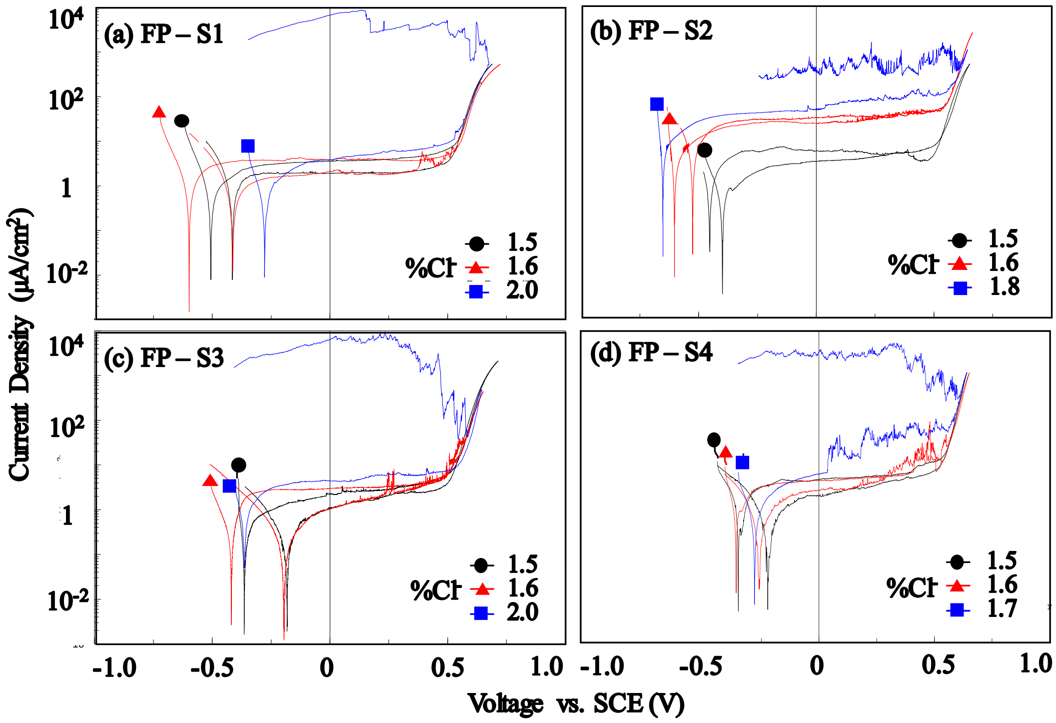

Figure 6.4: CPP test specimens of FP showing non-corrosive, initial pitting and unstable pitting stages

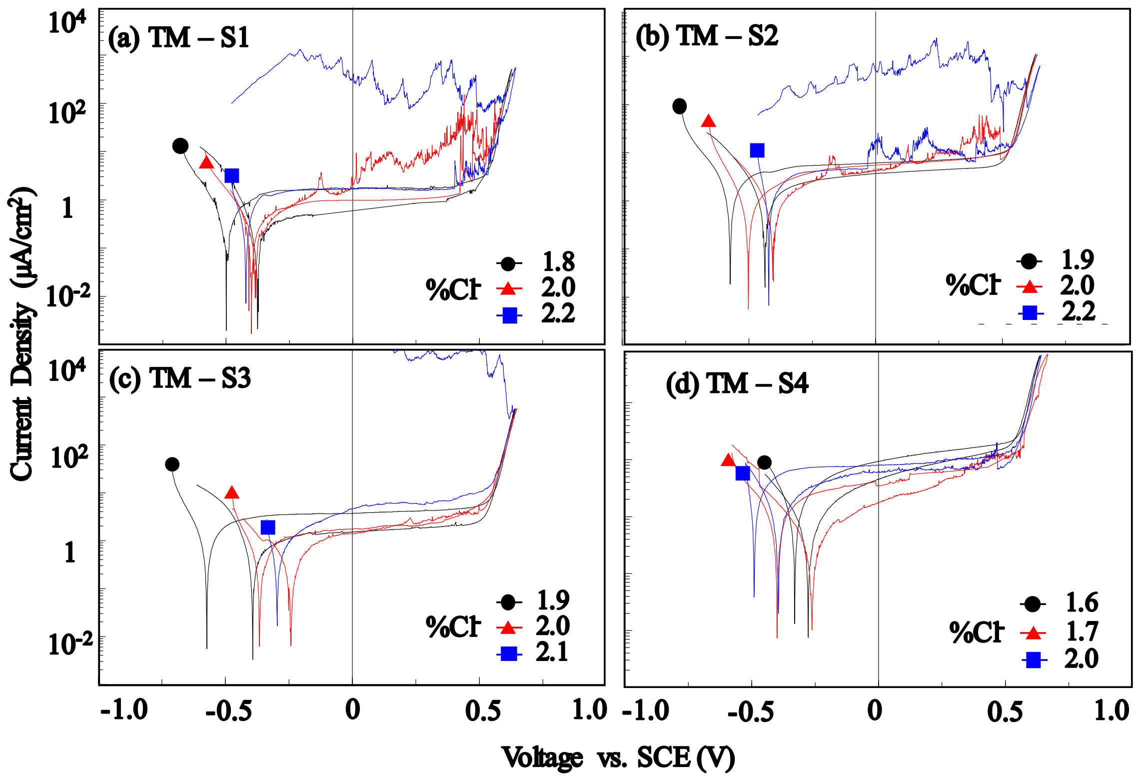

Figure 6.5: CPP test specimens of TM showing non-corrosive, initial pitting and unstable pitting stages

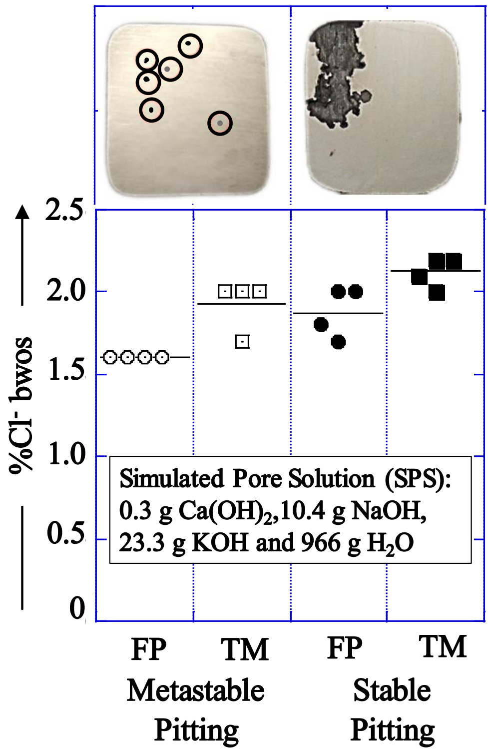

Figure 6.6: Estimated chloride threshold (Clth) of TM and FP in chloride contaminated pore solution

6.3 EFFECT OF DIFFERENTIAL CHLORIDE THRESHOLD ON SERVICE LIFE

Since the environment and experimental conditions are crucial for localized corrosion (involving pit nucleation), there are controversial discussions on the mechanisms and conclusions in pitting corrosion for steels (Strehblow 2002). However, it is expected that in similar systems with chloride contaminated pore solution, the underlying pitting mechanism (predominantly dependent on the anionic concentration) would be similar as in the current scope. Therefore, the relative percentage difference in the Cl_{th} values would remain approximately the same. The relative difference (in percentage) is associated with actual Cl_{th} values used in practice to predict the difference in the corrosion initiation time between good and poor quality steel rebars.

Based on the observations, Cl_{th} (for QST steel) is taken as that for FP for a poor quality rebar and for a good quality rebar as that of TM. As discussed in Section 6.2.2, two threshold values are considered for a rebar, one each for MSP and SP. MSP threshold may seem unimportant since the pits formed repassivate and do not affect the rebar. But, the probability of a metastable pit to grow to a stable one could not be predicted precisely

(Frankel et al. 1987). A pit nucleated out of the existing conditions need not surely repassivate and can propagate in a destructive manner. However, the observed pit is formed by the susceptibility of the material at its weak points (ferrite bands) to initiate pitting. Therefore, for SLP, MSP should also be considered as a possible point of corrosion initiation.

The absolute average Cl_{th} values (from Figure 6.6) for good quality and poor quality steel (in metastable and stable pitting cases) were not input in Life 365^{TM} for SLP. Instead, the percentage difference in threshold for poor quality steel from a good quality QST steel rebar is calculated and used as a 'reduction factor' on the absolute average Cl_{th}. The relative difference is 16% for MSP and 11% for SP. The threshold by weight of concrete (bwoC; required for input in Life 365^{TM}) is calculated from threshold by weight of cement (bwoc) by assuming the cement content as 350 kg/m^3.

An unpublished work done at the author's research lab recorded an average threshold (C_{TH}) of 1.36% bwoc (0.2% bwoC) as the chloride threshold in a good quality QST steel rebar-mortar system. Therefore, 1.36% bwoc is taken as the absolute Cl_{th} and the reduction factors are applied on C_{TH}. Thus, the absolute input values for Life365^{TM} were calculated as 0.84C_{TH} (16% reduction) in MSP and 0.89C_{TH} (11% reduction) in SP.

The concrete properties are assumed for a typical OPC concrete mix with 350 kg/m^3 of cement without any additives. To generalize the cases in different concrete mixes, all parametric inputs except diffusion coefficient and Cl_{th} were kept constant. The concrete cover is assumed as 60 mm with a surface chloride concentration of 0.8% bwoC built up in 1 year. This is a typical case at the marine tidal zone to limit the effect of surface chloride build-up time on service life. The diffusion coefficient (D_c) was varied in the assumed range of 10^{-13}(low permeability cover; high-performance concrete) to 10^{-11}(relatively permeable and low strength concrete) m^2/s with a decay factor (m) of 0.2. There is a marked reduction of 15-18% in the service life till MSP formation when compared to a 10-12% reduction in SP formation. Based on the conclusions from Section 5.3, lower diameter (predominantly 8,10 or 12 mm) rebars show the defective TM rings. Hence, the reduction in service life is crucial, since these rebars (where the defects are prominent) are mostly used as stirrup bars which become the first level of attack by the corrosive agents.

It is observed that the reduction in service life between a good quality to poor quality steel was significant in smaller D_c values and decreased with increasing D_c. This shows that the effect of differential Cl_{th} is notable when the quality of concrete used is high. Once the chlorides cross the concrete cover, the corrosion initiation depends predominantly on the corrosion resistance of the embedded steel. Although the reduction in service life (in percentage) is significant, the absolute service life should be read along with the other concrete parameters including mix type and cover provided. This is because both 4.5 (in 30 years) and 15 (in 100 years) year reductions in service life will correspond to the same 15% reduction. However, the former case may not be a significant example to substantiate the argument. In general, the corrosion initiation time over the service life could significantly reduce if a poor quality rebar (with defective TM-phase) is used over a good quality QST steel rebar.

6.4 IMMERSION CORROSION TEST RESULTS ON BARE QST STEEL BARS

6.4.1 Response in chloride contaminated SPS (1.6% Cl^-)

The Type 1 and Type 2 specimens did not respond to chloride concentrations of 1.6 to 2.8% in SPS. Even though the concentration was above sea water, the suppression effect by the continuous supply/availability of hydroxyl ions in the highly alkaline SPS tends to repassivate the passive layer breakage. Metastable pits were observed in points where the surface had near-micro dents. Hence, to accelerate the condition, the passivated steel rebar was transferred to 0.06% Cl^- in distilled water solution.

6.4.2 Response in chloride contaminated distilled water solution (1.6% Cl-)

In this case, TM and FP regions in the immersion test started corroding together without a distinguishable (visibly) preferential corrosion over a single phase in both Type 1 and Type 2 specimens. The corrosion initiation was fast and pitting started at multiple points in less than 30 minutes. The initial image when pits started forming is given in Figure 6.7(a) and Figure 6.7(d). The spots were seen in both FP and TM regions. However, the type of pitting (metastable or stable) could not be confirmed and was monitored on a daily basis. The dashed circle corresponds to an area of FP and the others correspond to TM.

The corrosion propagation was rigorous in the initial days and started to slow down after day 4. This is probably attributed to the settling of products over the surface of the steel hindering the penetration. The disturbance of these products to fall off the surface initiates further (visible) corrosion.

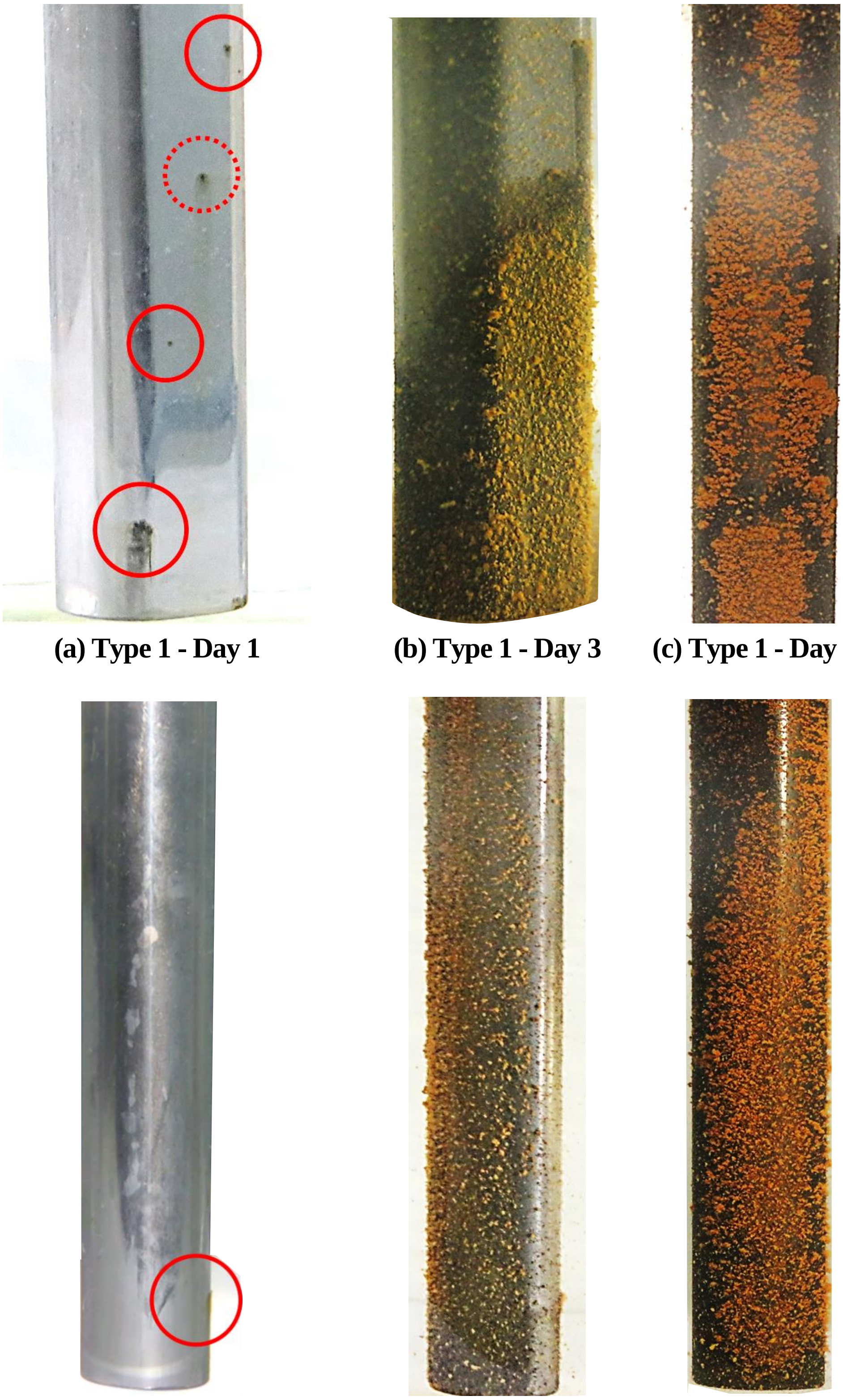

(a) Type 1 - Day 1 **(b) Type 1 - Day 3** **(c) Type 1 - Day 14**

(d) Type 2 - Day 1 **(e) Type 2 - Day 3** **(f) Type 2 - Day 14**

Figure 6.7: Immersion test – Pitting in Type 1 & Type 2 specimens

6.4.3 Response in chloride contaminated distilled water solution (0.06% Cl^-)

An additional Type 1 specimen was exposed to a lower concentration of Cl^- (0.06%) in distilled water for better control on the corrosion rate. Considering the rigorous reaction at 1.6% Cl^-, the concentration was reduced drastically to 0.06 % Cl^- to check the susceptibility of FP over TM in an as-received bar. However, similar to the previous case, there was sudden initiation in less than 30 minutes. This shows that the threshold in sea water without hydroxides are much less. The observations were the same as in the case of 1.6% in this case also. The exact points of initiation and the propagation could not be well-captured in this case too.

6.4.4 Analysis of surface cleaned specimens after pitting

Thus the initiation probability was not much different for a poor quality steel rebar owing to the high availability of chlorides. The chloride threshold in distilled water was expected to be less than that for chloride contaminated SPS. After the test for 14 days, the Type 1 and Type 2 specimens were cleaned using ASTM G1 solution to check the corroded surface after pitting. The surface profile for Type 1 and Type 2 specimens are given in Figure 6.8. The distribution of pits is scattered and cannot make a conclusive observation on the preferential pitting of FP over TM. Islands of pits are mostly observed near the TM-FP interface. Also, the pit depths are comparatively higher for the area of FP over TM.

However, the cross-section seems to have pits formed at FP preferentially over TM. This observation is common in both Type 1 and Type 2 specimens. The images are shown in Figure 6.8. This is in fact, an indication that FP might have localized corrosion over TM in an as received bar.

The random and continuous corrosion over the circumference could be a dominant mechanism due to the higher area and nearest availability of TM over FP in the solution. Also, the specimen dimensions and shape could have an effect on the circumferential pitting patterns observed. Also, the real-time specimens have a rough texture with oxide films while placing it inside the concrete. The mechanism observed here might not exactly simulate a site condition.

Hence, it is concluded from a metallurgists' point of view that there will be a preferential corrosion of FP over TM in the case of PQ steel rebars. However, in a civil engineer’s standpoint, this difference is not significant to make a significant difference in the performance or servile life of a concrete structure.

Figure 6.8: Immersion test – Pits on the cross-section and circumference visible in Type 1 (Left) & Type 2 (Right) specimens after cleaning

CHAPTER 7

RESULTS: MECHANICAL CHARACTERISTICS

7.1 INTRODUCTION

The tensile test results are given in the following sections. The test methods and materials involved in this section are given in Section 4.5.

7.2 COMPARISON OF MECHANICAL BEHAVIOUR OF FP AND TM

The tensile test was done for a specimen diameter of 5 mm in a gauge length of 25 mm. The specimen length was 20 mm and the gap length after setting up on UTM was 10 mm. The loading rate was 1.25 mm/s based on the codal provisions.

7.2.1 Stress-strain graphs of FP and TM

The stress-strain behaviour of the extracted FP and TM specimens are given in Figure 7.1. The characteristic values are also shown along with the graphs.

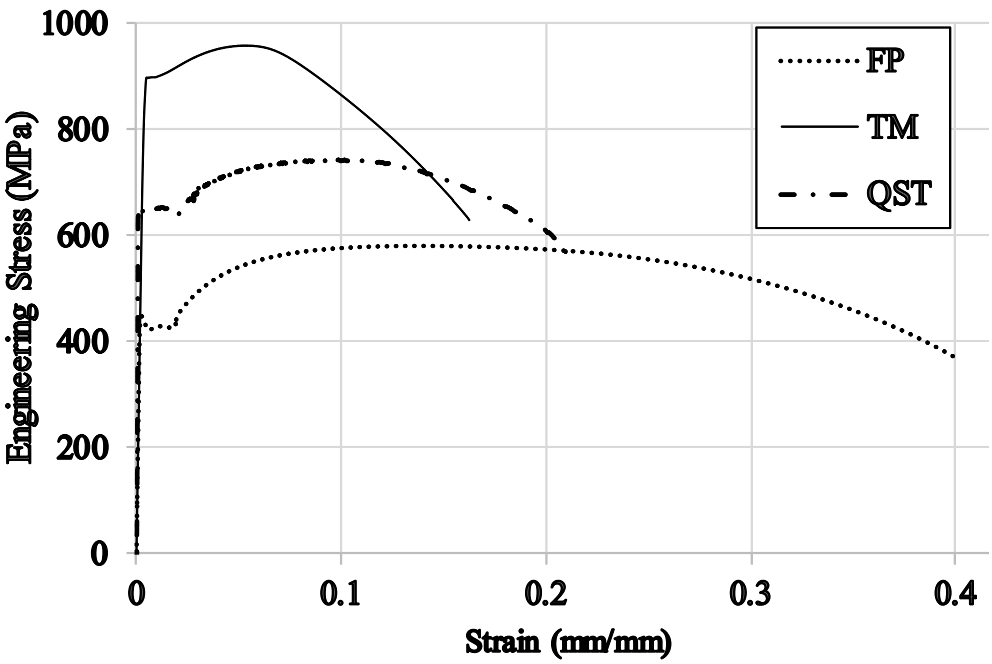

Figure 7.1: Stress-strain behaviour of FP and TM

It is clear that FP is more ductile (60% higher) than TM. However, FP has a 50% lower yield strength (around 450 MPa) than TM (around 900 MPa). E-value for both specimens were around 200 GPa. The TS/YS ratio for TM was lower than FP. The plateau near ultimate stress is relatively longer for FP which shows its ductile nature. This is reflected in a final elongation of 40% for FP when compared to 16% for TM (almost 2.5 times)

The third graph denotes an actual QST steel rebar with an intermediate behaviour between FP and TM. The lack of ductility in TM and strength for FP are cleared by pulling these values up in the composite response. The composite behaviour showed an increase of around 50% in the YS from FP and 30% in the final elongation from TM. It was found that the YS_{QST} was the average of YS_{FP} and YS_{TM}. The results conform with the strength characteristics of a QST steel rebar, which is predominantly given by TM, whereas the ductility is given by FP.

7.2.2 Failure pattern of FP and TM

The failure patterns closely agree to the theoretical formation as shown in Figure 7.2. FP showed a nearly ductile failure. There was a 'cup and cone' failure pattern. However, the end shear due to the jerk at failure causes a slip plane to form. Otherwise, the failure pattern of FP clearly resembles that of a typical ductile material.

Figure 7.2: Failure patterns of FP (top) and TM (bottom)

For TM, although a slight neck has occurred, the failure was by predominant shear with the shear planes visible in the image. The failure plane was not flat as in a typical brittle failure. However, multiple shear planes that slipped and ruptured is visible on the failed surface.

The failure pattern of QST steel rear is shown in Figure 7.3. The rebar was tested under tension at a loading rate of 1.25 mm/min. It is usually found that the core resembles that of a ductile material with semi-cup cone failure. However, since the periphery is brittle, towards the failure, the rebar shears off as clear from Figure 7.3. This closely follows the hypothesis and can be considered as a semi-ductile material.

Figure 7.3: Failure pattern of a QST steel rebar

7.3 VARIATION IN TENSILE PARAMETERS OF GOOD AND POOR QUALITY STEEL REBARS

Figure 7.4 shows the stress-strain graphs for a set of 4 - good and poor quality (GQ and PQ) steel rebars, tested under tension. The statistical parameters are calculated and given in Table 7-1. The strain under tension was measured using a low-cost indigenously designed and fabricated clip-on type extensometer discussed in Chapter 8. It was observed that the lower limits of tensile parameters are met by both sets. However, a relatively higher scatter is observed in the case of poor quality steel rebars. The difference in stress-strain behaviour of FP and TM in poor quality rebars, combined with inadequate CSPD is responsible for this scatter. The variation is clearly visible in the dot plot shown in Figure 7.5

Both sets of rebars almost met the upper limit of yield strength (600 MPa) given in the amendment for IS 13920: 1993 (See Figure 7.6). But, the required TS/YS value of 1.25 is not met by both sets. This makes them inadequate as per BIS standards for the use in seismic zones.

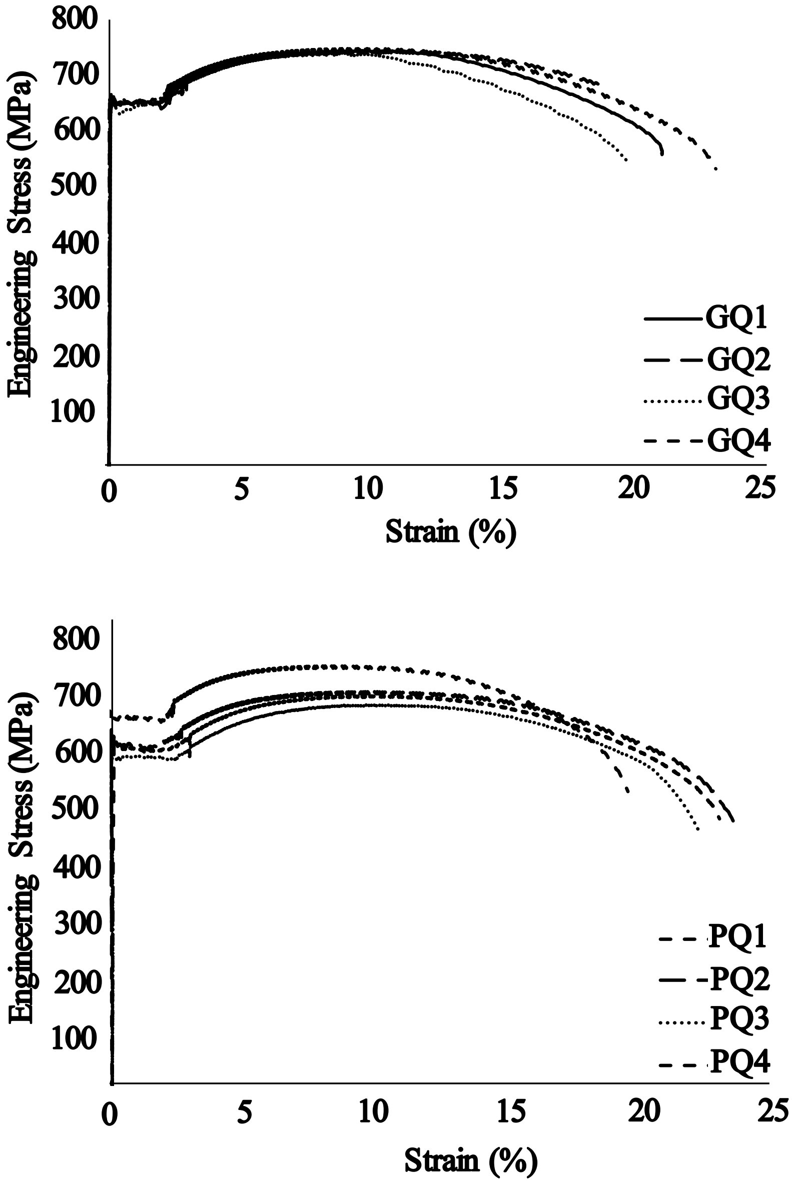

Figure 7.4: Stress-strain graphs for (a) good and (b) poor quality rebars in tension

The rebars tested were of 12 mm diameter. The variation would be profound even more in 8 mm diameter rebars since they undergo the least quality control in the manufacturing line. Since 8 mm rebars are not used as primary reinforcement, the variation might not be an issue in the primary design calculations. However, these are used in the design of shear stirrups and might pose an issue by exhibiting significant scatter in tensile behaviour, especially in seismic applications.

Table 7-1: Statistical variation in mechanical parameters

	YS	TS	% δ	TS/YS		YS	TS	% δ	TS/YS
GQ1	657.4	743.7	22.5	1.13	PQ1	638.2	720.6	24.32	1.13
GQ2	655.7	744.2	25.67	1.13	PQ2	555.7	649.9	20.57	1.17
GQ3	649.6	739.6	20	1.14	PQ3	588.0	675.9	25.53	1.15
GQ4	635.2	747.5	22.2	1.18	PQ4	596.8	669.1	23.08	1.12
μ	649.5	743.7	22.6	1.1	μ	594.7	678.9	23.4	1.1
σ	10.1	3.3	2.3	0.004	σ	34.0	29.9	2.1	0.022
CV	1.55	0.44	10.33	1.84	CV	5.72	4.40	9.07	1.91

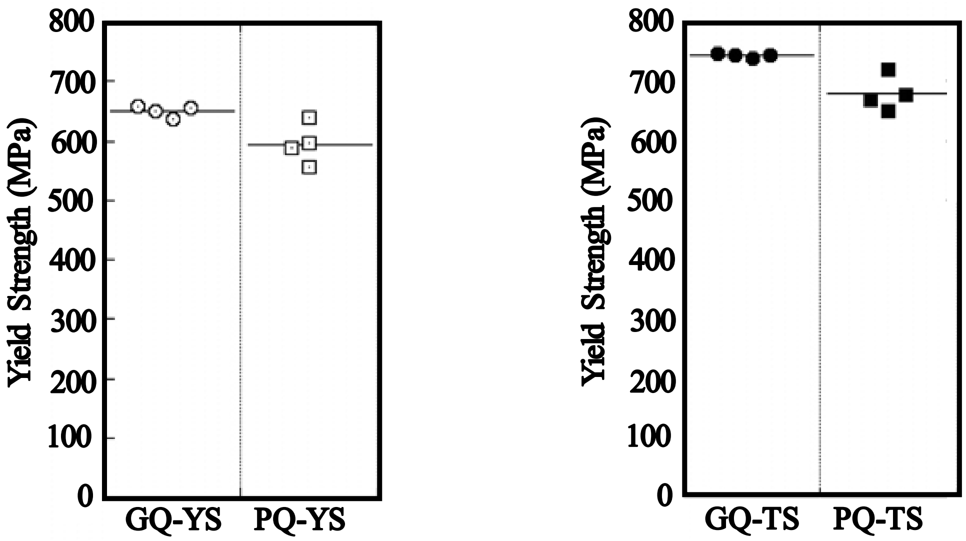

Figure 7.5: Dot plot showing the variation in yield and ultimate strength values

5.3 Steel reinforcement resisting earthquake-induced forces in RC frame members and in boundary elements of RC structural walls shall comply with **5.3.1**, **5.3.2** and **5.3.3.**

5.3.1 Steel reinforcements used shall be

(i) of grade Fe 415 (conforming to IS 1786), and

(ii) of grade Fe 500 and Fe 550, i.e., high strength deformed steel bars produced by thermo-mechanical treatment process having elongation more than 14.5 percent, and conforming to IS 1786.

5.3.2 The actual 0.2% proof strength of steel bars based on tensile test must not exceed their characteristic 0.2% proof strength by more than 20%.

5.3.3 The ratio of the actual ultimate strength to the actual 0.2% proof strength shall be at least 1.25.

Figure 7.6: Snapshot from the amendment for IS 13920: 2014

7.4 VARIATION IN CRACK RESISTANCE (BEND TEST)

7.4.1 Load v/s deflection graphs

The superimposed load-deflection graphs are given in Figure 7.7. It is evident that the scatter in the peak loads and overall load-deflection behaviour is more for poor quality steel rebars. Although the number of good quality QST steel rebar tested are less (2 sources – 2 specimens each), the scatter was less for the tested specimens. For poor quality specimens, the scatter is relatively high in terms of the angle at which peak load appears. The individual test results for each set of good and poor quality steel rebars are given in Figure 7.10. The good quality and poor quality QST steel rebars are shown in black and red colours, respectively. The dot plots showing the variation of peak loads (Figure 7.8) and the angle at peak loads (Figure 7.9) are also given.

The graphs for good quality QST steel rebar seem to coincide (approximately) as shown in Figure 7.10 (a and b). However, in Figure 7.10 (c to j), there are similar graphs which show that bending is uniform (probably owing to a good cross-section). There is a visible difference in the bending response in the same rebar in Cases d, f and h in Figure 7.10.

7.4.2 Cracking under bending

8 mm rebars are used in stirrups and hooks and are critical for achieving the desired service life. Hence, these rebars from good and poor quality lots were selected for bend test. All the rebars qualified the test for 45^{o} (or 135^{o} bend, as per IS 1786:2008 and IS 13920:1993). However, there were visible cracks in transverse (tensile cracks) and longitudinal direction by bending to an included angle of approximately 22.5^{o} (i.e. 22.5^{o} bending). A few cases of cracks were observed, as shown in Figure 7.11.

The frequency of cracking is less, and only a few of the poor quality rebars showed ‘visible cracks’ on 22.5^{o} bending. Among the 8 sources of poor quality steel rebars tested, 3 sources showed cracks under bending. However, based on the current observations, it is expected to observe cracks in rebars with close bends used in hooks. Also, the in-situ practices might not follow an exact included angle of 45^{o} for stirrups in seismic zones. Sometimes, these cracks are formed at the outer surface of the steel, which is near from the concrete surface. Then, this will be a governing factor for crevice corrosion initiation

(Jones 1996). Hence, the quality of steel rebars in stirrups with 22.5° bending (or higher) is crucial for structures in seismic zones.

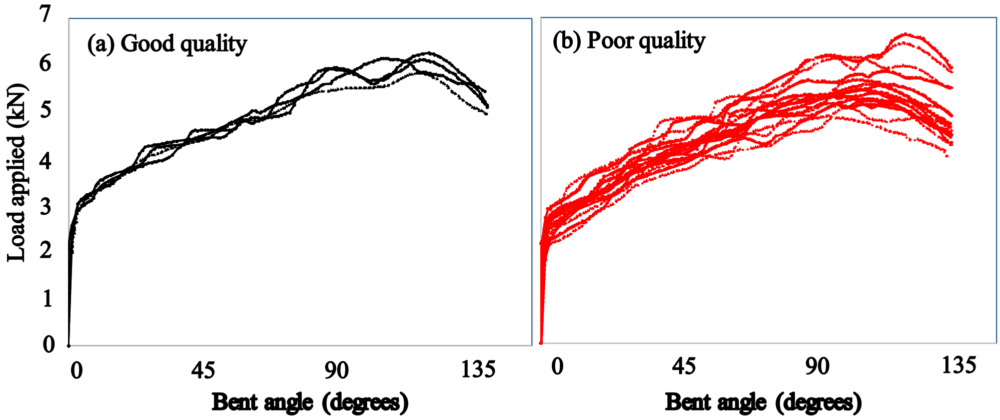

Figure 7.7: Bend test results - Load v/s bent angle

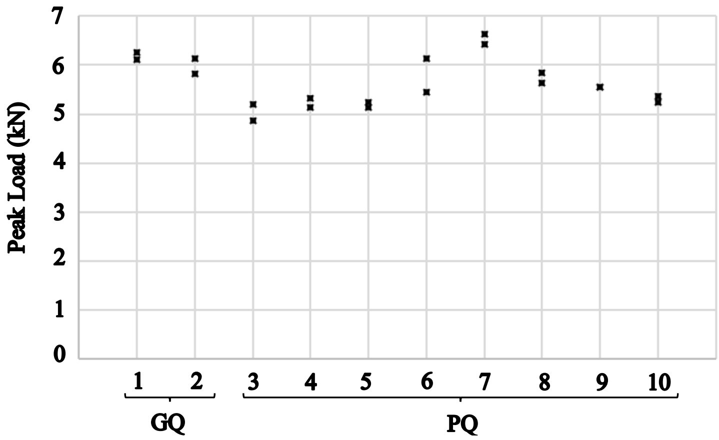

Figure 7.8: Dot plot showing peak loads in bend test

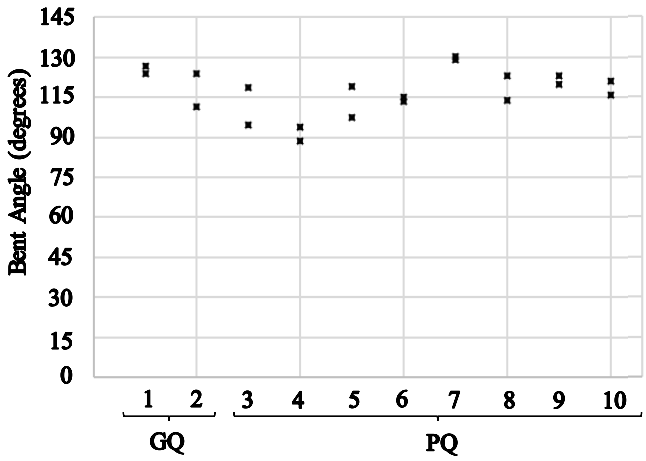

Figure 7.9: Dot plot showing angle at peak load in bend test

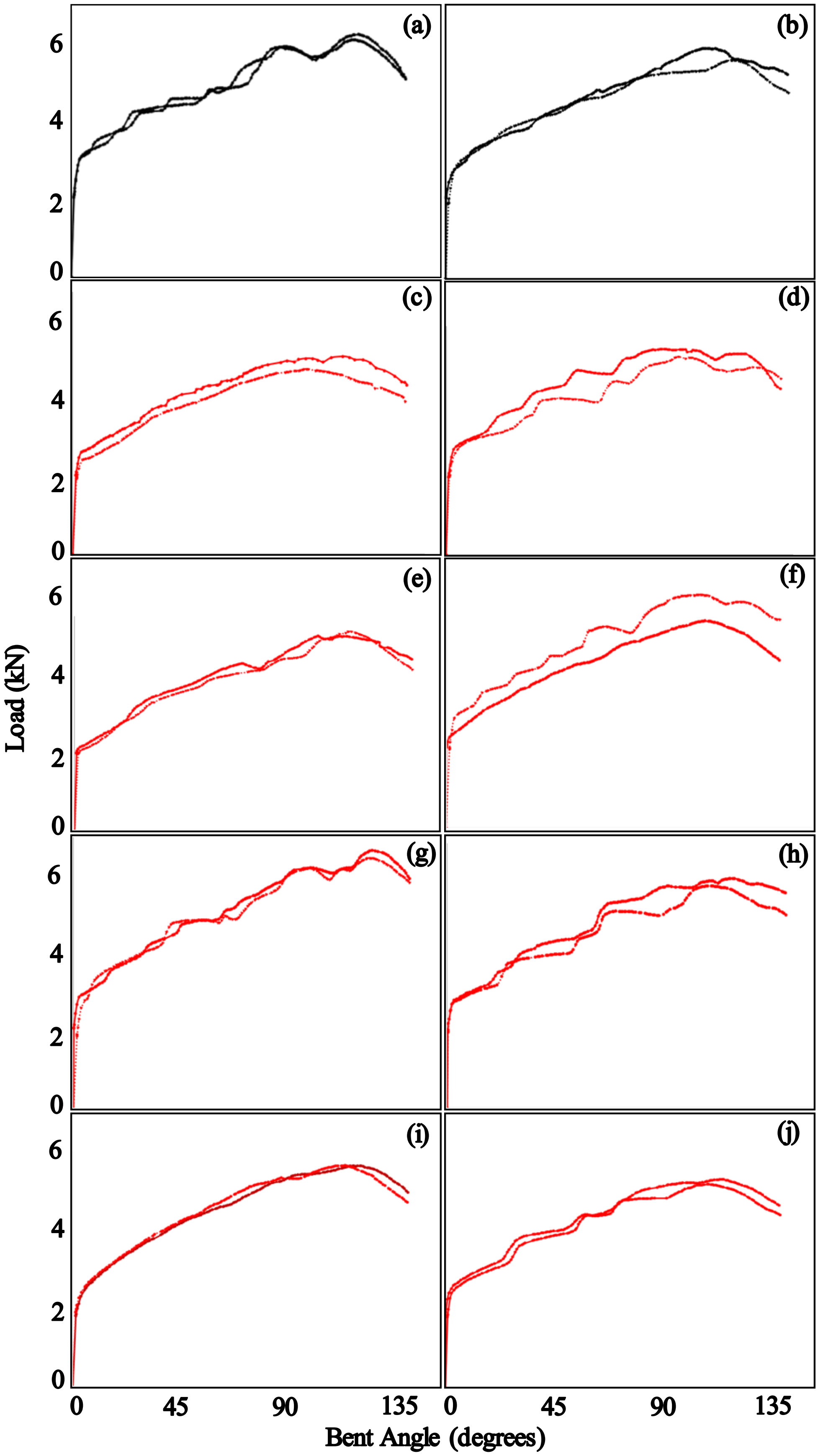

Figure 7.10: Bend test results - load versus bent-angle

Several poor quality QST steel rebar specimens showed stretch marks on the convex bent surface at 22.5^{o} bend. These could not be considered as visible cracks. However, the rebars would have started forming cracks at this angle and are located mostly near the rib roots. These comply with the observations made in the literature on stress concentrations near the rib roots. Few other specimens showed mill scales opening up which were also not considered as crack openings.

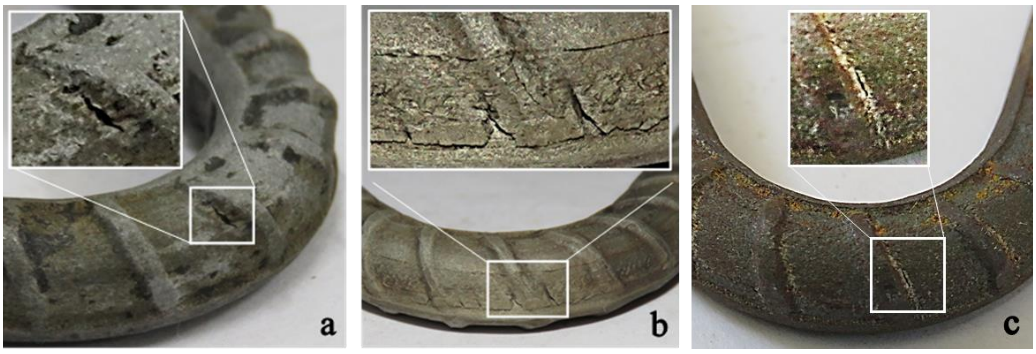

Figure 7.11: Cracks formed during bend test

7.4.3 Mechanism of cracking in poor quality QST steel rebars

Specimens from good quality and poor quality QST steel rebars were analyzed for CSPD in the bend region after the bed tests. This was done by milling the bent bar to a depth (from the surface) where the crack-ends were visible. The images of the macro-etched bent surface are given in Figure 7.12. It is evident that a good quality QST steel rebar has a perfect TM-ring and the bending stress at the extreme fibres are taken care by the hard TM. However, in a poor quality QST steel rebar, the specimen with severe cracking (both transverse and longitudinal) showed multiple locations of crack formation visible on the milled plane. It is noticed that the transverse cracks propagate in the longitudinal direction along the TM-FP interface. The delamination of TM over FP is probably due to the strain incompatibility at high loads.

The milling should ideally be done till the centre of the crack length where it would have originated. At this location, there is a probability of finding an FP phase. This defective CSPD will attract cracks at the locations of FP appearing at the extreme fibres. This is because FP has only 50% of the YS compared to TM. Once the crack starts, it propagates along the rib root/boundary. However, the reason for multiple crack formation could not be explained. Once a crack form, the failure could focus and stresses concentrate at the initiated point. However, in the current case, there is more than one point where the cracks have initiated. This could be explained if the cracks had started from the inside Hairline cracks are visible at the TM-FP interfacial region. When the stresses exceed the limiting stress of FP, hairline cracks start to form at the interface and propagate outward. This might result in multiple crack locations as shown in Figure 7.12.

An aternate bent-specimen which showed a single point of crack was milled till the centre of the crack. However, the milled section upopn etching did not show any FP near the periphery. It was noticed that the thickness of TM was varying in the case of poor quality steel rebars. This change in thickness of TM might also result in the crack formation due to higher stresses, at relatively thinner sections of TM.

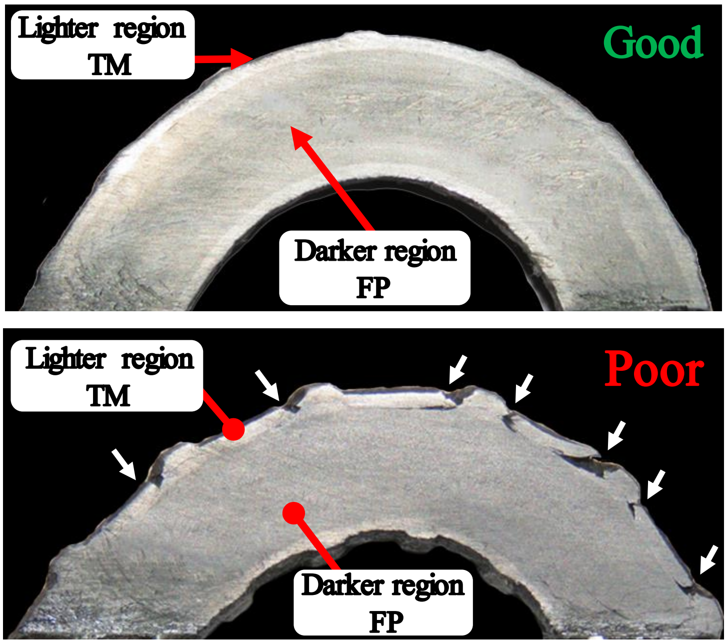

Figure 7.12: Bent sections of a good quality and poor quality rebar: milled and etched showing TM and FP

CHAPTER 8

DESIGN AND FABRICATION OF A CLIP-ON EXTENSOMETER

8.1 INTRODUCTION

Section 2.11.1 through 2.11.5 discussed the classification and history of extensometers, with a brief on transducers, strain gauges, and clip-on type extensometers. Section 8.4 is the overview of the extensometer fabricated and the working principle involved. Sections 8.5 through 8.7. explains the design and fabrication of the extensometer through the materials/methods involved, mechanical design, and electrical design. Sections 8.8 and 8.9 discusses the calibration and real-time tensile test using the prototype developed, respectively. Section 8.10 is on the cost analysis of the fabricated extensometer. Section 8.11 discusses the challenges faced in various stages of this instrumentation project.

8.2 STRAIN-GAUGE BASED CLIP-ON EXTENSOMETER (COE)

A clip-on extensometer (CoE) is named by the mode of contact of the device with the test specimen. Figure 8.1 shows a few examples of commercially available CoEs in the market for testing steel reinforcing bars ("rebars" herein). A typical extensometer has a movable element (physical or virtual), which detects the displacement in the tested specimen. In a CoE, the movable part is held (clipped-on) to the specimen using knife-edge and spring/clamp system. All the models shown in Figure 8.1 use clips/clamps. The latter design (bottom left image) is typically used for relatively longer gauge lengths than the former design (top left image) in Figure 8.1. Modern CoEs record the output data automatically. These automatic CoEs are classified into two types based on the measuring element viz. Linear Variable Differential Transformer (LVDT) devices and strain-gauge devices (Vial 2007); the latter being the focus of this article.

8.3 SIGNIFICANCE OF THE WORK

Extensometers are needed to understand the stress-strain behaviour of many reinforcing materials used in concrete construction industry. Generally, they are procured with high initial investments. Most of these extensometers would be compatible only with the test machines or data acquisition (DAQ) systems manufactured by the same or select providers.

There are service providers, who specialize in manufacturing extensometers alone and these devices would be compatible with any available test system. However, these customized extensometers are also relatively costly, making it unaffordable for the low-tier educational institutions and research labs. This project on the design and fabrication of an extensometer could help them to make indigenous extensometers at low cost and perform research projects on the performance of civil/structural materials. Also, the prototype developed in this work has flexibility for improvisation based on the user's test requirements.

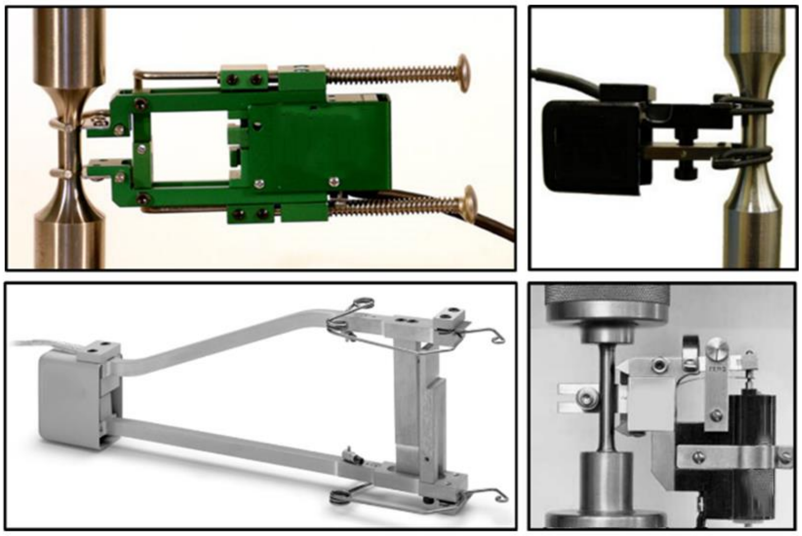

Figure 8.1: Some commercially available clip-on type extensometers

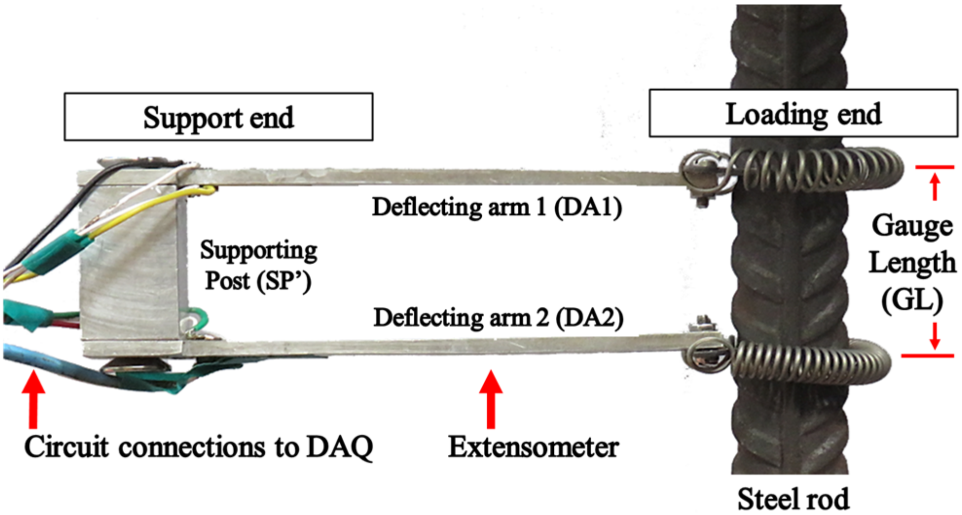

Figure 8.2: The clip-on extensometer (BTCoEM v1.0) fabricated in this project

8.4 OVERVIEW AND WORKING PRINCIPLE

This research tries to design and fabricate a CoE for the use in the tension tests for steel rebars. The CoE prototype fabricated in this research and mounted on a steel rebar for tension test is shown in Figure 8.2. The 'clipped-on' end is termed as the 'loading end' and the opposite end is termed as the 'support end'. The support end constitutes a supporting post (SP') which holds the deflecting arms (DAs). The deflecting arms are the primary part, which detects the deflection/strain experienced in the steel rod. An integrated electrical circuit employed using four strain gauges affixed to the deflecting arms determines the displacement (of the gauge length).

The CoE discussed in this article works under the principle of displacement-to-voltage translation. The fabricated CoE has a 3 part-physical body integrated with a Wheatstone Full Bridge (WFB) circuit. The resistances in the WFB circuit are four active strain gauges. Under a fixed input voltage (V_{input}), the WFB gives a unique output voltage (V_{output}) for a specific displacement of the CoE. A calibration chart is established for the CoE to correlate the specimen displacement to this change in V_{output}. The chart plots V_{output} from the WFB (on the ordinate) against the displacement at the deflecting arm's end (on the abscissa). During a tension test, the user will measure the V_{output} from the WFB circuit and calculate the actual displacement based on the calibration curve established for the CoE. The details of the mechanical and electrical circuit designs are given in the following sections.

8.5 MATERIALS AND METHODS

The materials used in the design and fabrication are divided into two: mechanical components and electrical components. The following are the materials used in the fabrication of the extensometer:

8.5.1 Mechanical components

The mechanical body of the CoE design includes a supporting post, a pair of deflecting arms, a pair of knife-edges, a pair of tension springs, and counter-sunk screws. The details on the design of these parts are given in Section 8.6.

(i) **Mechanical Body (supporting post and deflecting arm)**: The body should preferably be made of lightweight, elastic and fatigue resistant material. The final product should not be too heavy for the use in a tension test. The lightweight and small size would help in easy placement and control while testing. These are the conditions for material selection in the current scope.

Thus, the mechanical body was fabricated using a high strength and fatigue-resistant aircraft-grade aluminium (ASM 6061-T6). Relatively less durable materials like acrylic or stainless steel were not used based on this criterion. The mechanical parts were cut using conventional cutting/milling machines and Computerized Numerical Control (CNC) machines.

(ii) **Knife edge**: These should preferably be made using hardened steel. Stainless steel has been used on a trial basis in this scope. However, strength and longevity will be comparatively better for hardened steel over stainless steel. The hardness shall be value should be greater than that of the material tested. In the current scope, the surface hardness of the specimen is 280-320 BHN. The stainless steel knife-edges were prepared using laser cutting.

(iii) **Tension spring**: The tension spring anchors the CoE onto the test specimen. The stiffness and dimensions of the tension spring depend on the knife-edge design and the diameter of the rebar used. Stainless steel tension spring was used in the current work. For a 16 mm bar, the outer diameter and inner diameter of the springs were 4 mm and 3 mm respectively.

(iv) **Machine screws**: These were used for supporting post-to-deflecting arm and the knife-edge-to-deflecting arm joints. Stainless steel screws, nuts, and bolts were used for all the connections. The screws should preferably be countersunk.

8.5.2 Electrical components

The integral electrical circuit includes strain gauges, cyanoacrylate adhesive, single/double core shielded cable, bondable terminals, spade lugs and copper wires.

The strain gauges were of 350 ± 0.3% Ω resistance, 5 mm gauge length, and a self-temperature compensation (STC) factor of 23 (for aluminium). The strain range is ± 5 % and works at a temperature range of -75 ^{o}C to +175 ^{o}C. The constantan-backed strain gauges have a rated fatigue life of 10^6 cycles at a maximum strain level of 1500 με. Cyanoacrylate (CN) adhesive is used for the strong and durable bond between strain gauges and the aluminium body. Bondable terminals were used at soldering junctions to establish stable and neat connections using strain gauge leads and copper wires. The shielded cable (preferably double-core) shields the established circuit from the external electrical disturbances. A pair of wire (each from the 4-wire shielded cable) was used for input and output signal transfer. Spade lugs, terminal blocks and shielded cables were used to establish connections between the CoE and data acquisition system. The overall material requirement is shown in Figure 4.28.

8.6 DESIGN OF MECHANICAL PARTS

The mechanical design of the CoE has evolved through two designs (preliminary and modified). The design details are given in Sections 8.6.1 and 8.6.2. The general design of the CoE consists of a supporting post and two deflecting arms (as shown in Figure 8.2). The dimensions of the design are based on two factors: (1) the required travel length of the CoE and (2) the corresponding maximum stresses developed in the extreme fibres of deflecting arm near the support. The dimensions were decided by analyzing the stresses developed in the extreme tensile fibres of deflecting arm near the support end on a 'trial and error' basis. The deflecting arms were assumed as fixed cantilevers in the design calculations. The maximum deflections and corresponding stresses were calculated using 'simple bending theory' to arrive at an optimum set of dimensions for the CoE.

The fatigue strength should be considered instead of the yield strength for limiting stress calculations. This will keep the stresses developed within the safe limits and ensure prolonged usage of the CoE. In the absence of fatigue strength data, one-third of the yield strength may be taken as a reference. The mechanical parameters under consideration and the typical values of the materials chosen are given in Table 8-1.

Table 8-1: Material parameters of Aluminium 6061-T6

Modulus of Elasticity, E	68.9 GPa
Density, ρ	2.7 g/cc
Ultimate Tensile Strength, σ_{TS}	310 MPa
Tensile Yield Strength σ_{YS}	276 MPa
Fatigue Limit $\sigma_{fatigue}$	96.5 MPa

The knife-edges are fastened to the deflecting arms with the help of two through-holes at the end of the deflecting arm. During a tension test, the knife-edges will act as resting points for the CoE on the steel specimen. The small V-cuts on the sides of a knife - edge plate (See Figure 8.6) help in locking the tension spring. The tension spring anchors the CoE onto the specimen.

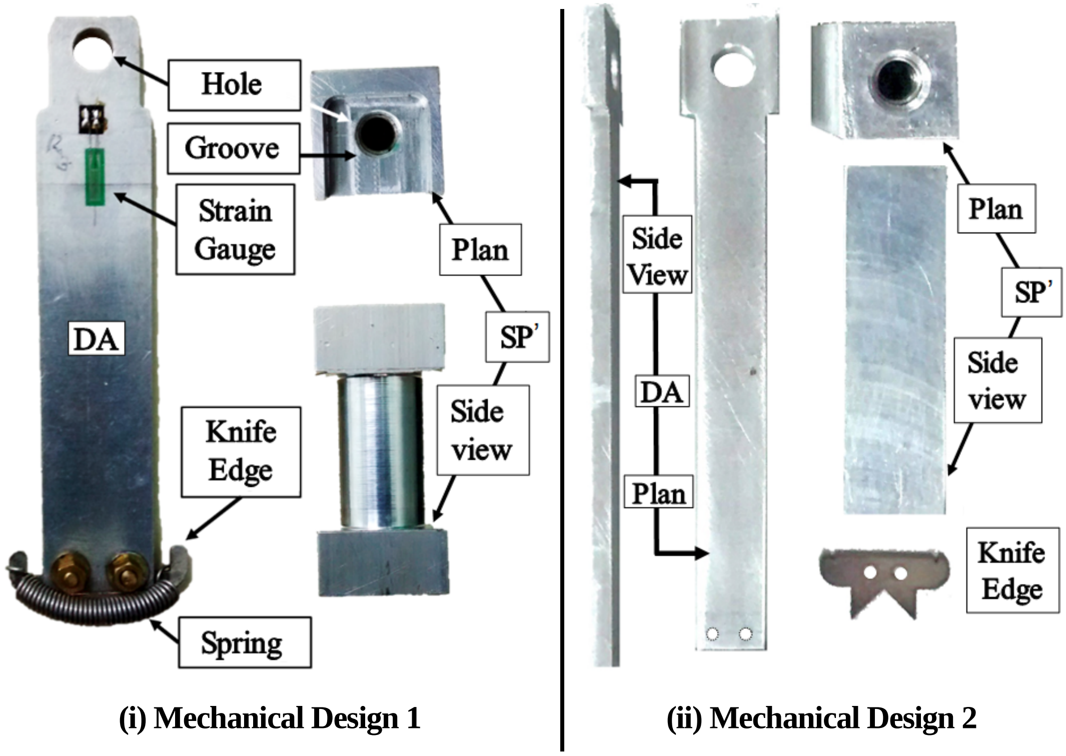

(i) Mechanical Design 1 (ii) Mechanical Design 2

Figure 8.3: Mechanical parts of the fabricated CoE

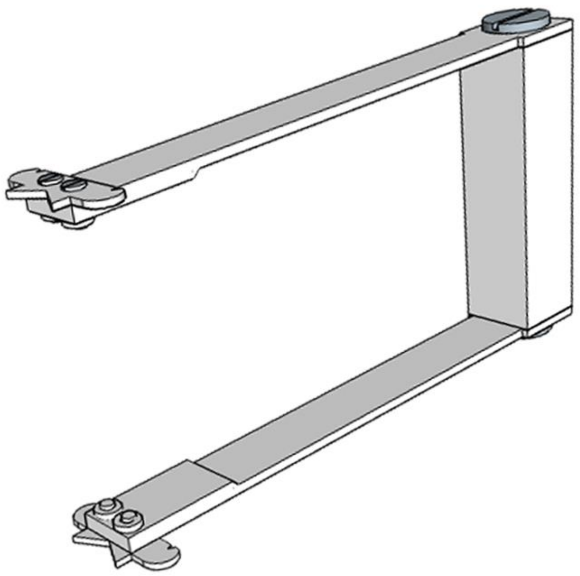

Figure 8.4: 3D model of the assembled CoE

8.6.1 Preliminary Design

The preliminary design was for QST steel rebars of diameters less than 20 mm. These rebars have a tensile strength in the range of 500 MPa along with a ductility ranging between

20 - 25% of the gauge length. Figure 8.3(i) shows the parts fabricated in preliminary design. Figure 8.4 gives a 3D-schematic of the CoE by assembling the parts shown in Figure 8.3(ii).

As shown in Figure 8.3(i), the deflecting arm was designed to fit in the seating groove (‘U’ shape) at the top and bottom sides of the supporting post. The depth of the groove was same as the thickness of the deflecting arm. The seating groove over the supporting post at the deflecting arm-supporting post connection will avoid the deflecting arm from rotating in the horizontal plane. The deflecting arm fastened on supporting post will act as a cantilever.

As per IS 1608: 2005, the proportional gauge length should be $5.65\sqrt{A}$, where A is the cross-sectional area of the rebar. This is equivalent to 5 times the diameter (eg. 50 mm for 10 mm diameter rebar) as given in ASTM E8 - 16a. If a non-proportional gauge length is used (say 50 mm gauge length for a 16 mm diameter rebar), then the values shall be factored to the proportional gauge length as per EN ISO 2566 – 1: 1999. Hence, the gauge length was fixed at 50 mm and the travel length as 25 % of the gauge length.

At the end of the deflecting arm, there are two more holes over which the knife - edges are anchored using a nut-bolt system. The knife-edge has two arms on the sides, which hold the tension spring. The tension springs hold the steel specimen towards the knife-edge during the tensile test and arrests the movement of knife-edge. A stiff and workable tension spring should be used to avoid the slippage of the tension spring over the surface of the specimen. Usually, the presence of ribs on the rebars sometimes can cause the springs to slip.

The calibration was done using a table-top calibrator (discussed in Section 8.8) connected to a universal tensile testing machine (UTM) and a data acquisition (DAQ) system. The results were satisfactory and confirmed that the integrated system is working. However, there were a few drawbacks for this design, which should be considered by the user while improving the mechanical body. The drawbacks were as follows.

1. The CoE (deflecting arms and supporting post) was bulky and heavy
2. The deflecting arm was too stiff that the maximum deflection, which the CoE could undergo, was limited (for a gauge length = 50 mm)
3. Due to the stiffness, the stress induced in the supporting post-to-deflecting arm connection was very high at the maximum displacement (Internal stress in deflecting arms were within safe limits)

8.6.2 Modified Design (BTCoEM v1.0)

The dimensions of the modified design were reduced significantly to rectify the issues faced in the preliminary design (See Figure 8.3b). The modified design was made for a travel length of 15 mm (maximum 30% for 50 mm gauge length) The maximum stress developed in the extreme tensile fibres of deflecting arm is approximately 50% of the yield stress. It is to be noted that the calculations are done assuming that the joints between the supporting post and deflecting arm are fixed. For the maximum design stress of 140 MPa in the extreme fibre, the fatigue cycle curve for aluminium 6061-T6 allows 10^6 cycles (S-N curve given in Figure 8.5) before reaching the endurance limit (Yahr 1993).

The designs of deflecting arm and supporting post were modified to make the CoE as light as possible. This was done by milling off the portions from the deflecting arm and supporting post where minimal stresses are induced.

The knife-edge detailing is shown in See Figure 8.6(e). The diameters upto 20 mm are compatible with the developed prototype. A user could modify the angle of knife-edge (shown as 30 degrees in the current design) to control the range of diameters compatible with the CoE.

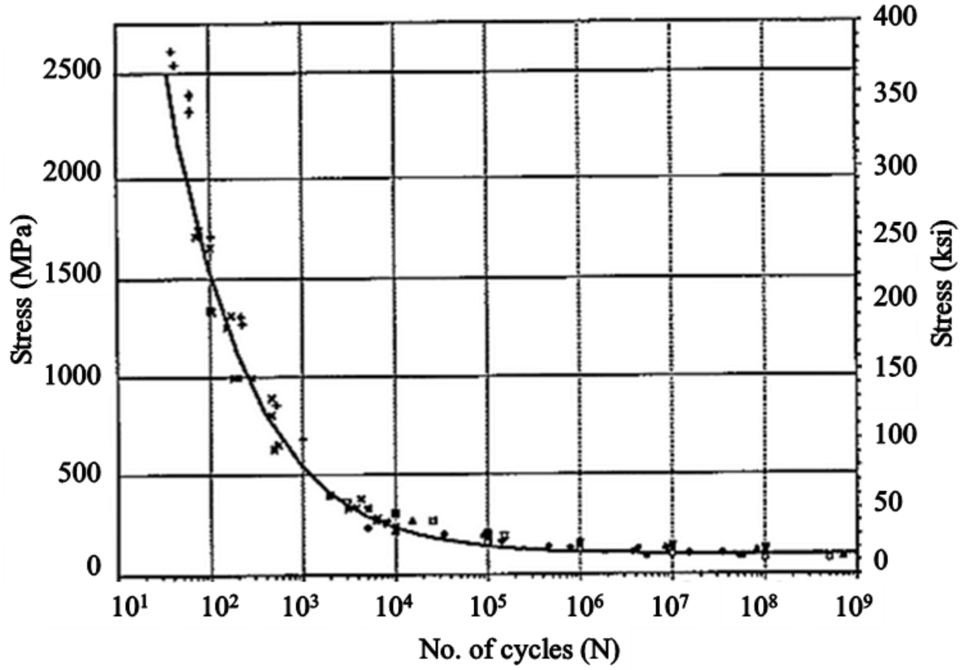

Figure 8.5: Fatigue curve for aluminium 6061- T6 (Yahr 1993)

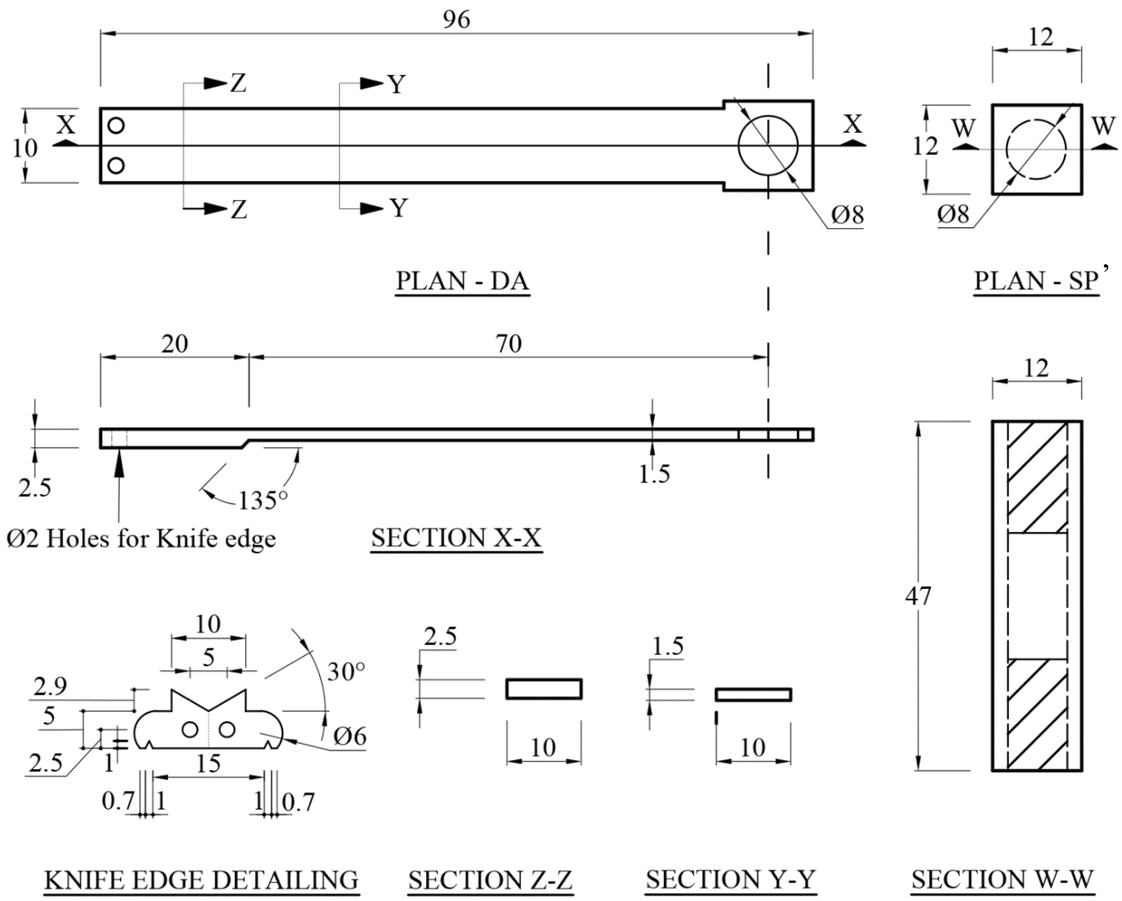

Figure 8.6: Design detailing of the mechanical parts of CoE

8.7 DESIGN OF ELECTRICAL PARTS OF BTCOEM V1.0

The electrical circuitry for the CoE involves an integrated WFB circuit. This detects the strain developed within the gauge length of the test specimen. The detection mechanism is a 3-stage process shown in Figure 8.7 from Stages 2-4 and described below.

Stage 2: As the steel specimen is axially strained under tension, the deflecting arms move apart. The bending of the deflecting arms will induce stresses in its fibres.

Stage 3: The strain gauges are pasted on the surface of the deflecting arm near the support end, one each on the inside and outside surfaces (See Figure 8.8a). The tensile and compressive strains at the extreme, inside and outside fibres respectively are thus captured by these strain gauges.

Stage 4: The strains developed result in changes in the resistance of the strain gauges. There will be four such strain gauges (See Figure 8.8a), which are connected in a WFB combination (See Figure 8.8b).The change in resistance is detected as an equivalent change in V_{output} from the WFB circuit.

1. **Test specimen** is axially pulled/elongated
2. **Deflection of the arm** at the end with knife-edge
3. **Linear strain in the arm** is taken by 2 strain gauges on either side of the arm
4. Change in **WFB output Voltage** recorded
5. **Elongation is calculated** using the output voltage
6. **Stress-Strain graph** is plotted

Figure 8.7: The flow of process in recording the stress-strain behaviour using CoE

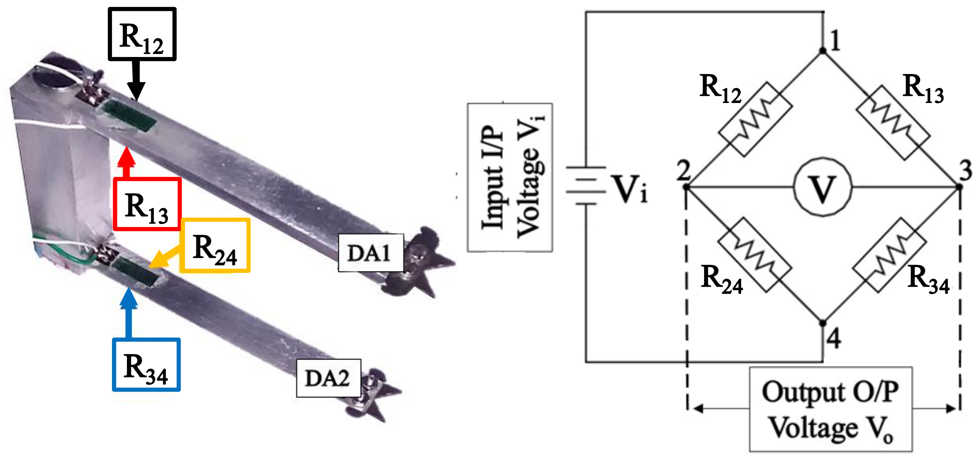

(a) (b)

Notes: R_{12} and R_{34} are pasted on the outside surface of Deflecting Arms 1 and 2, respectively

R_{13} and R_{24} are pasted on the inside surface of Deflecting Arms 1 and 2, respectively

Figure 8.8: Strain gauge placement on a CoE

In effect, the strain in steel specimen (at Stage 1) is reflected as a change in V_{output} (at stage 4). Further details on stage 3 are explained in Sections 8.7.2 and 8.7.3.

8.7.1 Strain gauge placement and specifications

The strain gauge placement has an importance in the WFB employed. The extreme fibres near the support will experience the maximum strains. To ensure the maximum sensitivity of the WFB, the strain gauges are placed near the support, where the maximum strains are experienced. However, the strain developed in a strain gauge should not exceed its maximum limits. Higher the resistance, better the sensitivity; i.e., the output voltage for a unit deflection will be sufficient if a 350 Ω resistance is used. Hence, strain gauges of 350 Ω were used to achieve the desired resolution in the displacement measurements.

8.7.2 Balanced WSFB at unstressed condition

Figure 8.8a shows the placement of strain gauges to establish a WFB circuit. Assume a WFB circuit with all the bridge resistances as 350 Ω (See Figure 8.8b). Let the V_{input} = 6 V. The following conditions are applicable in the unstressed condition as shown in Figure 8.8b.

$$\mathrm{V_{input}} = 6\ \mathrm{V} \qquad \mathrm{R_j} = 350\ \Omega\ \forall\ \mathrm{j} \in [1,4] \qquad \text{(Eq. 1)}$$

$$\mathrm{i_{14}} = \mathrm{i_{12}} + \mathrm{i_{13}} = \mathrm{i_{24}} + \mathrm{i_{34}} (\,\mathrm{i_{23}} \approx 0) \qquad \text{where } \mathrm{i_{12}} = \mathrm{i_{13}}\,,\ \mathrm{i_{24}} = \mathrm{i_{34}} \qquad \text{(Eq. 2)}$$

i_{jk} corresponds to the current in line ‘j-k’ where j, k ϵ [1, 4]. The voltage drops and resultant voltages in the circuit are given below:

$$\Delta\mathrm{V_{12}} = \mathrm{i_{12}}.\mathrm{R_{12}} \qquad \text{(Eq. 3)}$$

$$\Delta\mathrm{V_{13}} = \mathrm{i_{13}}.\mathrm{R_{13}} \qquad \text{(Eq. 4)}$$

$$\mathrm{V_2} = \mathrm{V_{input}} - \Delta\mathrm{V_{12}} \qquad \text{(Eq. 5)}$$

$$\mathrm{V_3} = \mathrm{V_{input}} - \Delta\mathrm{V_{13}} \qquad \text{(Eq. 6)}$$

Substituting the values from Eq. 1 and Eq. 2, Eq. 3 and 4 give $\Delta\mathrm{V_{12}} = \Delta\mathrm{V_{13}}$

$\Rightarrow \mathrm{V_2} = \mathrm{V_3}$ (From Eq. 5 and 6)

$\therefore \mathrm{V_{output}} = \mathrm{V_{23}} = \mathrm{V_2} - \mathrm{V_3} = 0.$

Hence, the bridge is balanced and the resultant V_{output} = 0 V in its initial position when the deflecting arm is not loaded. This is because the potential drops across R_{12} and R_{13} are the same (See Eq. 3 and Eq. 4).

8.7.3 Unbalanced WSFB at stressed condition

When the deflecting arms deflect in a real-time tension test, the WFB becomes unbalanced. Figure 8.9 shows the deflection and change in resistance of strain gauges in a single deflecting arm under a stressed condition. There are 2 strain gauges adhered on the deflecting arm near the support end, where the maximum strains are experienced. The deflecting arm under deflection will experience maximum tension on inside face and maximum compression on the outside face near the support. The strain gauge-R_{13} and strain gauge-R_{14} (in Figure 8.11) are placed at these locations on the deflecting arm to capture the strains in tension and compression, respectively. The resistance R_{13} will increase under tension and R_{14} will decrease under compression.

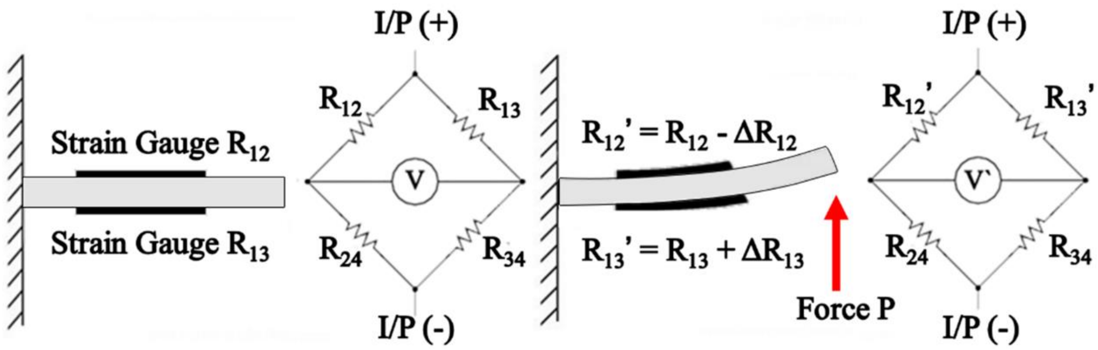

(a) Unstressed condition (b) Stressed condition

Figure 8.9: Schematic of the response of strain gauges on a deflecting arm under (a) unstressed and (b) stressed condition

Figure 8.10 shows the condition when both the deflecting arms have deflected during a tension test. In this case, resistances R_{12}, R_{24}, R_{13}, and R_{34} varies simultaneously. The resistances R_{12} and R_{13} are on the compression side whereas R_{24} and R_{34} are on the tension side. Assuming that the compressive and tensile strains are equal (and opposite) in magnitude, the net resistance of strain gauges across Lines 1-2-4 and 1-3-4 will still remain the same. Hence, Eq. 2 remains applicable in the unbalanced case. However, the unequal resistances across Lines 1-2 and 1-3 results in a non-zero potential difference between Points 2 and 3 (V_2 and V_3, respectively). Thus an unbalanced WFB gives a non-zero V_{output}.

$$\Delta V_{12} = i_{12}.R'_{12} \quad \text{(Eq. 7)}$$

$$\Delta V_{13} = i_{13}.R'_{13} \quad \text{(Eq. 8)}$$

$$V_2 = V_{input} - \Delta V_{12} \quad \text{(Eq. 9)}$$

$$V_3 = V_{input} - \Delta V_{13} \quad \text{(Eq. 10)}$$

$$\because\ \Delta V_{12} \neq \Delta V_{13} \Rightarrow V_2 \neq V_3.$$

$$\therefore\ V_{output} = V_{23} = V_2 - V_3 > 0.$$

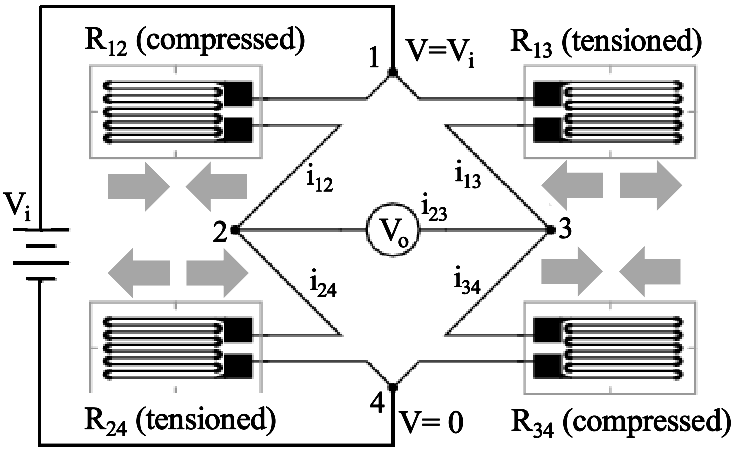

Figure 8.10: Schematic of strain gauge combination as a WFB in a CoE

Figure 8.11: Strain gauge placed and adhered over the inside and outside faces of the deflecting arm

Based on Eq. 6, the V_{output} increases as the tensile/compressive strains increase with respect to the displacement at the loading end. Hence, a single value of V_{output} from the

WFB circuit is related to a unique value of displacement at the loading end. This relation between the V_{output} and displacement is obtained by calibrating the device (discussed in Section 8.8).

8.7.4 Bridge configuration and features

A balanced bridge condition depends on the position of the strain gauge (angle of placement), actual gauge resistance (350 ± 0.3 %), temperature effects, and additional wire resistances. If the WFB shows a non-zero V_{output} at the unstressed condition, the value can be offset and the V_{output} can be recorded. The change in V_{output} per unit displacement at the loading end is of a primary concern than the absolute V_{output}. Hence, an unbalanced bridge caused by circuitry errors or improper preparation could still be used, provided the unbalanced V_{output} is approximately zero (say V_{output} = 0.5 mV for a full range of 20 to 30 mV). This zero error can be offset as a zero correction during data acquisition.

On successful fabrication, the user may give a V_{input} of 5 ± 1 V and check if the WFB is giving a non-zero V_{output}. The increase in the gap between the deflecting arms will result in a consistent increase (or decrease) in the value of V_{output}. This could be used to check if the bridge configuration is properly working.

The SGs are placed in WSFB has an indirect advantage of nullifying the temperature strains, called Self-Temperature Compensation. Assume an unstressed condition of the device where V_{output} = 0 V. At this condition, say the room temperature has increased by 10 ^{o}C and caused temperature strains in the device. However, the SG placement is such that the strains developed will be equal for the SGs and the bridge remains balanced. Hence, there is no/negligible effect on the output voltage.

8.8 CALIBRATION

8.8.1 Calibration apparatus

The calibration for an extensometer establishes the relationship between the displacement at the loading end and the V_{output}. This is established with the help of a table-top calibration apparatus. The verification procedure is given in Section 4.1 of *ASTM E83: Standard Practice for Verification and Classification of Extensometer Systems* suggests an apparatus which *'…may consist of a rigid frame, suitable coaxial spindles, or other fixtures to accommodate the extensometer being verified, a mechanism for moving one spindle or* *fixture axially with respect to the other, and a means for measuring accurately the change in length so produced…'*. It is also mentioned that *'…any other device or mechanism that will accomplish the purpose equally well…'* could be used.

An apparatus meeting these requirements was fabricated and used in this study. (See Figure 8.12) The CoE is calibrated using a table-top calibrator with a horizontal arrangement in this study (See Figure 8.13). There are four supports (numbered and shown in Figure 8.13) involved in the mechanism and discussed below.

(i) Support 1: Anchors and hold the knife edge of deflecting arm 1 on the frictionless/movable table
(ii) Support 2: Anchors and hold the knife edge deflecting arm 2 (fixed)
(iii) Support 3: Holding post for the retracing-spring that pulls the frictionless table towards the micrometer.
(iv) Support 4: Holds the micrometer in contact with the frictionless table.

The deflecting arms of the CoE are held/gripped between Support 1 and Support 2 by a suitable mechanism. The deflecting arms are anchored into grooves available at the top of these supports. A horizontally supported micrometer (at Support 1) is in contact with a 'frictionless table' (Support 4). The frictionless table is an arrangement with a platform that could easily move horizontally over a set of ball bearings with minimal friction. The platform can slide in a uniaxial direction in the horizontal plane within a maximum travel length of 15 mm). A retracing-spring arrangement between the frictionless table and Support 3 is provided. The retracing-spring will always try to pull the frictionless table towards the micrometer. Thus, micrometer could move the frictionless table for a known displacement, which in turn adjusts the gap between Supports 3 and 4.

The micrometer is adjusted to a position of 'X' mm such that the gap between support 1 and support 2 equals the gauge length of the CoE. The retracting spring is stretched to this position. The CoE is placed in the grooves, and the deflecting arms are anchored by using screws or springs to avoid sway. The micrometer reading is adjusted with respect to 'X' which moves the frictionless table and increase the displacement between the deflecting arms. At specific intervals (say every 0.5 mm) of displacements, the V_{output} is measured and recorded.

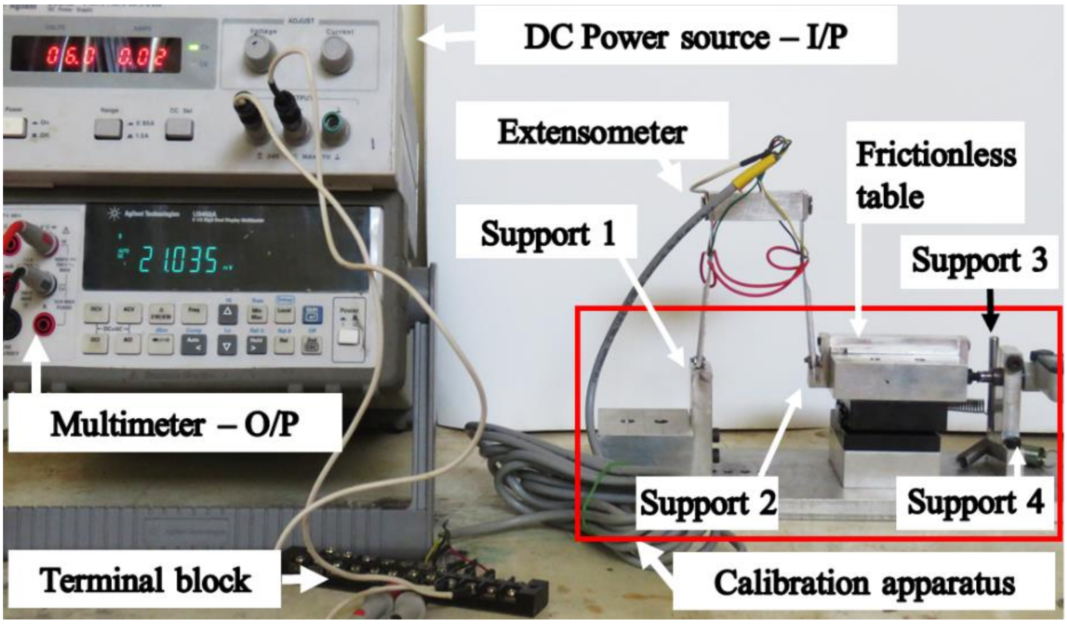

Figure 8.12: Calibration setup including table-top calibrator for the clip-on extensometer used in this study

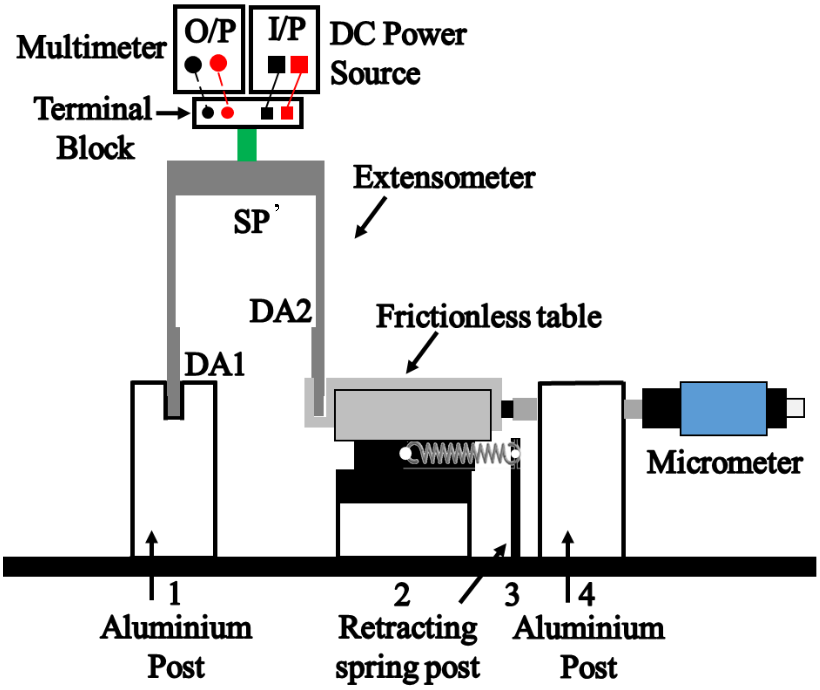

Figure 8.13: Schematic of table-top calibrator for the CoE used in this study

8.8.2 Calibration procedure

The calibration was done using the above-mentioned table-top calibrator at discrete steps of displacement, as per the following steps:

1. Setup the calibration package which includes a DC Power Supply (for applying V_{input}), a multimeter (to measure the V_{output}) and a table-top calibrator (which holds the CoE for calibration).
2. Connect the CoE to the DCPS and the multimeter to establish the WFB-response. Apply a V_{input} of 6 V and set the multimeter preferably with a least count of 0.001 mV to capture slight movements.
3. Place and anchor the CoE between Supports 1 and 2 as mentioned in Section 8.8.1. Make sure that the initial gap (between the two knife-edges) after it is placed in the table-top calibrator is almost equal to the pre-defined gauge length i.e. zero deflection at the loading end. Offset the initial V_{output} if the bridge is not balanced.
4. Slowly increase the micrometer reading in steps of 0.5 mm and measure the V_{output}. Increase the end-displacement upto the design travel length (15 mm).
5. Repeat the measurement in the reverse direction from +15 mm to −5 mm. Come back to zero from −5 mm to complete a full hysteresis loop. The cyclic calibration can be done in the displacement range for which the CoE is designed to measure.

Plot the calibration graph between the V_{output} (on the ordinate) and end-displacement (on the abscissa).

Figure 8.12a shows the CoE setup for a continuous point calibration. The continuous calibration can be done using a displacement controlled UTM. This is done by automating the CoE movement at a fixed displacement rate to execute a complete displacement cycle. The data acquisition system associated with the UTM could measure the V_{output} continuously (actuator/piston displacement) at a specific data acquisition rate (say 10 points per second). This setup is similar to the commercially available table-top calibrator.

8.8.3 Calibration chart

Figure 8.14b shows the calibration chart for the BTCoEM v1.0. Ideally, the calibration chart is a straight line. Hence, there is a constant voltage difference per unit deflection (of the CoE) at the loading end. A continuous calibration was found to be more reliable than a discrete calibration in the current study. This is probably because of the absence of lag between the readings taken and the control on the speed of the displacement. Figure 8.14b shows the calibration chart established by continuous calibration method at the displacement rate of 1.25 mm/min for 3 cycles and linearly fitted. V_{output} is assumed to be zero at zero deflection as an additional boundary condition in the linear fit.

A user could also do a continuous calibration instead of a discrete step calibration. The continuous calibration can be done using a displacement controlled UTM. This is by moving the extensometer at a fixed displacement rate to execute a complete displacement cycle. The DAQ associated with the UTM could measure the output voltage for the known displacement (actuator/piston displacement) at an instant. The required data acquisition rate depends on the design. Figure 8.14(a) shows the CoE setup for a continuous point calibration. Figure 8.14(b) shows the calibration chart established by continuous calibration method at the displacement rate of 1.25 mm/min for 3 cycles and linearly fitted.

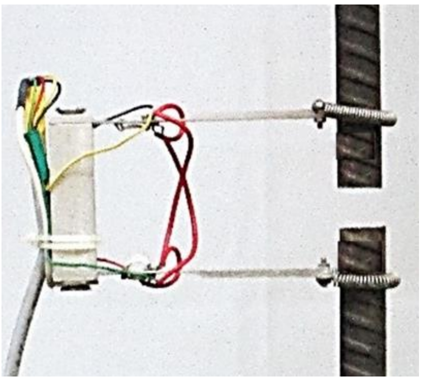

(a) BTCoEM mounted for calibration

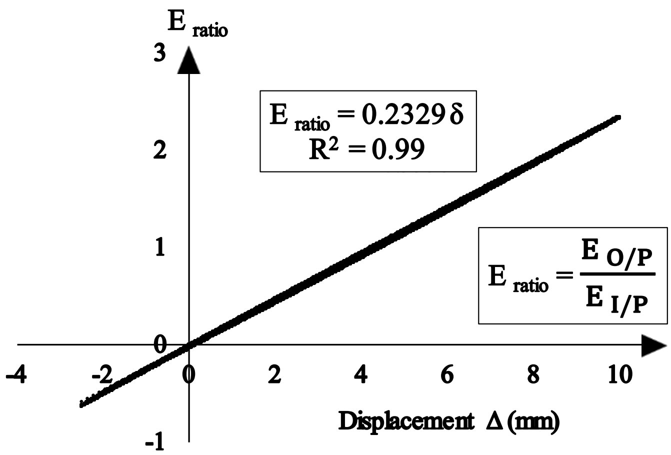

(b) Calibration chart obtained for 3-cycle data and linearly fit

Figure 8.14: Calibration chart for CoE using continuous calibration

8.9 TENSILE TESTING OF STEEL REBAR USING 'COE'

The features of the CoE fabricated in this study (Model BTCoEM v1.0) has been given in Table 8-2 and was ready for testing on successful calibration. The calibration equation was fed into the data acquisition system. Figure 8.7 from Section 8.7 gives the step by step flow in the determination of displacement using the CoE during the tension test. The displacement of the steel rod results in a deflection of the attached deflecting arm. The corresponding strains in the extreme fibres of the deflecting arm are measured by the respective strain gauges, translated to V_{output}, and recorded (Steps 2 to 6). The flow between Steps 2 through 6 is a continuous process until the specimen breaks. The recorded V_{output} is used to determine the deflection, using the calibration chart. This is used to calculate the strain in the test specimen and subsequently plot the stress-strain behaviour. Figure 8.15 shows the stress-strain behaviour recorded for a 500D grade QST steel rebar of 12 mm diameter tested using the fabricated CoE.

Table 8-2: Specifications of the fabricated BCoEM v1.0

Overall Weight	60 g
Maximum travel length	15 mm
Input voltage	6 V
Resolution	0.001 mm
Accuracy	± 5 %
Fatigue rating	10^6

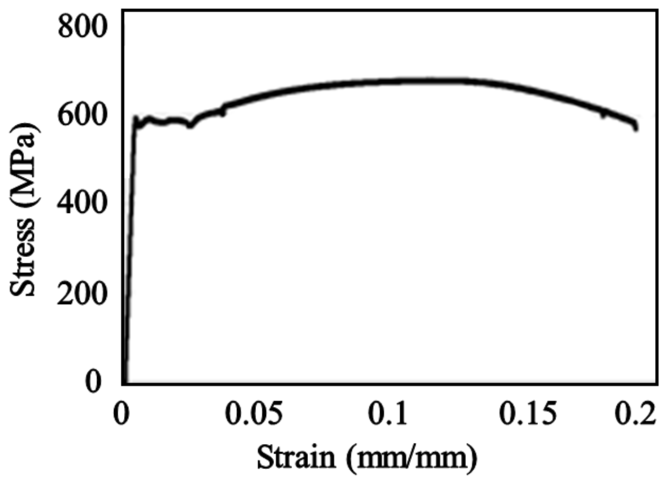

Figure 8.15: Stress-strain curve recorded using the fabricated CoE

8.10 COST ANALYSIS

The cost of the extensometer is about one-tenth the price of commercially available extensometers available in the industry with similar specifications. The approximate cost of the components is given in Table 8-3. A comparison of the final product with a few commercially available extensometers are given in Table 8-4.

Table 8-3: Cost analysis of BTCoEM v1.0 (in INR)

Part/Item	Cost (INR)	Per unit
Aluminium 6061-T6	2000	25x25x500 mm rod 260x260x5 mm plate
Other mechanical	~1000	-
Strain gauges	1500	4 Nos.
CN adhesive	2100	1 No.
Other electrical	~1000	-
Machining	~5000	-

Table 8-4: Comparison of commercially available extensometers

Company		**Epsilon**	**MTS**	**Tinius Olsen**	**IIT Madras**
Model		3542-050M-025-ST	634.25	-	BTCoeM v1.0
Classification (As per ASTM E83)		B1	B1	B1	E
Gauge Length	mm	50	50	50	50
Resolution	mm	0.0005-0.00175	0.001	0.001	0.001
Travel Length	mm	−5 to +12.5	−5 to +25	15	−5 to 25
Weight	g	30	30	-	65
Approximate Cost	INR	~1,52,000	~2,00,000	~5,00,000	~20,000

8.11 CHALLENGES FACED AND LIMITATIONS

There were several challenges faced during the design and fabrication of the prototype model. The primary challenges include the following:

1. The structural design of mechanical parts and the electrical circuit to meet the test requirements – Optimizing the dimensions of the CoE for a relatively light-weight design and required test specifications is a challenge. If the calculations go wrong, the user will end up with a design that is too stiff or stresses exceeding the fatigue or yield strength of the material with which the COE is fabricated.
2. Proper placement of strain gauges - The strain gauges on the deflecting arm should be placed by following the standard strain gauge placement procedures. The quality of the circuit integrated with the mechanical body is important. In the case of an improper alignment of a strain gauge, the WFB will be unbalanced in an unstressed state. If the strain gauges are not pasted properly using the CN adhesive, the bond will easily get damaged, and the strain gauges will be detached from the surface.

3. The rotation or sway at the supporting post-to-deflecting arm joints – This is a significant problem for a sensitive CoE. The linearity in calibration will be lost which results in error in the measurements. Care should be taken in the design to arrest these motions.
4. Proper alignment of strain gauges - It is better to avoid the errors in the WSFB by preparation errors. Follow a standard preparation manual to properly employ the circuit and have minimum zero errors.
5. Delamination of strain gauges – At times when the device is overstressed during a tensile test or if the wires are stretched while handling, the strain gauges may delaminate by shearing off the surface along with the adhesive as shown in Figure 8.16

Figure 8.16: Delamination of bondable terminals and strain gauges under stress

The following are few limitations in this study which could be considered for replicating or improvising the current design:

1. The CoE is highly sensitive to the speed of testing. The calibration and test values are valid only at low speeds (say 1.25 mm/min which is the minimum allowed as per ASTM E8 -16a).
2. The slight slip in tension springs are not accounted for, and the error may accumulate with the displacement measured (while calibration or testing).
3. The development of fatigue strains with time and its effect on the drift in calibration chart need to be studied.

The user is expected to consider these challenges while replicating this model. The limitations could be rectified, and the features could be incorporated in further improvisations of this model. The prototype developed has a lot of scope for future study to address the limitation mentioned in Section 8.10, along with varying the materials and design, to optimize the performance of the CoE.

The connectors might be different across machines, and there will be difficulty in establishing a connection between the extensometer and the UTM. Say the user have a connector as in Figure 8.17. How will a user be able to connect the fabricated extensometer is a question. Here, the user should identify the leads/ports on the pin which corresponds to input and output as shown in Figure 8.17 and Figure 8.18. Then, the connections could be established through soldering wires to those specific leads/ports (for input and output) and connecting these to the corresponding wires in the shielded cable from the extensometer through a terminal block connection. However, the compatibility and DAQ rate will depend on the system. It is advantageous to have a separate DAQ system to which direct connections could be made without any difficulty with compatible connectors/limited usage.

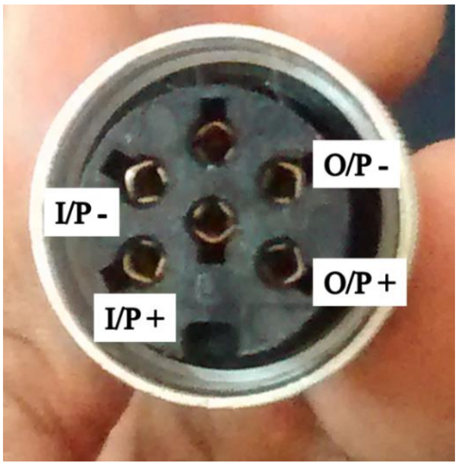

Figure 8.17: A sample male connector from CONTROLS UTM

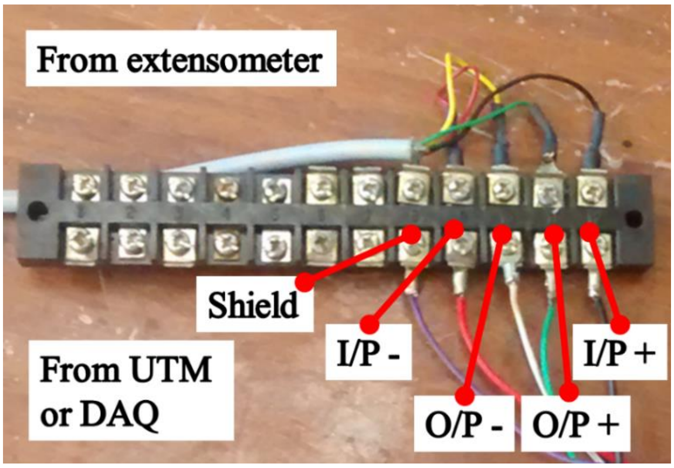

Figure 8.18: The connections joined through a terminal block

CHAPTER 9

CONCLUSIONS AND SCOPE FOR FUTURE STUDY

9.1 SUMMARY OF THE RESEARCH

Within its scope, this study introduces a potential quality control issue in the manufacturing of QST steel rebars in the Indian market. The study was executed in 3 stages viz. microstructural corrosion and mechanical studies on QST steel rebars. The presence of defects in the peripheral tempered martensite (TM) ring and ferrite-pearlite (FP) core, respectively, in QST steel rebars of 8, 12 and 16 mm diameters were identified. The potential defects were classified broadly into discontinuous or non-uniform TM-phase, and eccentric FP core. In this context, the bars were categorized as good quality QST steel rebars and poor quality QST steel rebars.

The effect of the cross-sectional defects in poor quality QST steel rebars on the corrosion resistance was evaluated by studying the individual phases (FP and TM) extracted from a QST steel rebar. These specimens were subjected to linear polarization resistance (LPR) and cyclic potentiodynamic polarization (CPP) tests. The tests were done on TM and FP phases isolated from a QST steel rebar. The results from these tests were validated using the immersion tests. The effect of the cross-sectional defects on mechanical properties was studied by comparing good quality and poor quality QST steel rebars subjected to tension tests and bend tests. The results from the corrosion and mechanical tests were correlated to the cross-sectional observations.

A ‘TM-ring test’ protocol has been developed/documented to evaluate the CSPD in QST steel rebars. The test protocol includes guidelines for specimen extraction, preparation, macroetching, analysis and documentation of results. The developed ‘TM-Ring test’ could be used by the technicians at the steel plant and construction sites to assess the quality in terms of CSPD. A 2-level acceptance criteria have also been provided.

9.2 SPECIFIC CONCLUSIONS

The major conclusions from the three different stages of this study are as follows.

9.2.1 Identification of defects in CSPD of QST steel rebars

- Discontinuities in the peripheral TM phase could occur under improper quenching.
- The defective TM-phase was observed in many cases, predominantly in rebars of lower diameter in the rebars from the Indian subcontinent.
- It was also found that the CSPD could vary across sources, across the same batch from a single source, and along a single rebar length itself.
- The cross-sectional image analysis of rebars showed that in general, TM constitutes a 35-45% of the total area of cross-section.

9.2.2 Effect of defects in CSPD on the corrosion resistance of QST steel rebars

- The effect of these TM-phase defects on the potential localized corrosion was based on CPP test results at incremental chloride concentrations. It is concluded that FP is more susceptible to pitting corrosion than TM. FP is recorded to have an 11% and 16% lesser chloride threshold (Cl_{th}) values than TM, until MSP and SP, respectively. Hence, in the presence of a discontinuity, there could be a preferential pitting at a lower chloride level (on FP) when compared to the Cl_{th} in a case with continuous TM-ring. This shows a 20% reduction in the service life between RC embedded with good quality and poor quality steel.
- The immersion tests to validate the composite action of TM and FP in a corrosive environment showed mixed observations. Most of the TM area was subjected to pitting in the circumferential area. However, FP showed preferentially more pitting in the cross-section. It was concluded that the corrosion due to surface imperfections may be predominant over the microstructural differences.

9.2.3 Effect of defects in CSPD on the mechanical response of QST steel rebars

- The bent tests on poor quality steel rebars showed visible cracks, which could result in crevice corrosion. The mechanism behind the crack formation in a poor quality steel rebar under bending need to be studied for further information.
- The mechanical parameters were found to be satisfactory for good and poor quality steel rebars. However, there is a relatively higher scatter in tensile test results for poor quality steel rebars. This is due to the variation in the area of TM and FP in steel bars with inadequate CSPD. The defective bars could also show cracks in

stirrups or bent-up bars, owing to the strain incompatibility between FP present in the extreme TM tensile fibres. Hence, the study suggests considering a check for CSPD of QST steel rebars as a mandatory regulation.

9.2.4 Design and fabrication of an indigenous extensometer for testing QST steel rebars

- As part of the mechanical study, a low-cost clip-on extensometer was designed and fabricated. The approximate cost (20000 INR) is around 1/10th the market value of a similar gauge and meets the test specifications and results satisfactorily.
- Although the accuracy is relatively less than the commercially available products, the fabricated CoE could be used in tests which could tolerate the error recorded. The calibration chart recorded was linear with a good fit. The resolution and travel length were chosen for testing QST steel rebars, with a fixed gauge length of 50 mm. The prototype developed can cater to the needs of research in low-tier educational institutions and research lab.

9.3 RECOMMENDATIONS FOR FUTURE STUDY

The scope for future studies is given below for each section of this thesis.

9.3.1 Microstructural phase distribution in different QST steel rebars

The present study has focused on 8,12 and 16 mm diameters. This work could be extended to the following aspects:

1. The study could be executed for other Indian steel grades including 415, 500, 550, 415D and 550D. The grade used is 500D in the current study.
2. Rebars including 6, 10 and 14 mm diameters can be tested for validation of the current test results. The study on higher diameter rebars (greater than 16 mm) can confirm whether the quenching process is better in higher diameters. The TM area analysis will confirm the variation and stabilization of quality of quenching for the wide spectrum of diameters.
3. The study has focused on the macrostructural response of the QST steel rebar cross-sections. The parameters including chemical composition, micro-level phase distribution, and effect of quenching parameters on the observations lay the scope for further studies in this regard

4. The presence and effect of bainite are neglected in the scope of this study. Additional information on the formation and identification of bainite is required.
5. The solution to this problem as a quality check test has been reported. However, studies in the level of quenching process and quench-boxes could be done to propose a solution to this quality control issue.
6. Along with the ‘TM-ring test’, the variation in mechanical properties and variation in hardness values along the periphery could serve as destructive methods of quality check to identify a good CSPD. Further studies could be done to frame a test procedure and acceptance criteria in this regard.
7. An alternate solution in the quality control test could be studied and proposed using magnetic techniques, if FP and TM are significantly different in their magnetic characteristics. This could serve as a non-destructive test which could be advantageous and easy for the site personnel to execute the quality check on a day-to-day basis.

9.3.2 Mechanism and susceptibility to corrosion in TM and FP

1. The present study has focused on cyclic potentiodynamic polarization tests and linear polarization resistance tests. This scope could be extended to other test methods including EIS and galvanic corrosion tests. The test results can be compared to the results from various tests and the conclusions from this study could be validated.
2. The study has isolated TM and FP microstructural specimens used to compare the corrosion susceptibility under pitting. A composite specimen under the presence of both the microstructures still need to addressed properly. The current study has shown that the mechanism of corrosion could be the dominant factor over the microstructural difference which could be validated. Hence further studies focusing on the type of corrosion and the mechanism remains a need for future study.

9.3.3 Mechanical response in poor quality QST steel rebars

1. Similar as in the case of microstructural studies, the scope could be extended to bars of higher grades and diameters, especially in earthquake grade ‘S’ bars included in the last revision of IS 1786: 2008.

2. The hardness test could be done on a comparative basis to see if there's a difference in the microstructure of good quality and poor quality QST steel rebars. However, the current results could be validated by checking the variation of hardness along the periphery of a QST rebar cross-section in a poor quality QST steel rebar. This method could also serve as a site practice to confirm if a QST steel rebar has undergone improper quenching.

9.3.4 Refinement of the extensometer design

Based on the previous section, the user is expected to consider the following suggestions while replicating this model:

1. Stopper for fixed gauge length - Place a stopper or self-centering mechanism to fix an initial gauge length, accurate to 1 decimal point in millimetres.
2. Better springs and hardened knife-edges - The springs were not designed carefully and were randomly chosen to fit the need. Also, the knife-edges were made of stainless steel, which will get worn off with time. Better springs and hardened knife-edges shall be preferred for better performance.
3. Different materials for the mechanical body (say Aluminium 2024 grade, stainless steel, or acrylic) could be used and compared in performance.

It is generally observed that the studies on QST steel rears are focussed on the mechanical and corrosion properties and reported on a comparative basis across different grades and types of rebars. However, the presence of defective CSPD and its effect on the performance of the rebars have a lot of scope for future studies. The solution to this problem lies in the quality control of quenching process especially in maintaining the quench boxes and identifying the defects as and when it happens. It is expected that further studies in this area will lead to better quality control and awareness of quality required in site practices which would benefit in the quality and durability of RC structures.

REFERENCES

Alfimov, P. T., Lamashevskii, V. P., & Makovetskii, I. V. (1983), Extensometer for measuring axial and tangential strains in tubular specimens, Strength of Materials, 15(1), 141-143.

Alonso C., Andrade C., Castellote M., Castro P. (2000), Chloride threshold values to depassivate reinforcing bars embedded in a standardized OPC mortar, Cement and Concrete Research, 30: 1047-1055.

Alonso-Falleiros, N., Hakim, A., & Wolynec, S. (1999), Comparison between potentiodynamic and potentiostatic tests for pitting potential measurement of duplex stainless steels. Corrosion, 55(5), 443-448.Gamble W. L., Thermex-processed reinforcing bars, Concrete International, 25(7), 2003 p.p. 85-88.

Al-rubaiey, S.I., Anoon, E.A. & Hanoon, M.M. (2013), The influence of microstructure on the corrosion rate of carbon steels, Eng. & Tech. Journal, 31: 1825–1836.

Ambuja Cement (2005), Steel Reinforcements – Technological Innovations, Ambuja Technical Literature Series, 107, Ambuja Cements Ltd., Gujarat.

Angst, U., Elsener, B., Larsen, C. K., & Vennesland (2009), Critical chloride content in reinforced concrete—a review. Cement and Concrete Research, 39(12): 1122-1138.

Angst, U. M., & Elsener, B. (2016), Forecasting chloride-induced reinforcement corrosion in concrete — effect of realistic reinforcement steel surface conditions, Concrete Repair, Rehabilitation and Retrofitting IV – Dehn et al. (Eds), 177–184.

AS/NZS 4671 (2001) Steel reinforcing materials, Standards Association of New Zealand, New Zealand.

ASTM A615/A615M -16 (2016) Standard specification for deformed and plain carbon-steel bars for concrete reinforcement, American Society for Testing Materials, USA.

ASTM A706/A706M -14: 2014, Standard specification for deformed and plain low-alloy steel bars for concrete reinforcement, American Society for Testing Materials, USA.

ASTM A913/A913M-15, Standard Specification for High-Strength Low-Alloy Steel Shapes of Structural Quality, Produced by Quenching and Self-Tempering Process (QST), ASTM International, West Conshohocken, PA, 2015.

ASTM E3 - 11: 1921 (reapproved 2011), Standard guide for preparation of metallographic specimens, American Society for Testing Materials, USA.

ASTM E340 -15: 1968 (reapproved 2013), Standard practice for macroetching metals and alloys, American Society for Testing Materials, USA.

ASTM G9-07: 2013 e1, Standard Test Method for Water Penetration into Pipeline Coatings, ASTM International, West Conshohocken, PA, 2013

Augusti A. (1995), In-line thermal treatment applies to straight and coiled rebars, Steel Times International, 19.2, 44.

Bannister, B. R., & Whitehead, D. C. (1991), Interfacing. In Instrumentation: Transducers and Interfacing (pp. 121-149), Springer Netherlands.

Barbieri, M., & Corvi, A. (1988), An extensometer for fracture mechanics testing of thin composite laminates, Engineering Fracture Mechanics, 30(1), 1-4.

Bartlett, M. L., Saxena, A., & Brown, R. G. (1987), Telemetric Laser Extensometry Technique for Monitoring Deflections in Small Cracks, Fatigue '87., 3, 1449-1458.

Belyakov, E. Y. (1962). Extensometer attachment for measuring long distances. Measurement Techniques, 5(3), 191-191.

Bennett, F. N. B. (1980), The no-contact extensometer, Polymer Testing, 1(2), 91-95.

Bergqvist, B., & Scherling, G. (1987), A prototype for a resistive extensometer as a strain measuring standard, Strain, 23(4), 167-174.

Bhagavathi, L. R., Chaudhari, G. P., & Nath, S. K. (2011) Mechanical and corrosion behavior of plain low carbon dual-phase steels. Materials & Design, 32(1): 433-440.

Blair, S. C., Sweider, D., Trettenero, S., & Boro, C. (1997). A new reflective optical extensometer (ROX) system for geomechanical deformation measurements, International Journal of Rock Mechanics and Mining Sciences, 34(3-4), 29-e1.

Boyle, H. B. (1992), Transducer Handbook, BH Newness Publications.

Brace, P. H. (1919), Wire testing extensometer, Journal of the Franklin Institute, 188(3), 407.

Bramfitt, B. L., & Benscoter, A. O., Metallographer's Guide: Practices and Procedures for Irons and Steels, ASM International, USA, 3, 2002.

BS 4449 (2005) Steel for the reinforcement of concrete - Weldable reinforcing steel - Bar, coil and decoiled product – Specification, British Standards Institute, United Kingdom.

Cadoni, E., Dotta, M., Forni, D., Tesio, N., & Albertini, C. (2013). Mechanical behaviour of quenched and self-tempered reinforcing steel in tension under high strain rate. Materials & Design, 49, 657-666.

Campbell, P. C. (1989). Application of microstructural engineering to the controlled cooling of steel wire rod (Doctoral dissertation, University of British Columbia).

CED 39 : 7941, Ductile detailing of reinforced concrete structures subjected to seismic forces - code of practice (First Revision of IS 13920), Bureau of Indian Standards, New Delhi, India, 2014.

Central Public Works Department (2008), Modification in special conditions for steel under para 26.2 of CPWD Works Manual 2007, CPWD Office Memorandum.

Central Public Works Department (2009), CPWD Specifications (Vol.1), CPWD Specifications.

Chenchanna, P., Krishnankutty, V. K., Mukherjee, A., & Samanta, M. (1970), Development of resonance extensometer, Experimental Mechanics, 10(3), 130-132.

Collins, S. (1965). The RF cavity extensometer, Strain, 1(2), 3-6.

Concrete Reinforcing Steel Institute (2001), Evaluation of reinforcing bars in old reinforced concrete structures, Engineering Data Report Number 48, 48, p.p. 1-6.

DIN 488-1 (2009) Reinforcing Steels – Part 1, Deutsches Institut für Normung, Germany.

Frankel, G. S., Stockert, L., Hunkeler, F., & Boehni, H. (1987). Metastable pitting of stainless steel. Corrosion, 43(7), 429-436.

Geels, K., Fowler, D. B., Kopp, W. U., & Ruckert, M., Metallographic and materialographic specimen preparation, light microscopy, image analysis, and hardness testing, ASTM International, USA, 46, 2007.

Grédiac, M., Hachani, A., & Vautrin, A. (1991), Applying a quadriaxial extensometer to the strain analysis of anisotropic structures, Composite Structures, 17(1), 37-49.

H&K India, THERMEX QST SYSTEMS Installed by H&K India, Available Online at www.thermex-qst.com/reference-list.html, Last accessed on August 2016.

Herbert Rothe Consulting Engineers, ThermoQuench© for the temperature controlled rolling of wire rod and bar products, Available Online at www.steel-consulting.de/cooling/turboq2.htm, Last Accessed on August 2016.

Hoar, T. P. (1937). The corrosion of tin in nearly neutral solutions. Transactions of the Faraday Society, 33, 1152-1167.

Holister, G. S., Jones, W. E. M., & Luxmoore, A. R. (1966), A moiré extensometer, Strain, 2(4), 27-34.

Holm, D. (1984), Installing an Axial Extensometer on a Test Specimen, Experimental Techniques, 8(12), 33-33.

IS : 13920 : 1993, Ductile detailing of reinforced concrete structures subjected to seismic forces – code of practice, Bureau of Indian Standards, New Delhi, India.

IS : 1786 : 2008, High strength deformed steel bars and wires for concrete reinforcement, Bureau of Indian Standards, New Delhi, India.

IS : 7739 (Part I) : 1975, Code of practice for preparation of metallographic specimens; Part 1 – General features, Bureau of Indian Standards, New Delhi, India.

IS : 7739 (Part V) : 1976, Code of practice for preparation of metallographic specimens; Part 5 – Iron and steel and their examination, Bureau of Indian Standards, New Delhi, India.

Islam M. A. (2010), Thermo-mechanically-treated advanced steels for structural applications, Proceedings of the international conference on marine technology (MARTEC) 2010, Dhaka, Bangladesh, 2010 p.p. 149-153.

Jang, J. W., Iwasaki, I., & Moore, J. J. (1988). Effect of martensite and austenite on grinding media wear. Wear, 122(3), 285-299.

JIS : G3112 : 2004, Steel bars for concrete reinforcement, Japan Industrial Standards Association, Japan.

Jones, D. A. (1992), Principles and prevention of corrosion, Macmillan.

Johnstone, P. G., & Elms, D. G. (1972), A ten-inch extensometer measuring small low-frequency strains, Experimental Mechanics, 12(9), 429-430.

Kabir, I. R., and Islam, M. a. (2014). "Hardened Case Properties and Tensile Behaviours of TMT Steel Bars." American Journal of Mechanical Engineering, 2(1), 8–14.

Karuppanasamy, J., and Pillai, R. G. (2016) Probabilistic corrosion rates of cold-twisted deformed and thermo-mechanically treated steel in choride contaminated mortar, The Indian Concrete Journal, 90(11): 45-55.

Kenner, V. H., Popelar, G. F., & Popelar, C. H. (1992), A Simple Extensometer for Transverse Strain Measurements during Uniaxial Loading of Moderately Compliant Materials, Experimental Techniques, 16(2), 17-19.

Kobayashi, K., & Yamaguchi, I. (2011), High Accuracy and Wide Temperature Measurement by Non-Contact Speckle Extensometer, Strain, 47(s1).

Lazarus, L. (1980), Torsional extensometer, Experimental Techniques, 4(2), 6-6.

Lebow, M. J. (1966), Extensometers, Experimental Mechanics, 6(6), 21A-28A.

Life-365 (2014) Life-365TM service life prediction modelTM and computer program for predicting the service life and life-cycle cost of reinforced concrete exposed to chlorides, URL: http://www.life-365.org/download.html/; Last accessed on February 13, 2016.

Lu, B., Li, W., Luo, J., & Chiovelli, S. (2012) Pitting susceptibility of induction-quenched pipeline with microstructural heterogeneity. Journal of Materials Science, 47(19): 6823-6834.

Lundberg, S. E. (2002). Optimization of corrosion resistance and mechanical properties on quenched and tempered rebar. Scandinavian journal of metallurgy, 31(3), 234-240.

Maffei, B., Salvatore, W., & Valentini, R. (2007). Dual-phase steel rebars for high-ductile rc structures, Part 1: Microstructural and mechanical characterization of steel rebars. Engineering Structures, 29(12), 3325-3332.

Magee, J. H., and Schnell, R. E. (2002). Stainless steel rebar. Advanced Materials and Processes, October 2002, 43-45.

Mamun Al Rashed H. M. and Shorowordi K. M., The advantage of hot-rolling process without reheating furnace on TMT/QST quality, Ranisteel, India, 2015.

Motoie, K., Sakane, M., & Schmidt, J. (1983), An extensometer for axial strain measurement at high temperature, Mechanics of Materials, 2(2), 179-182.

Markan, R. K. (2005) Steel reinforcement for India: relevance of quenching and tempering technology, Steel World, 3: 4-9.

Nair S. A. O, Gokul P.R., Sethuraj R., Nandipati S., and Pillai R. G., Variations in microstructure and mechanical properties of Thermo-Mechanically-Treated (TMT/QST) steel reinforcement bars, Proceedings of the 4th Asian Conference on Ecstasy in Concrete (ACECON), Kolkata, India, October, 2015 p.p. 325-331.

Nair, S. A. O., Pillai, R. G., Gettu, R. (2016) Corrosion characteristics of Quenched & Self-Tempered steel reinforcement bars, Proceedings of the International RILEM conference on Materials, Systems, and Structures in Civil Engineering 2016, Aug 21-24, 2016, Lyngby, Denmark, RILEM.

Nair, S. A. O, and Pillai, R. G., 'TM-ring test' - A quality control test for TMT (or QST) steel reinforcing bars used in reinforced concrete systems, Indian Concrete Institute Journal (Accepted for publication).

Nandi, S. K., Tewary, N. K., Saha, J. K., & Ghosh, S. K. (2016) Microstructure, mechanical properties and corrosion performance of a few TMT rebars. Corrosion Engineering, Science, and Technology, 51(7): 476-488.

National Institute of Health (USA), ImageJ™ (computer software), URL: http://imagej.nih.gov/ij/; Last accessed on February 13, 2016.

Nikolaou, J., & Papadimitriou, G. D. (2004). Microstructures and mechanical properties after heating of reinforcing 500 MPa class weldable steels produced by various processes (Tempcore, microalloyed with vanadium and work-hardened). Construction and Building Materials, 18(4), 243-254.

Noville J. F. (2015), Tempcore®, the most convenient process to produce low cost high strength rebars from 8 to 75 mm, Proceedings of the 2nd European Steel Technology and Application Days (ESTAD) conference, Dusseldorf, Germany, June 15-19.

Paul, S. K., Rana, P. K., Das, D., Chandra, S., and Kundu, S. (2014). "High and low cycle fatigue performance comparison between micro-alloyed and TMT rebar." Construction and Building Materials, 54, 170–179.

Pillai, R.G., Annapareddy, A. (2013) Service life prediction models for chloride-laden concrete structures: A review and nomographs, International Journal of 3 R's, 4 (2): 563-580.

Pistorius, P. C., & Burstein, G. T. (1992) Metastable pitting corrosion of stainless steel and the transition to stability. Philosophical Transactions of the Royal Society of London A: Mathematical, Physical and Engineering Sciences, 341(1662): 531-559.

Postlethwaite, J. (1983). Electrochemical tests for pitting and crevice corrosion susceptibility. Canadian Metallurgical Quarterly, 22(1), 133-141.

Poulsen, S., & Sorensen, H. (2012) Chloride threshold values–state of the art. Danish Expert Centre for Infrastructure Constructions, Danish Expert Centre for Infrastructure Constructions.

Poursaee, A., & Hansson, C. M. (2007). Reinforcing steel passivation in mortar and pore solution. Cement and Concrete Research, 37(7), 1127-1133.

Princeton Applied Research, "Application Note CORR-4". Princeton Applied Research, Oak Ridge, TN.

Rehm, G., & Russwurm, D. (1977). Assessment of concrete reinforcing bars made by the Tempcore process. C. R. M. Metall. Rep., (51), 3-16.

Renganathan, S. (2003), Transducer engineering, Allied Publishers Limited.

Rai, D. C., Jain, S. K., & Chakrabarti, I (2012). Evaluation of Properties of Steel Reinforcing Bars for Seismic Design. Proceedings of the fifteenth world conference on earthquake engineering, Lisbon, Portugal.

Ray, A., Mukerjee, D., Sen, S. K., Bhattacharya, A., Dhua, S. K., Prasad, M. S., Sahu, A. K. (1997) Microstructure and Properties of Thermomechanically Strengthened Reinforcement Bars : A Comparative Assessment of Plain-Carbon and Low-Alloy Steel Grades, Journal of Materials Engineering and Performance, 6(3): 335–343.

Rocha, M., Brühwiler, E., & Nussbaumer, A. (2016). Geometrical and Material Characterization of Quenched and Self-Tempered Steel Reinforcement Bars. Journal of Materials in Civil Engineering, 28(6), 04016012.

Samoilenko, V. N. (1960), Portable extensometer for measuring deformations at high temperatures, Measurement Techniques, 3(10), 856-857.

Sarkar, P. P., Kumar, P., Manna, M. K., & Chakraborti, P. C. (2005). Microstructural influence on the electrochemical corrosion behaviour of dual-phase steels in 3.5% NaCl solution. Materials Letters, 59(19), 2488-2491.

Schafer, G. J., Gabriel, J. R., & Foster, P. K. (1960). On the Role of the Oxygen Concentration Cell in Crevice Corrosion and Pitting. Journal of the Electrochemical Society, 107(12), 1002-1004.

Selig, E. and Reinig, I. (1982), Vertical Soil Extensometer, Geotechnical Testing Journal, 5 (3/4), pp. 76-84.

Siemens VAI (2010), Solutions for long product rolling mills, Metals technologies

Simon, P., Economopoulos, M., & Nilles, P. (1984). TEMPCORE, an economical process for the production of high quality rebars. In METEC 84(Steel Rolling, Second International Conference) (p. 1984).

Sinclair, I. (2000), Sensors and transducers, Newness Publications.

Sjöström, S. (1961), An equiangular rosette-type extensometer., Experimental Mechanics, 1(10), 129-133.

Smart, B. G. D., Singh, R. N., & Isaac, A. K. (1978), Design and development of the magnetic cantilever extensometer, International Journal of Rock Mechanics and Mining Sciences & Geomechanics Abstracts, 15 (6), pp. 269-276.

Smarter Building Systems LLC., Basalt Rebar from smarter building systems, Available Online at http://basalt-rebar.com/, Last accessed on May 2017.

Sommer, C., & Sommer, S. (2005). Complete EDM Handbook: Wire EDM, RAM EDM, Small Hole EDM; Practical Information for Designers, Engineers, Machinists, Tool and Die Makers, Mold Makers and Others in the Metal Machining Fields. Advance Publications.

Szklarska-Smialowska, Z. (2002) Mechanism of pit nucleation by electrical breakdown of the passive film. Corrosion Science, 44(5): 1143-1149.

Szklarska-Smialowska, Z., & Mankowski, J. (1978). Crevice corrosion of stainless steels in sodium chloride solution. Corrosion Science, 18(11), 953-960.

Strehblow, H. H. (2002). Mechanisms of pitting corrosion. In: Corrosion Mechanisms in Theory and Practice, CRC Press, 243-285.

McCafferty, E. (2010). Crevice corrosion and pitting. In Introduction to Corrosion Science (pp. 263-313). Springer New York.

Tourlonias, M., Bueno, M. A., Bigué, L., Durand, B., & Renner, M. (2005), Contactless optical extensometer for textile materials, Experimental mechanics, 45(5), 420-426.

Usher, M., & Keating, D. (1996). Sensors and Transducers: Characteristics, Applications, Instrumentation, Interfacing. Maxmillan.

Vekey, R. C. (1974), An LVDT extensometer for tensile studies of composite materials, Journal of Materials Science, 9(11), 1898-1900.

Vial, G.: Automatic extensometers. Advanced materials & processes. 163(9), 49-51 (2005)

Vishay™: Introduction to strain gauge technology, http://www.egr.unlv.edu/~bj/MEG_302L_web/Student_strain_gage_Manual-001.PDF. (2001). 31 March 2016.

Viswanatha C. S., Prasad L.N., Radhakrishna and Nataraja H. S., Sub-standard rebars in the Indian market: An insight, The Indian Concrete Journal, January 2004, p.p. 52-55.

Zeingsheim H.P. and Pab G., An inductive extensometer measuring microstrains on flat and cylindrical bars (1969), Wear, 13(2), pp. 142.

Zenxiang, F., Jize, S., & Shichun, W. (1997), A theoretical study of the optimum linearity conditions of the structure of an axial extensometer, Journal of materials processing technology, 69(1-3), 152-154.

APPENDICES

Appendix A: HARDNESS PROFILES FROM LITERATURE

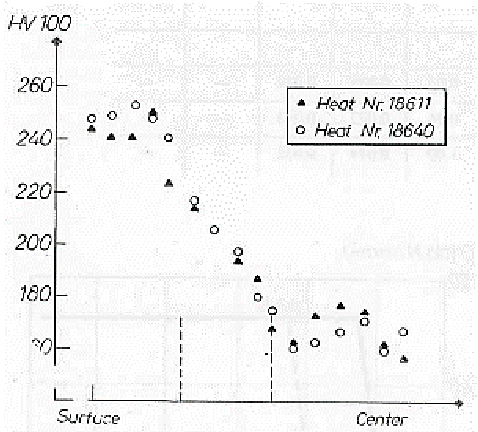

Rehm and Russwurm 1977

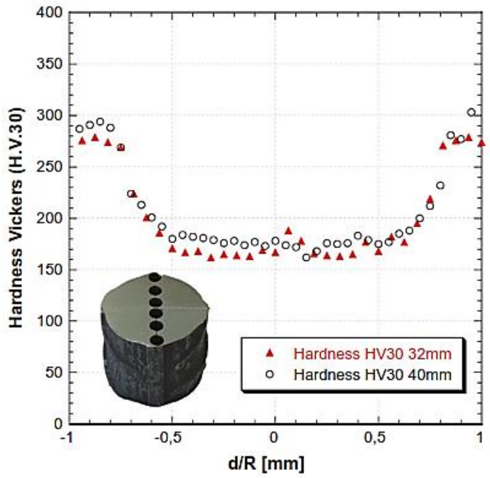

Cadoni et al. 2013

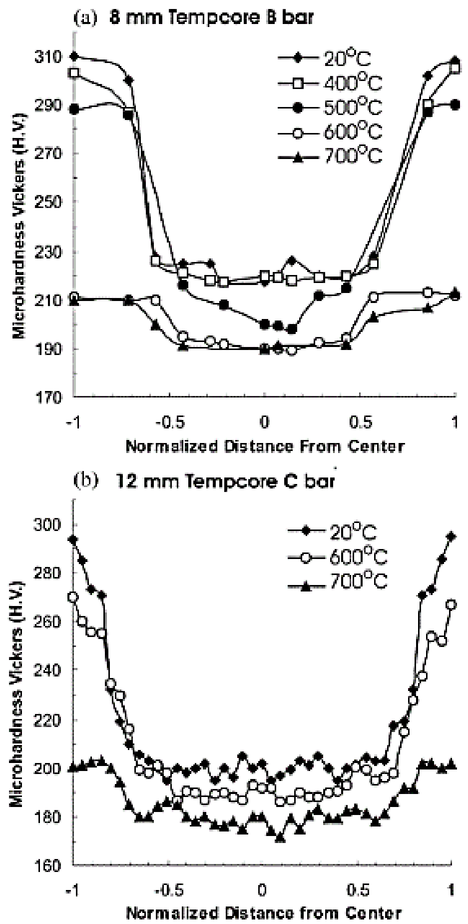

Nikalaou 2004

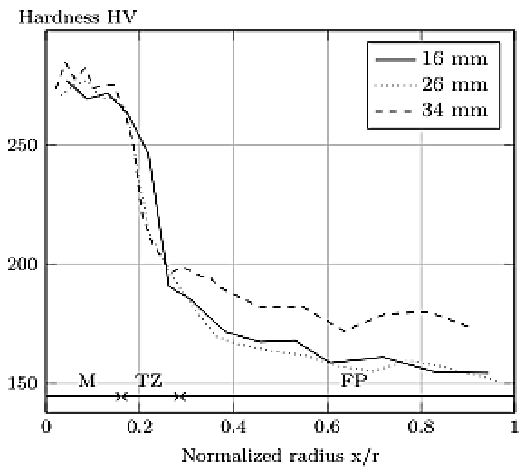

Rocha et al. 2016

Appendix B: NITAL TEST RESULTS – INDIAN SAMPLES

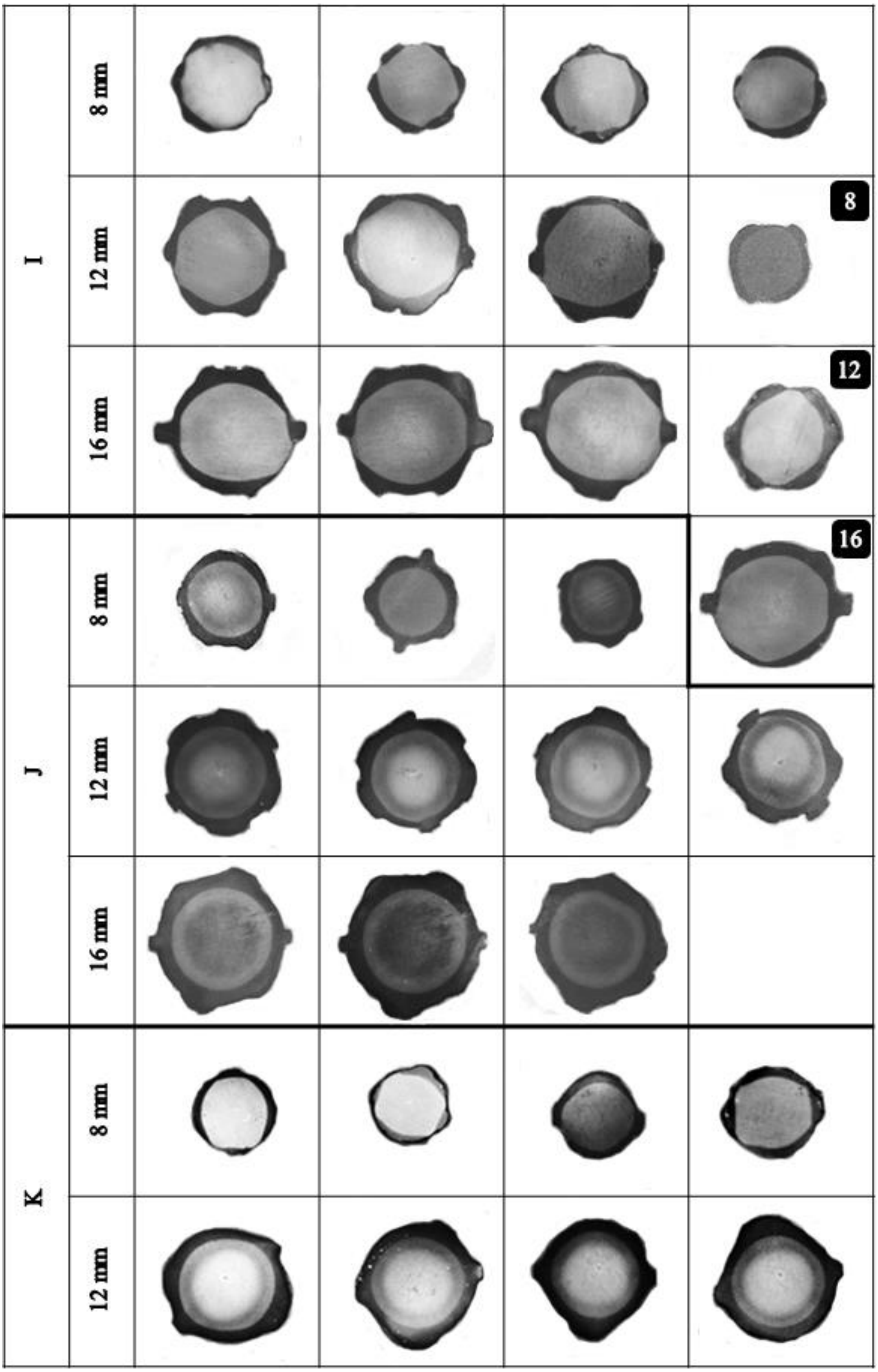

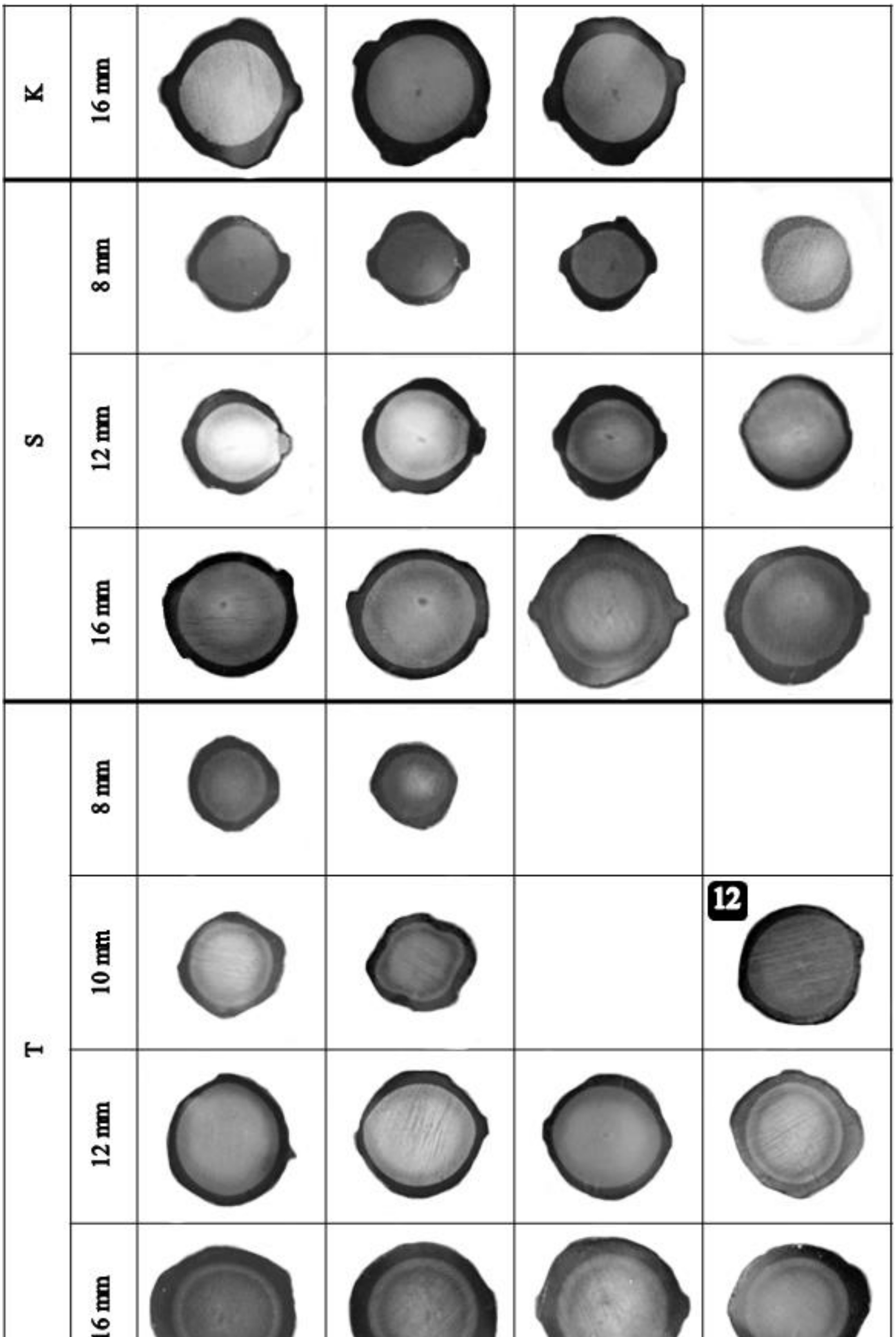
K
16 mm
S
8 mm
12 mm
16 mm
T
8 mm
10 mm
12 mm
16 mm
12

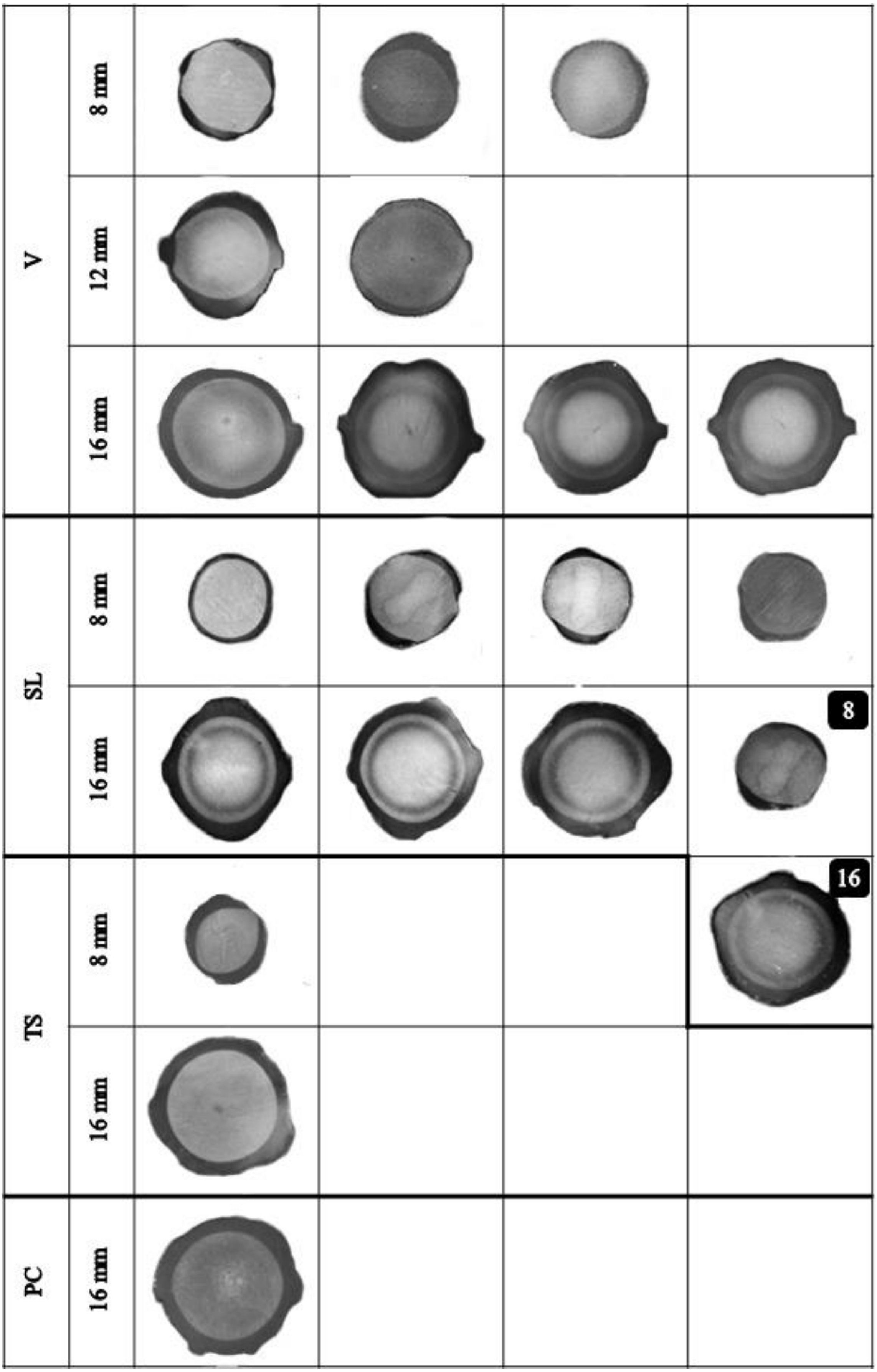
V
8 mm
12 mm
16 mm
SL
8 mm
16 mm
8
TS
8 mm
16 mm
16
PC
16 mm

A	AG	GB			SD
8 mm	8 mm	16 mm	12 mm	8 mm	12 mm
		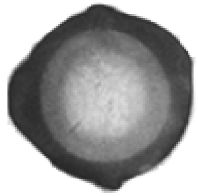		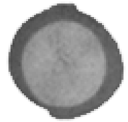	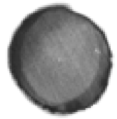
		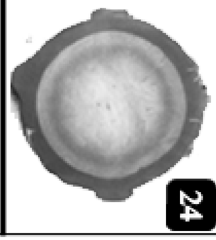	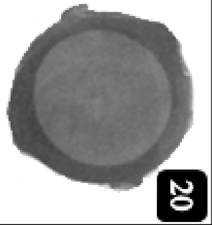	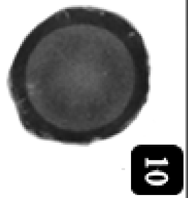	

Appendix C: **NITAL TEST RESULTS – FOREIGN SAMPLES**

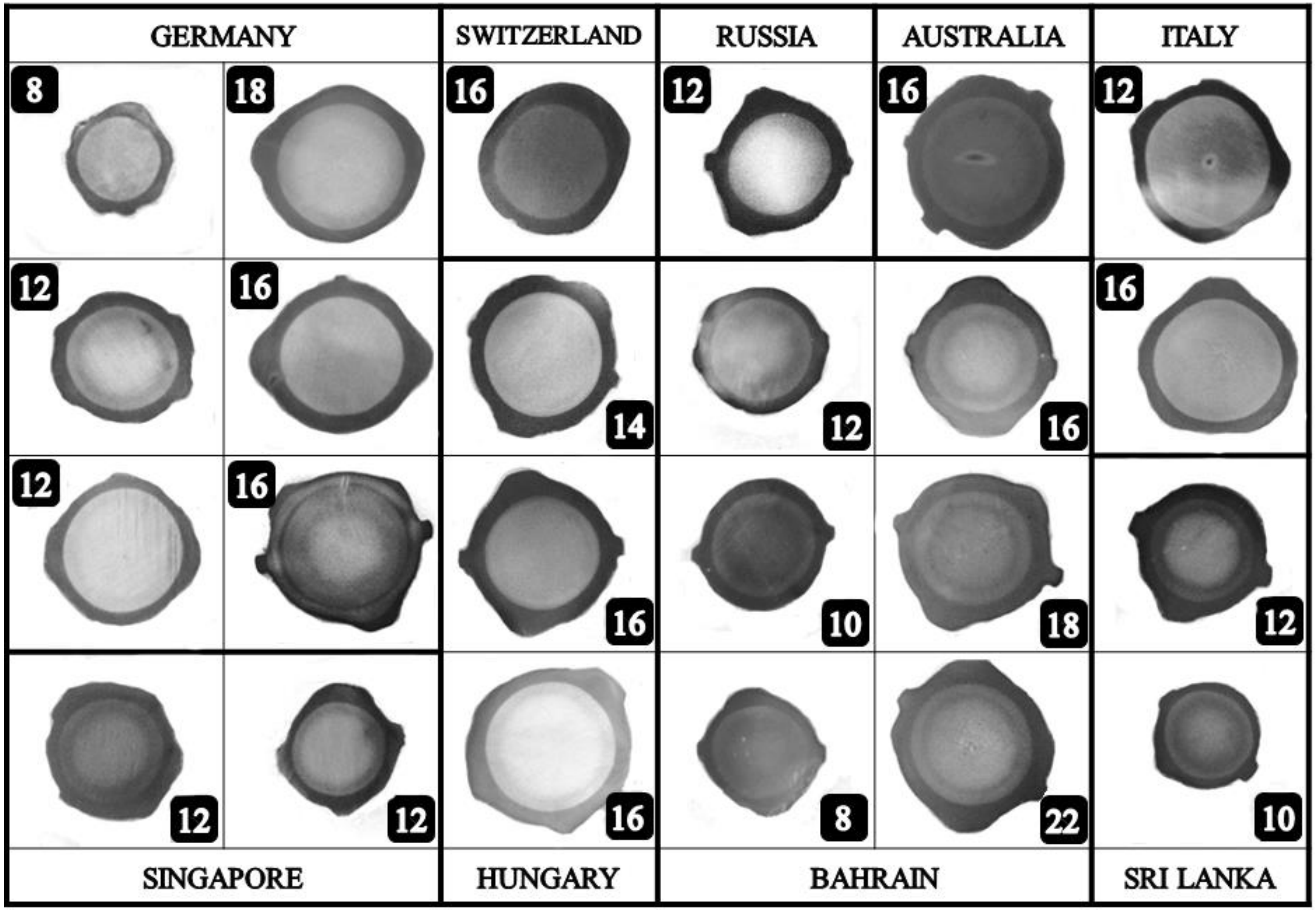

Appendix D: LONGITUDINAL C/S STUDY – PQ VS. GQ 12 MM

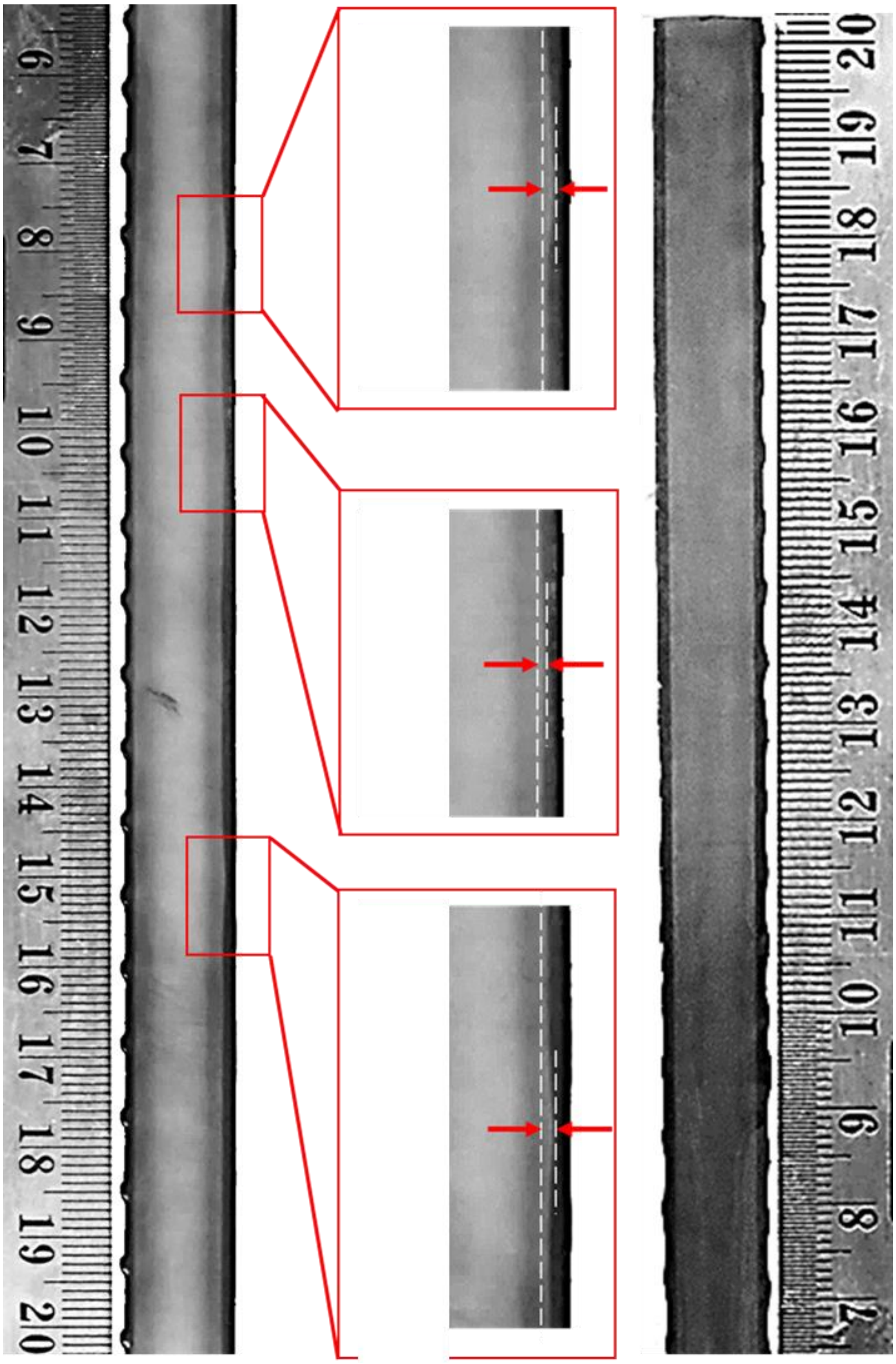

LIST OF PUBLICATIONS ON THE BASIS OF THIS THESIS

REFEREED JOURNALS

1. **Sooraj A. O. Nair and Radhakrishna G. Pillai**, 'TM-ring test' - A quality control test for TMT (or QST) steel reinforcing bars used in reinforced concrete systems, Indian Concrete Institute Journal (Accepted for publication in April-June 2017 issue).
2. **Sooraj A. O. Nair and Radhakrishna G. Pillai**, Microstructural and corrosion characteristics of Quenched and Self-Tempered (QST) steel bars used in reinforced concrete structures, Materials and Structures (In preparation).
3. **Sooraj A. O. Nair, Vellore S. Gopalaratnam and Radhakrishna G. Pillai**, A low-cost design and fabrication of a clip-on extensometer for tensile test on steel bars, Experimental Techniques (In preparation).
4. **Sooraj A. O. Nair and Radhakrishna G. Pillai**, Microstructural, electrochemical and mechanical characteristics of Quenched and Self-Tempered (QST) or TMT steel bars in reinforced concrete, Indian Concrete Institute Journal (In preparation).

PRESENTATIONS/POSTER IN INTERNATIONAL CONFERENCES

1. ***Sooraj A.O. Nair, Gokul P.R., Sethuraj R., Nandipati S., Radhakrishna G. Pillai.**, "Variations in microstructure and mechanical properties of Thermo-Mechanically-Treated (TMT) steel reinforcement bars", *Proceedings of the 4th Asian Conference on Ecstasy in Concrete (ACECON)*, Oct 08-10, 2015, Kolkata, 325-331, Indian Concrete Institute.
2. ***Sooraj A.O. Nair, Radhakrishna G. Pillai**. "Localized chloride-induced corrosion of quenched and self-tempered (QST) steel rebar due to discontinuous peripheral tempered martensite phase", *Proceedings of the Concrete Service Life Extension Conference*, May 23-25, 2016, Florida, NACE International.
3. **Sooraj A.O. Nair, Radhakrishna G. Pillai, *Ravindra Gettu**. "Corrosion characteristics of Quenched & Self-Tempered steel reinforcement bars", *Proceedings of the International RILEM Conference on Materials, Systems, and Structures in Civil Engineering 2016*, Aug 21-24, 2016, Lyngby, Denmark, RILEM.

4. ***Sooraj A.O. Nair, Abhinav R., Mitra Pradeep, Aiswarya R., Suhail Ishack, Radhakrishna G. Pillai**. "Microstructural phase distribution and corrosion characteristics of Thermo Mechanically Treated(TMT) steel reinforcement bars", *CORCON 2016 – International conference and expo on corrosion*, Poster Presentation, September 18-21, 2016, New Delhi, NACE International.

(* indicates presenter)

GRADUATE TEST COMMITTEE

CHAIRPERSON	Dr. K. Ramamurthy Professor and Head Department of Civil Engineering
GUIDE	Dr. Radhakrishna G. Pillai Assistant Professor Department of Civil Engineering
MEMBERS	Dr. Ravindra Gettu Professor Department of Civil Engineering
	Dr. Srinivasan Chandrasekaran Professor Department of Ocean Engineering

CURRICULUM VITAE

Name	:	Sooraj Kumar A. O.

Education qualifications

2014	**:**	**Bachelor of Technology (B.Tech.)**
Institution	:	National Institute of Technology Calicut, Calicut
Department	:	Civil Engineering
2017	**:**	**Master of Science (M.S.)**
Institution	:	Indian Institute of Technology Madras, Chennai
Department	:	Civil Engineering
Specialization	:	Building Technology and Construction Management
Registration Date	:	15 July 2014